

**Numerical methods for improved signal to noise ratios in
spatio-temporal biomedical data**

Dissertation

Zur Erlangung des akademischen Grades

Doktoringenieur (Dr.-Ing.)

**vorgelegt der Fakultät für Informatik und Automatisierung
der Technischen Universität Ilmenau**

von Dipl.-Ing. Dania Di Pietro Paolo

geboren am 21. August 1978 in Teramo

Tag der Einreichung: 20. Oktober 2009

Tag der wissenschaftlichen Aussprache: 05. Mai 2010

Gutachter: 1. Prof. Dr.-Ing. Habil. Jens Haueisen

2. PD Dr. rer. medic. Peter van Leeuwen

3. Dir. u. Prof. Dr. Lutz Trahms

urn:nbn:de:gbv:ilm1-2010000179

To the memory of one of my best friends: Tony

Contents

Abstract	ix
Zusammenfassung	xi
1 Introduction	1
1.1 Motivation	1
1.2 Introduction to denoising techniques	3
1.3 Aim of the thesis	10
1.4 Overview	12
2 Materials and Methods	13
2.1 Basis of Magnetocardiography	13
2.2 Physiological basis of MCG	16
2.3 Technical basis for MCG detection	16
2.3.1 SQUID sensor	16
2.3.2 Magnetometer and Gradiometer	18
2.3.3 Cryostat-Dewars	20
2.3.4 Magnetically Shielding Room	20
2.4 Equipment	20
2.4.1 MCG System	20
2.4.2 Ergometer	22
2.5 Patients	24
2.6 Acquisition Paradigma	25
2.6.1 Rest Data	25
2.6.2 Stress Magnetocardiographic Data	25

2.7	Averaging procedure	28
2.7.1	Overview	28
2.7.2	Segmentation	29
2.7.3	Cluster Analysis	32
2.8	Blind Source Separation	36
2.8.1	Introduction	36
2.8.2	Singular Value Decomposition	39
2.8.3	Independent Component Analysis	40
2.8.4	Overfitting: Bumps and spikes	48
2.8.5	Singular Value Decomposition vs Independent Component Analysis . .	48
2.8.6	Finding the cardiac signals	49
2.8.7	Reconstruction	53
2.8.8	ICs validations	53
3	Results	55
3.1	SNR improvement in averaged data using categorized data analysis	55
3.1.1	Theoretical explanation	55
3.1.2	Examples	58
3.2	Noise Reduction using Blind Source Separation	61
3.2.1	Choosing the optimal BSS algorithm	61
3.2.2	Identification Phase-Finding the cardiac components	67
3.2.3	Validation Phase-Cleaned data	75
3.3	Computation time	88
4	Discussion	93
5	Conclusions	101
	Acknowledgments	127

Abbreviations

ABP	auditory brain stem
ABR	auditory brain stem responses
AC	alternate current
BSE	blind source extraction
BSPM	body surface potential map
BSS	blind source separation
CCA	categorized cluster analysis
CHD	coronary heart disease
CpT	computation time
CRM	cardiac rhythm management
CT	correlation threshold
EA	ensemble averaging
ECG	electrocardiography / electrocardiogram
EEG	electroencephalography
EI	electric interference
EVD	eigen value decomposition
fECG	fetal electrocardiography

fICA	fast independent component analysis
fMCG	fetal magnetocardiography
FT	flux transformator
HCA	hierarchical cluster analysis
HOS	high order statistics
HR	high resolution
HRECG	high resolution ECG
HRV	heart rate variability
ICA	independent component analysis
ICD	implanted cardiac defibrillator
JADE	joint approximation diagonalization
JJ	josephson junctions
KT	kurtosis threshold
LVEF	left ventricular ejection fraction
MCG	magnetocardiography / magnetocardiogram
MEG	magnetoencephalography
MF	magnetic field
MI	magnetic interference
MSR	magnetic shielded room
NPA	negative predictive accuracy
NS	non stationarity
PCA	principal component analysis
PDF	probability density function

PL	power-line
PPA	positive predictive accuracy
PPU	patient position unit
PSMCG	pharmacological stress magnetocardiography
RMS	root mean square
SD	standard deviation
SHIBBS	shifted block blind separation
SMCG	stress magnetocardiography
SNR	signal to noise ratio
SOBI	second-order blind identification
SOS	second order statistics
SQUID	super-conducting quantum interference device
SVD	singular value decomposition
TDSEP	temporal decorrelation source separation
VT	ventricular tachycardia
WHO	world health organization
WPW	wolf parkinson white

Abstract

Magnetocardiography (MCG) is a non-invasive and side-effect-free cardiac diagnostic technique allowing body-surface recording of the magnetic fields generated by the electrical activity of the heart. The fields of interest are manifold; e.g., risk stratification of ventricular tachycardia, fetal rhythm assessment, detection of ischemia etc. One problem is that the interpretation of MCG signals is jeopardized by different kinds of disturbances and noise, making its analysis difficult.

Several methods have been suggested for noise reduction in MCG data such as averaging, pass or stop band filters, and statistical based methods, but a unified framework that takes into account different typologies of MCG signals (rest MCG, stress MCG and rest MCG in patient with an ICD -Implanted Cardioverter Defibrillator- implanted) using an adequate number of recordings was still missing. Consequently, the main aim of the thesis was to develop methods for noise and artifacts treatment.

Due to the non-stationarity (NS) of the noise and the *per se* variability of the cardiac signal, the conventional ensemble averaging of the data, using *en block* all cardiac beats, did not yield the theoretical improvement. In order to overcome this problem a new averaging procedure has been applied, that ignored the noisiest beats and those with high variability. The results of this averaging procedure have confirmed that in case of NS, the SNR (Signal to Noise Ratio) reached a maximum after a certain number of *selected* beats. Although this behavior was already described in the literature, a mathematical expression was up to now still missing. The approach used to reach the formulation was to extend the SNR derivation after the averaging procedure to the NS of the noise, or better the piecewise stationarity: In fact the optimum SNR could be reached whenever the condition $\sigma_{x+1}^2 > 2\sigma_{avg}^2$ was verified; in other words if the variance σ calculated using $x + 1$ beats was at least twice the averaged variance calculated using x beats (where x is the number of averaged beats).

The second part of the thesis has dealt with techniques based on Blind Source Separation (BSS), used in case of low SNR. BSS were used, in this work, as preprocessing step in the averaging procedure. Different BSS algorithms were compared in order to find the best one in terms of noise reduction, separation, and computational time for each data typology. A drawback of BSS techniques is the order of the independent components that is ambiguous and cannot be determined *a priori*: the heart related sources have to be detected by visual inspection once all sources are found. In order to overcome this problem three methods (kurtosis, correlation and frequency analysis), based on different statistical principles, have been developed in order to automatically retrieve the cardiac signals discarding the other ones. The approach used was to separate the patients enrolled into two groups: one identification group where the thresholds related to each of the aforementioned methods were calculated and a validation group where these thresholds were tested.

The last part of the thesis studied the application of BSS methods to a category of signals that was not yet analyzed: patients with ICD implanted. In fact, the presence of this device in the thorax of the patient leads to very strong interferences, that are orders of magnitude larger than the biomagnetic signal of the heart. For this reason, ICDs and pacemakers were up to now among the exclusion criteria for studies concerning MCG. It was shown that it was possible to extract the cardiac signal also in such noisy data, although not automatically.

The Temporal Decorrelation source SEParation (TDSEP) algorithm outperforms the other BSS methods.

This thesis showed that, applying novel automatic routines for the removal of noise and artifacts, MCG data can be used in clinical environments.

Zusammenfassung

Magnetokardiographie (MKG) ist eine nicht-invasive und belastungsfreie diagnostische Technik, die die Aufnahme des magnetischen Feldes, welches durch die elektrische Aktivität des Herzens generiert wird, erlaubt. Die Anwendungsfelder dieser Technik sind vielfältig: Risikostratifizierung bei ventrikulären Tachykardien, Ischämiedetektion, Analyse von fetalen Rhythmen usw. Die Analyse und Interpretation des MKG Signals wird jedoch durch verschiedene Störungen und Rauschen erschwert.

In der Vergangenheit wurden einige Methoden zur Störsignalunterdrückung beim MKG beschrieben. Dazu gehören Mittelungstechniken, Filter oder statistische Methoden. Jedoch wurde bisher kein einheitliches Rahmenwerk vorgestellt, welches die unterschiedlichen Typen von MKG Signalen (rest MKG, stress MKG und Patienten mit implantiertem ICD -Intrakardialer Defibrillator) und adäquate Mittelungszahlen berücksichtigt. Daher war das Hauptziel der vorliegenden Arbeit die Entwicklung von generischen Methoden zur Behandlung von Artefakten und Rauschen im MKG.

Auf Grund der Nichtstationarität des Rauschens und der per se Variabilität des Herzsignals ist die Verbesserung des Signal-zu-Rausch-Verhältnisses (SNR) durch Mittelung aller einzelnen Herzschläge theoretisch limitiert. Zur Lösung dieses Problems wird eine neue Mittelungsherangehensweise vorgeschlagen, die stark verrauschte Schläge und solche mit hoher Variabilität ignoriert. Das Ergebnis dieser neuen Mittelungstechnik zeigte ein Maximum im SNR nach einer bestimmten Anzahl von ausgewählten Schlägen (oder Gruppen von Schlägen). Obwohl dieses Verhalten bereits in der Literatur beschrieben wurde, gab es bisher keinen mathematischen Ausdruck dafür. Es wurde ein theoretisches Kriterium für das Optimum im SNR abgeleitet. Dazu wurde das SNR stückweise (pro Block x , wobei ein Block aus einer bestimmten Auswahl von ähnlichen Schlägen besteht) unter der Annahme der Stationarität pro Block betrachtet. Es wurde gefunden, dass unter der Bedingung $\sigma_{x+1}^2 > 2\sigma_{avg}^2$ das optimale

SNR erreicht wurde, wobei σ_{x+1}^2 für die Varianz des Blockes $x + 1$ und σ_{avg}^2 für die Varianz der bis dahin ausgeführten Mittelung steht.

Der zweite Teil der vorliegenden Arbeit beschäftigt sich mit dem Einsatz der Blind Source Separation (BSS) als Vorverarbeitungsschritt vor der Mittelung bei sehr geringen SNRs. Es wurden verschiedene BSS Algorithmen bezüglich ihrer Rauschunterdrückung, ihrer Separierung und ihrer Rechenzeit bei verschiedenen Datentypen verglichen. Ein Nachteil der BSS Algorithmen besteht in ihrer Mehrdeutigkeit und der nicht a priori feststellbaren Reihenfolge der zerlegten Quellen. Oft werden die Quellen des Herzschlages durch eine visuelle Inspektion separiert. Daher wurden drei Ansätze (Kurtosis, Korrelation und Frequenzanalyse), basierend auf verschiedenen statistischen Prinzipien, entwickelt, die die Rückgewinnung des Herzsignals aus dem zerlegten Multikanal-MKG realisieren. Die notwendigen Schwellwerte wurden dabei an einem Trainingsset von Patienten bestimmt und anschließend an einem Testset von Patienten getestet.

Im letzten Teil der vorliegenden Arbeit wurden die BSS Methoden auf Messungen an Patienten mit implantierten ICDs angewendet. Das Vorhanden sein der ICDs im Thorax der Patienten führt zu starken Interferenzen, die um mehrere Größenordnungen größer sind als das biomagnetische Signal des Herzens. Aus diesem Grund sind ICDs bis jetzt ein Ausschlusskriterium für MKG Studien. Die Ergebnisse zeigten, dass es möglich war das Herzsignal zu extrahieren, wenn auch nicht mit einer automatischen Prozedur.

Der Temporal Decorrelation source SEParation (TDSEP) Algorithmus übertrifft die anderen BSS Methoden.

Zusammenfassend konnte gezeigt werden, dass auch unter den schwierigen Bedingungen klinischer Routine ein Einsatz von neu entwickelten und automatischen Routinen zur Verbesserung des SNRs zur klinischen Nutzung des MKGs möglich ist.

Chapter 1

Introduction

1.1 Motivation

Biomedical signals arising from many sources including heart, brain and lungs pose a challenge to researchers who may have to separate the signals arriving from multiple sources contaminated with stochastic and non-stochastic contributions (Widrow and Walach (1996); Jung et al. (2000b)).

The information of interest contained in these signals is often a combination of features that are either well localized temporally (e.g., spikes) or more diffuse (e.g., small oscillations). This mix of properties requires the use of analysis methods that are sufficiently versatile to handle events that can be at opposite extremes in terms of time-frequency localization. The main difficulty in dealing with biomedical signal processing is the extreme variability of the signals and the necessity to operate on a case by case basis (Unser and Aldroubi (1996)).

Each physiological process in a biomedical signal is associated with certain types of signals that reflect their nature and activities. Such signals can be of different types:

- Biochemical: hormones and neurotransmitters;
- Electrical: potentials and currents;
- Mechanical: pressure and temperature.

The electrical activity generates a magnetic field (MF) that can be measured with magnetic sensors. Biological MFs are very weak and the MF of a single human cell is below the detectable threshold. Transient biomagnetic activity can only be measured if thousands of cells are activated synchronously which is the case with focal pathological activity, whereas in the propagation of activity mostly only nerve bundles of a few hundred nerve cells are involved. Yet,

with the improvement of acquisition devices and signal-processing techniques, first attempts to localize the propagation of electric activity have been made, e.g., the localization of very prominent pathways of electrical excitation such as Atrio Ventricular (AV) - His activity in the heart (Fenici et al. (1983); Patrick et al. (1983); Erne (1985)) and the localization of evoked potentials sources in the brain (Romani et al. (1982a,b)). Since these first developments in the late 1980s, many progresses have been made by the Superconducting Quantum Interference Device (SQUID) technology.

Remarkable success is obtained applying these systems to Magnetoencephalography (MEG): In fact 90% of all SQUIDS systems are related to neurological biomagnetic investigation, since here basic research still plays a strong role and the users are more receptive to new technology. For the same motivation, Magnetocardiography (MCG) is facing far more difficulties in becoming an accepted diagnostic tool, but perspectives are increasing since the cause of death for heart disease is the most common cause of mortality in industrialized countries (Figure 1.1) (Koch (2001)) and a non-invasive diagnostic tool with great sensitivity and specificity is still missing.

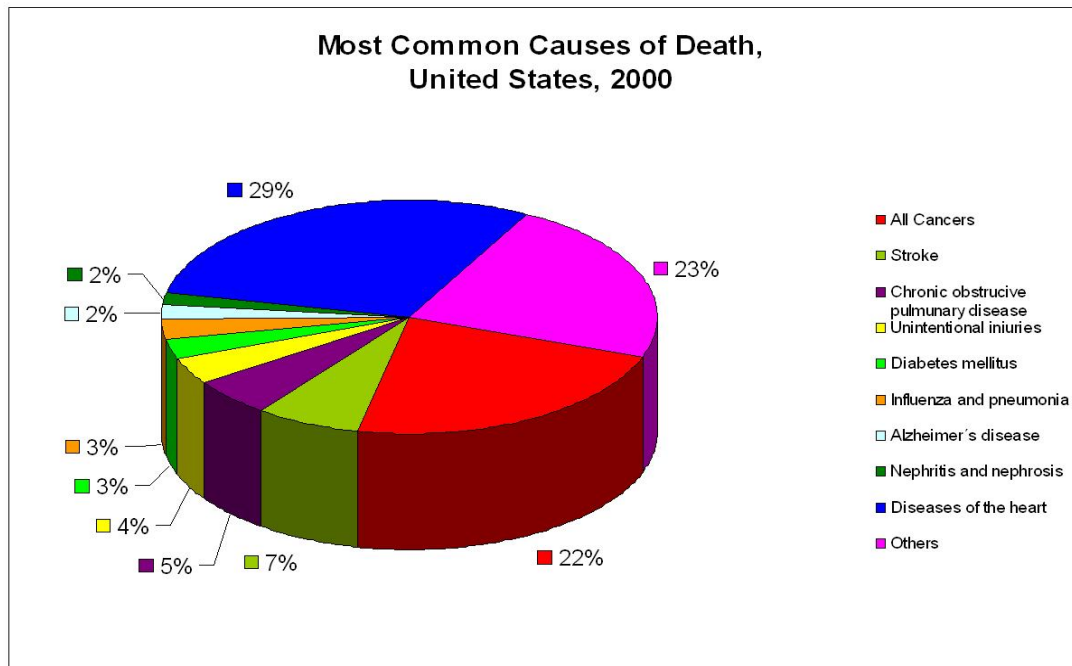


Figure 1.1: Percentage of death caused by heart disease: Heart disease is the first cause of death in USA according to the National Center for Health Statistic. The trend is the same in almost all industrialized countries (Anderson (2002))

In this thesis the attention will be focused on the cardiac signal activity, recorded by means of MCG. Magnetocardiography monitors the spontaneous activity of the heart by measuring the weak MF variations associated with the primary ionic currents flowing through the myocardium during the cardiac cycle (Siltanen (1989)). Such multi-channel acquisition is usually recorded with a known spatial distribution of recording sensors with respect to the human thorax, hence giving rise to a set of temporally and spatially correlated measurements.

1.2 Introduction to denoising techniques

Magnetocardiographic signals, as most of the biomedical signals, are contaminated by different sources of noise that can be classified into two main categories: endogenic and exogenic interferences, where the former are related to noise sources within the body and the latter are caused by external noise sources. Endogenic noise sources are for example caused by muscular activity whereas exogenic interferences are produced by equipment generating electrical charges or electromagnetic fields. In a hospital for MCG recording, most of electrical and magnetic devices must be properly shielded in order to minimize the influence of exogenic noise. Exogenic noise sources can be further divided according to their origin:

- Electric interference (EI), arises from differing potentials in various parts of the body and, as result, a current flows which interferes with the sensors. Electrical motors and transformers may generate this kind of interference (Dawson et al. (2000));
- Magnetic interference (MI), has only a minor influence on the body. However, for unipolar electrodes, the flux from the MF induces a current in the coil formed between the electrode tip and a cardiac rhythm management (CRM) device;
- Electromagnetic Interference (EMI), arises from television transmitters, police radios, and cellular phones. It can cause medical monitors and other hospital devices to malfunction.

Noise is often modeled as gaussian white noise, but this is not the reality: Noise is often correlated (with itself or with the signal), it is not continuous, but it can be concentrated in short time intervals, and it is not stationary: Its statistical properties change over time. Table 1.1 illustrates the range of signal contamination for a MCG signal according to the frequency content and the time duration: There are continuous noise such as power-line interferences or sensor noise and transient noise such as an airplane flying by, a slammed door etc.

Due to these different noise sources the signal to noise ratio (SNR) in MCG is quite low and, for this reason, several epochs have to be recorded in different space-points: The result is

Table 1.1: Possible contaminations of a MCG recording and their nature: for each of them the frequency range and time duration are shown

Noise sources	Characteristics	Frequency Range	Time Duration
	earth field	broad band	continuous
	power line	narrow band: 50-60 ± 2 Hz	continuous
	urban noise	broad/narrow band	continuous
	train	narrow band: 16 ± 2 Hz	transient
	airplane	broad band	transient
	movement baseline	narrow band: < 0.5 Hz	continuous/transient
	wander		
	respiration	narrow band: < 2 .Hz	continuous/transient
	muscle activity	broad band	transient
	sensor noise	broad band	continuous

a multidimensional time series, coming from the recording of such activities, highly redundant and containing artifacts and noise. The difficulty in recording MCG is the weakness of the signal if compared with the electrical counterpart (Electrocardiogram): The MF generated by currents flowing in the heart is in the order of 10^{-10} to 10^{-12} Tesla, which is much weaker than the earth's MF and urban noise (refer to Chapter 2). As a consequence, special care is required in obtaining MCG signals in order to reduce time disturbances, such as fluctuations of the earth's MF and those generated by electrical devices and power-lines.

Since superconducting multi-channel systems have become available, the cardiac MF can be recorded with high sensitivity simultaneously from a number of positions over the chest (Pasquarelli and Di Luzio (1993); Tavarozzi et al. (2002a)), hence allowing accurate field mapping during the cardiac cycle, useful for several clinical applications, particularly for arrhythmias (Brockmeier et al. (1997); Hren et al. (1999); Kandori et al. (2001); Tavarozzi et al. (2002b)) and for patients prone to ventricular tachycardia (Müller et al. (1999)).

Different methods can be used for improving the SNR in MCG: They can be divided into different groups depending on whether they are frequency based (i.e. pass or stop band filter), statistical based (i.e. autocorrelation, autoregressive model, singular value decomposition

(SVD) or based on blind source separation (BSS) methods) or a process of averaging.

In this work, different methods for reducing noise and artifacts in MCG data are presented. The first illustrated method is a *modified* averaging algorithm that considers the spatio-temporal properties of the MCG data. Often a conventional ensemble averaging (EA) of the data, using *en block* all cardiac beats is used. Unfortunately, the classical hypothesis of cardiac signal embedded in random uncorrelated noise and same noise level in all epochs is quite improbable. Nevertheless, in case all these requirements (random, stationary uncorrelated noise) were satisfied, the well-know improvement of the SNR with the square root of the number of cardiac beats would be obtained. In reality, the stationarity is frequently violated by muscular activity (artifacts), respiration, slow movements of the patient and heart rate variability (HRV), to mention only endogenic noise.

Several average algorithms have been developed in order to examine these effects, but most of them are related to brain activity (Riedel et al. (1999)), that is a quite different problem when compared with the cardiac one. In fact, in brain activity several epochs are needed for the average procedure since the SNR is very low and an estimation of the noise amplitude is straightforward. If the average of brain stem response is analyzed, two methods are normally used to minimize the undesirable effects of noise instability on the SNR. The former and most common method is artifact rejection i.e., the elimination of realizations with signal amplitudes exceeding a certain level from the averaging process, but this method has a drawback: The threshold must be known *a priori*. The latter one is weighted averaging i.e., the weighting of realizations or blocks of realizations inversely to the estimated power of background noise (Hoke et al. (1984)), but in this case the underestimation of the signal amplitude is unavoidable (Lutkenhoner et al. (1985)). Mühler and von Specht (1999) (Mühler and von Specht (1999)) have suggested the method of sorted averaging on a single sweep basis so as to determine the sweeps entering an average *a posteriori*: This means that before averaging, the recorded epochs are sorted according to their (estimated) contamination by noise. Only sweeps containing less than a certain degree of noise are included in the average.

Heretofore, the amount of papers that have been published on MCG noise reduction is not so high, since in MCG cardiac signal (if recorded inside a shielded room) the SNR is generally quite high and normally an *en block* procedure seems to be sufficient. Unfortunately if MCG is performed either in a slightly shielded or in an unshielded room, environments nearer to clinical applications, an alternative averaging procedure is needed: In this case the SNR is much lower

and the use of an *en block* algorithm is not optimal especially in those channels with the lowest SNR (close to the zero line).

In 1999 Willemsen et al. (Willemsen et al. (1999)) published a paper concerning the signal averaging of non-stationary noise applied to ECG using as parameters some weights that depend on the variance of a beat. This method showed that the use of weighted averaging decreases the number of complexes needed to achieve a predefined noise level, but no experiments on real data were performed.

The main problem is that the procedure of averaging works well if the noise level is sufficient small to correctly estimate the fiducial points (in general, a point in the QRS complex), as a synchronization reference. In fact, it can happen that due to highly correlated noise (such as residual 50 Hz) the R-peak (or any other fiducial point used for averaging, e.g., Q-onset) is not well estimated, hampering in this way the averaging process. In order to eliminate this problem a preprocessing is needed. The main source of electrical interference is the 50 Hz or 60 Hz superposition due to power-line (PL) AC interference (Huhta and Webster (1973)). The pursuit of a convenient method for the elimination of such interference in biological signals has been the topic of many papers (Glover (1987); McManus et al. (1993); Mortara (1977); Ferdjallah and Barr (1990)). Unfortunately, PL-interference is not the only noise source: In case of a stress acquisition the sources of noise increase.

The stress measurements are generally longer than their rest counterpart: This leads to a higher probability of artifacts, patient movements, especially if an ergometer is used. In this case the signals are very noisy, causing the averaging to be not effective as should and, for this reason, a filtering on the raw data has to be performed (see section 3.2.3). Analog and digital filters (such as Butterworth and Tchebyshev filters) are usually used to eliminate such interferences, but the spectrum of some artifacts and disturbances overlaps with that of the cardiac signal invalidating the usage of these filters (Thakor and Zhu (1991); Lander et al. (1995)). Thus, not only the interference is removed, albeit non completely, but also part of the signal of interest (Nolte and Curio (1999)). During denoising, care has to be practiced to preserve the features contained in the original signal since they are often relevant and necessary for appropriate diagnosis. In general, it is very difficult to differentiate between biologically important characteristics of the signal and the noise contained in the signal: The biological signals may not be consistent and may differ. Therefore, a reliable, robust, and versatile denoising method applicable in different circumstances is needed.

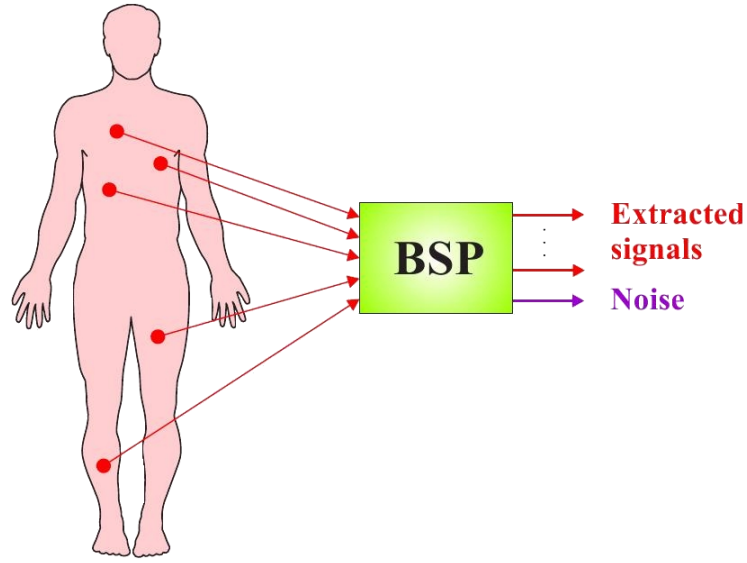
In the last few years, a bunch of new methodologies, based on Blind Source Separation (BSS) and/or Blind Signal Processing (BSP), has been developed for solving this problem. These methods are applied in several aspects of the signal processing in MEG, EEG, Electromyography (EMG) (Figure 1.2a) for denoising purpose.

Cichocki and Vorobyov (2000) (Cichocki and Vorobyov (2000)) have proposed several methods for signal detection such as kurtosis for detecting white (colored) gaussian noise, gradient descendant techniques and Hurst exponent. Delorme et al. (2001, 2007) (Delorme et al. (2001, 2007)) have developed five different statistical signal processing methods for detecting artifactual data epochs on Independent Component Analysis (ICA) decomposed sources, Greco et al. (2005) (Greco et al. (2005)) have enhanced the techniques of Delorme et al. (2001) (Delorme et al. (2001)) introducing the Renyi 's entropy instead of the Shannon 's entropy that showed some failures.

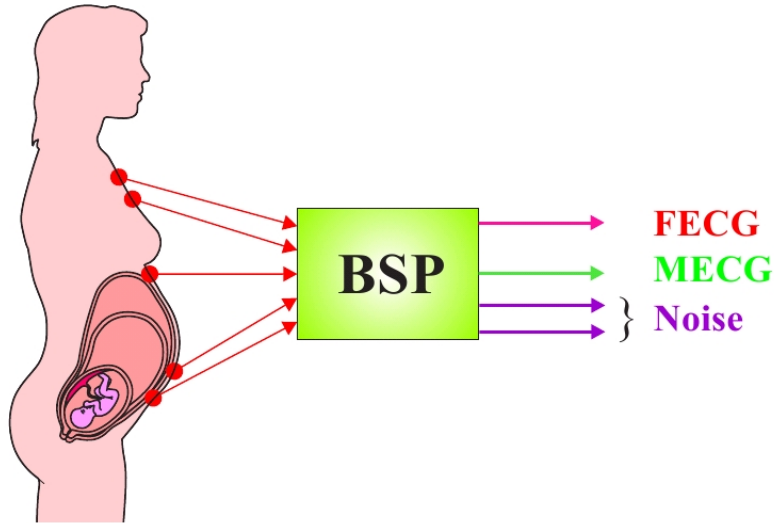
In ECG and fECG, BSS is normally used for separating fetal and maternal activity (de Lathauwer et al. (1995); Zarzoso et al. (1997); de Lathauwer et al. (2000)) (Figure 1.2b), for the analysis of atrial fibrillation (Rieta et al. (2000, 2004); Phlypo et al. (2007)), for the classification of arrhythmia (Owis et al. (2002); Azemi et al. (2007)) and for denoising (Barros et al. (1998); He et al. (2006)).

He et al. (2006) (He et al. (2006)) has proposed for ECG two different procedures for automatically identify the sources after the application of the joint approximation diagonalization (JADE) algorithm: kurtosis for detecting the continuous noise and an index based on the variance. The values of kurtosis have been found on 10s epochs of ECG and the variance has been calculated after having divided the sources into 10 non overlapping blocks. These routines have the disadvantage of being very sensitive to noise: In fact in the only example of low SNR, ICA and the related automatic methods fail in removing the artifacts. Another possible problem can be the variance method: it assumes that ECG signals have a heart rate of circa 1s and are quasi periodic, but this is not the case if patients with arrhythmia are considered.

In MCG, BSS methods are mainly used for fetal cardiac extraction (Comani et al. (2004); Hild et al. (2007); Comani et al. (2009)) even in twin gestation (Burghoff and VanLeeuwen (2004)). In fMCG, BSS is also used as preprocessing step for the evaluation of key parameters involving fetal arrhythmias, heart rate variability and autonomic control (Hoyer et al. (2009)): Studying these pathologies could permit an earlier detection of developmental problems and improved therapeutic strategies. On the contrary not so many papers are published dealing



(a)



(b)

Figure 1.2: Examples of biomedical applications for Blind Signal Processing (BSP) such as biomedical signals acquired with multi-electrode/channel devices: a) Enhancement of low-level ECG components, noise reduction in EMG signals, separation of residual original heart signal from the transplanted heart signal, separation of heart sounds from gastrointestinal acoustic phenomena, separation of heart sounds from lung sounds, cancellation or reduction of artifacts; b) blind separation of the fetal electrocardiogram (FECG) and maternal electrocardiogram from skin electrode signals recorded from a pregnant woman (Cichocki and Amari (2002))

with noise reduction at rest, under stress MCG (SMCG) and in general MCG in noisy conditions (Kobayashi et al. (2005); Steinhoff (2005); Lee et al. (2004)).

Lee et al. (2004) (Lee et al. (2004)) have introduced a spatial filter method based on fast ICA (fICA) for reducing magnetic noise in MCG: In this work the noise components are subjectively chosen among the sources and the evaluation of the noise reduction performances is done using the SNR of the MCG signal in the interval between the T-wave and the P-wave. As mentioned in section 3.2.3 this interval is not very effectual in case the RR interval is too short.

Kobayashi et al. (2005) (Kobayashi et al. (2005)) have applied ICA on MCG signals, disturbed by a wire fixed in the sternum, but the number of examinations is inadequate: In fact only an acquisition with a volunteer was recorded with and without wire.

Steinhoff (2005) (Steinhoff (2005)) has published a paper where the temporal decorrelation source separation method followed by joint diagonalization (TDSEP-JD) is applied to MCG data for noise reduction (power-supply, breathing and patient movements), in fECG and for separating atrial and ventricular activity in atrial flutter, but the number of subjects utilized is unknown and the resulting independent components are automatically classified only according to their spectral power in selected frequency bands.

The methods, that will be used in this PhD thesis are the following: a well known second order method for noise reduction such as SVD and other 5 ICA/BSS (Vorobyov and Cichocki (2002); Barros et al. (1998); James and Hesse (2005); Jung et al. (2000b,a); Rieta et al. (2002); Noel et al. (2001); Cichocki and Amari (2002)) methods. These algorithms are applied to different types of MCG signals, such as rest MCG, stress MCG etc.

Eventually, another important application of BSS methods is in patients with an already implanted Implantable Cardioverter Defibrillator (ICD). Implantation rates of ICDs have been rising to around 25 cases per million population in western European countries and North America. The costs for one additional year of life in chronic heart failure range from US 34,000\$ in older trials (CABG Patch, DINAMIT) up to US 70,200\$ (Zipes et al. (2006); Buxton et al. (2006)).

Because of this unprecedented expansion of ICD implantation, that only in few cases (between 21 to 35%) (Bardy et al. (2005)) leads to an appropriate therapy (arrhythmic events followed by a shock), there is a renewed interest in a non-invasive predictor for risk-stratification. For example the indication for an ICD implantation based on the parameter left ventricular ejection fraction (LVEF%) has been "coupled" in the MADIT II (Moss et al. (2004)) with the

ECG-derived QRS duration and heart rate variability without success. In the last 10 years, another risk stratifier has been applied: T-wave alternans (Hohnloser et al. (1998)), but the results are controversial (Chow et al. (2007)).

Korhonen et al. (2006) (Korhonen et al. (2006)) have performed a pioneer clinical study analyzing the intra QRS-fragmentation in averaged magnetocardiographic data (Link et al. (1994); Müller et al. (1999)). The results show the superiority of the method in comparison to signal averaged ECG and, in all-cause mortality, an abnormal MCG score together with a LVEF < 30% had a positive predictive accuracy (PPA) of 50% and negative predictive accuracy (NPA) of 91%. The population enrolled in that work is quite small (158 patients after myocardial infarction- MI) and therefore a bigger perspective clinical study is needed for validating the role of QRS-fragmentation as a risk stratificator. The problem is that this kind of study is time consuming (in the order of years, if the follow-up phase is included in the study). An alternative approach is to perform retrospective studies on patients with already implanted ICDs.

So far, it has been not possible to perform MCG and succeeding QRS-fragmentation analysis in such patients. In fact, the presence of an ICD in the thorax (usually it is located inside the chest, close to the left shoulder) of the patient leads to very strong interferences in the MCG measurements due to ferromagnetic components. The signal intensities of these interferences are up to orders of magnitude higher than the biomagnetic signal of the heart. Since the ICDs are normally placed on the left shoulder, the sensors are more influenced by this device close to the head: This means that the spatio-temporal properties of the recording change in relation to the position (Figure 1.3). For this reason, ICDs are still among the exclusion criteria for studies concerning MCG. However, using dedicated algorithms based on BSS, the extraction of these cardiac signals becomes possible.

1.3 Aim of the thesis

MCG still plays a strong role in basic research, but it is facing more difficulties in becoming an accepted diagnostic tool used in clinical environment. Difficult is the restricted SNR caused by artifacts, disturbances and external noise.

Although several papers have been presented for noise reduction in MCG data, a study that analyzes the different MCG data typologies in a unique framework with an adequate number of data is still missing.

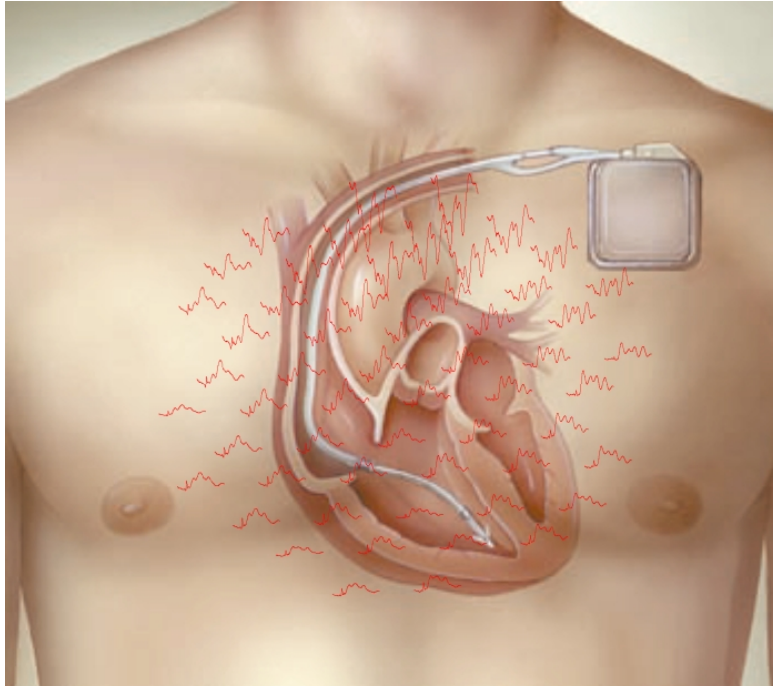


Figure 1.3: A schematic representation of the position of the ICD in the patient torso. Overlapped the sensor arrangement of a patient with ICD: Note the different properties of the signal according to the relative position with the ICD

The goal of the thesis is to present a general strategy, how to cope with the different noise sources in MCG signals in order to make MCG applicable in clinical use. To make it possible the tools for the denoising have to be user-independent and the computational load has to be low.

The first problem to be considered is the choice of a user-independent tool that is able to denoise data with low SNR, for this reason BSS algorithms and a novel average procedure will be evaluated. The BSS methods require that the users, after a visual inspection, select the cardiac sources among the estimated components for the denoising: This approach, as mentioned above, is too time demanding in case these algorithms have to be used in a clinical environment. Aim of the thesis is to develop routines, based on different statistical properties, for the automatic detection of cardiac signals in order to make the noise reduction procedure a user-independent tool.

The second problem that will be addressed is the computational speed of the algorithms that has to be reduced to use them also in clinical environment. Solutions for this problem will be proposed, thanks to the new technology of workstations that makes it possible to scale

the routines using multi processors and multi-threading approaches, in order to get an almost on-line result.

1.4 Overview

In the following a summary of the thesis content is listed.

Chapter 2 gives an overview of the used MCG data, acquisition systems and methods: It can be divided into more sections:

- a brief technical description of the MCG systems;
- the electrical conduction system of the heart;
- patient population;
- average procedure;
- BSS methods.

In *Chapter 3* the results for the different types of signal are presented. First of all an example of the theoretical findings in section 2.6.2 is shown: A mathematical explanation of why the optimal average is reached only after averaging a *selected* number of beats (or group of beats) is given, yielding as result the variance to not be exceeded during the average. In the second part of the chapter the results concerning BSS and their computational load are indicated. The methods used for the automatically selection of the sources are introduced.

In *Chapter 4* a discussion of the thesis findings are analyzed thoroughly.

In *Chapter 5* the conclusion about the relevance of methods for improving SNR in MCG has been drawn .

Chapter 2

Materials and Methods

2.1 Basis of Magnetocardiography

Magnetocardiography is a non-invasive and risk-free technique allowing a contact-free recording of the MFs generated by the electrical activity of the heart. The difficulty in recording MCG is the weakness of the signal; indeed the MF generated by currents flowing in the heart is of the order of 10^{-10} to 10^{-12} Tesla. As a consequence, special care is required in obtaining MCG signals for reducing disturbances, such as fluctuations of the earth's MF, MFs generated by electrical devices and power-lines. Figure 2.1 shows the strength of the human heart MF when compared to the environmental fields and the other biomagnetic fields produced by the body (for comparison a car at 50 m distance produces a MF that is about 1000 times larger than the heart signal).

Due to the closeness to the electrophysiology it is worthwhile to discuss the advantages of MCG compared with non invasive electrical acquisitions, e.g., BSPM (Body Surface Potential Map) and ECG. First of all, MCG is contact free, so all artifacts due to the skin-electrodes interfaces are avoided: This is especially important for stress measurements, where often the skin properties can change dramatically during the acquisitions jeopardizing them. The second main difference is that the electrical potential distribution measured at the body surface is governed by the geometry and the inhomogeneities of the different organs inside the torso. The MF recorded is, in first approximation, independent from "volume currents" affected by the aforementioned conditions. The third difference is the higher spatial resolution of the sensors that detect the MF compared with the lead field of the electrodes: In general the measuring points (sensors) in MCG are more than the electrodes used in a normal ECG.

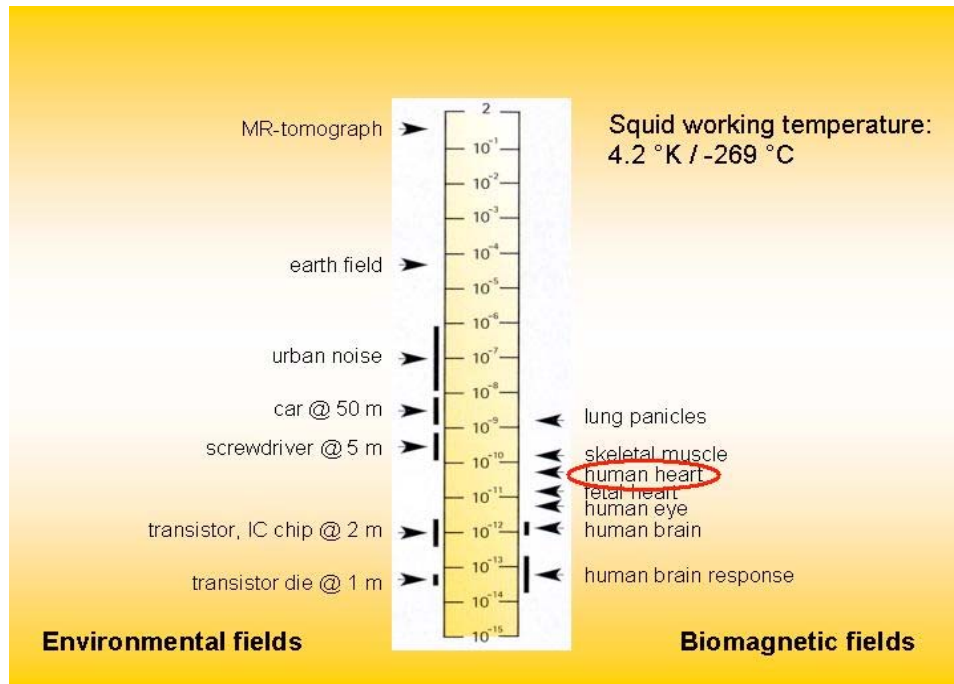


Figure 2.1: Comparison of selected biomagnetic fields and environmental disturbances: Note the amplitude of the heart MF when compared to the earth magnetic field and urban noise (Vrba (1996))

Among all differences, the most important one consists in the capability of MCG to detect vortex currents. According to the theoretical predictions of Wikswo (Wikswo et al. (1982); Wikswo (1983)), due to the cyto-architecture of the myocardium, the current, flowing during the excitation, has vortex components (Figure 2.2), that can be detected magnetically but not electrically. In normal heart the main direction of the activation wave front is radial, from the endocardium to the epicardium: Thus, MCG may show deviation from the normal activation direction induced (Figure 2.2b), e.g., myocardial ischemia with better accuracy than ECG (Siltanen (1989)).

More than one decade ago Brockmeier et al. (1997) (Brockmeier et al. (1997)) have been able to confirm experimentally this theoretical prediction performing simultaneous magnetical and electrical acquisitions under stress. This difference could be given by the vortical structure of the generating current distribution as it has been discussed in Kosch et al. (2000) (Kosch et al. (2000)). The influence of the active (Liehr et al. (2005)) and passive (Dutz et al. (2006)) vortex currents on the strength of magnetic signals was quantified with the help of a phantom torso.

The first report of a human body MF dates back to the 1960s with Baule and McFee (Baule

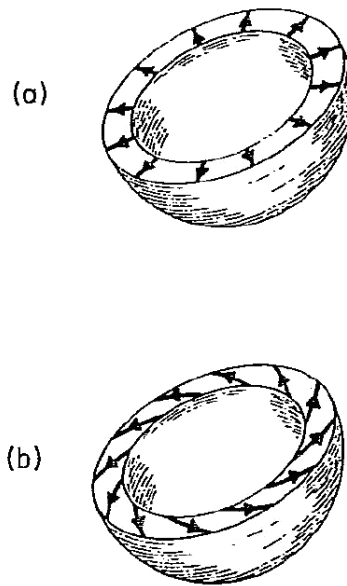


Figure 2.2: a) A uniform double-layer model of cardiac activity; b) Another double layer model of the cardiac activity where also the tangential part of the current distribution is shown. These tangential currents produce a MF, but their electrical field is silent (Wikswo et al. (1982))

and McFee (1963)) that used an induction coil magnetometer, made by winding two million turns of copper wire around a ferrite core. The progress of this discipline has been hampered by the fact that MFs produced by the biological activity are extremely weak, and at that time conventional instruments had difficulties in resolving all but the strongest biomagnetic fields.

The breakthrough came in the 1970s with the development in low temperature physics laboratories of a field sensor, known as the Superconducting Quantum Interference Device (SQUID), with dramatically improved sensitivity. This instrument provides the possibility to measure the MFs from many organs of the body. As these fields are much weaker than the magnetic noise of the environment, the earliest applications have been limited to type of acquisitions that could be recorded in either a remote location or in an elaborately shielded chamber.

The first magnetic shielded room (MSR) consisted of two layers of ferromagnetic shielding and one layer of aluminium (Cohen et al. (1970)). This room required a large space for installation and the working space was very small.

More recently built MSRs have fewer shells, provide more working space, and yield acceptable shielding for most purposes (Nakaya and Mori (1992)).

2.2 Physiological basis of MCG

A typical MCG tracing of a normal heartbeat (or cardiac cycle) consists of a P-wave, a QRS complex and a T-wave (a small U-wave is normally visible). The frequency of the cardiac cycle is the heart rate. Every single beat of the heart involves three major stages: atrial systole, ventricular systole and complete cardiac diastole.

The term diastole is synonymous with relaxation of a muscle. The cardiac cycle is coordinated by a series of electrical impulses that are produced by specialized heart cells found within the sinus node (S node) and the atrio-ventricular node (AV node). The electrical impulses in the S node pass through the atria using as conduction medium the myocardial tissue; the region between the atria and the ventricles is basically not conducting; only the AV-node and the following His bundle, as part of the specific conduction system, provide a mean for further propagation of the excitation toward the ventricles. The His bundle consists of Purkinje fibers with a fast conduction velocity, therefore the time between the activation of the His Bundle and the onset of ventricular activation is circa 40 ms. For a better understanding in Figure 2.3 the development of the MCG trace is shown in parallel with the schematic representation of the progress of the excitation in the heart: At the time corresponding to the maximum of P-wave, the excitation of the atria is almost completed, during the PQ interval, the atrial excitation is completed and the His-Purkinje system activated. In correspondence to the Q wave, the apex of the ventricle is activate and with the R-peak (corresponding to the maximum of the heart beat) the heart activation extends to the total septum and in the large part of the ventricles. During the S and the ST segment the excitation of the ventricles is completed. During the T-wave the depolarization of the ventricles is ongoing, and at the end of the beat (post T) the MCG signal goes theoretically to 0, and the heart is at rest (Rosendorff (2005)).

2.3 Technical basis for MCG detection

2.3.1 SQUID sensor

Superconducting quantum interference device is the most sensitive detector of magnetic flux available, made of superconducting material. The traditional superconducting materials for SQUIDs are pure niobium or a lead alloy with 10% gold or indium, as pure lead is unstable when its temperature is repeatedly changed. To maintain superconductivity (zero resistance)

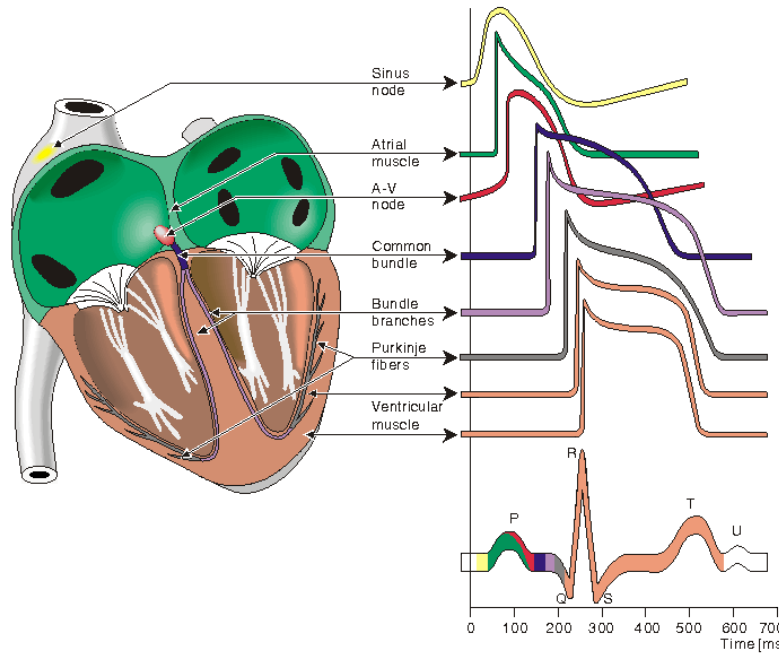


Figure 2.3: *Electrophysiology of the heart: the relationship between the spread of cardiac electrical activation represented at various time instants by a summing vector and the genesis of the MCG/ECG is shown (Webster (1992))*

the entire device needs to operate within a few degrees above the absolute zero, below a certain temperature, the so called critical temperature T_c (4,2 K with liquid helium or 77 K with nitrogen).

The SQUID, at critical temperature T_c using quantum-mechanical effects, provides a transfer from magnetic flux to electrical-impedance variations.

The basic phenomena governing the operation of SQUID devices are flux quantization in superconducting loops and the Josephson effect. A SQUID sensor consists of one (r.f. SQUID) or two (d.c. SQUID) Josephson Junctions (JJ). In the first case a single JJ interrupts the current flow around a superconducting loop and the r.f. SQUID is operated with a radio frequency flux bias. In the second case, d.c. SQUIDs, the two JJs are connected in parallel in a superconducting loop and are called in this way since they can be operated with a steady current bias.

To use the SQUID in practical instrumentation, a linearization circuit is necessary to minimize the non linearity; for this reason the SQUID is normally used as zero detector in a feedback loop. SQUID can operate in two different modalities according to what is kept constant: either

the flux or the current I_{sc} (Andrä and Nowak (2007)).

2.3.2 Magnetometer and Gradiometer

The most direct way of connecting the SQUID with the external world is to use a so called flux transformer (FT) consisting of a single coil system connected inductively to a SQUID sensor or combined in software or firmware. The simplest FT is the magnetometer that measures the projection of the MF B_z along the coil. In this case the pick-up coil should be designed so that the inductance $L_i = L$ (Figure 2.4).

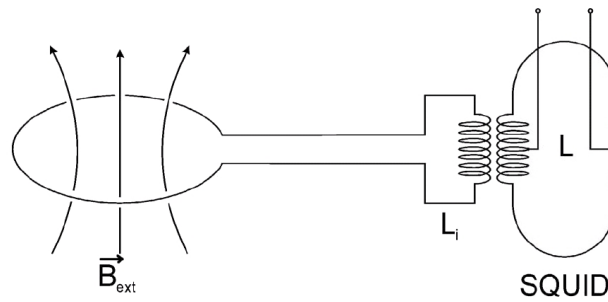


Figure 2.4: Schematic illustration of the coupling with a magnetometer, L_i inductance of the antenna and L inductance of the SQUID loop (Andrä and Nowak (2007))

The magnetometer configuration provides the best field sensitivity achievable when a FT is coupled to a SQUID. Nevertheless it can be used only inside an MSR. In case the examinations have to be carried out in an unshielded environment or in a moderate shielding the magnetometer is not appropriate. For this reason other FT configurations have been developed: At a distance of about 5-6 cm (SQUID baseline) from the pick-up coil another coil, defined reference coil, is added: This coil has the same area and the same number of turns as the pick-up coil, but it is wound in opposite sense. This configuration is insensitive to spatially uniform fields (the field is canceled out) and it is sensitive to any field having spatial gradient. A detection coil with these properties is called gradiometer (Figure 2.5). There are different types of gradiometers: They differentiate for order, symmetry, spacing among the turns etc (Figure 2.6).

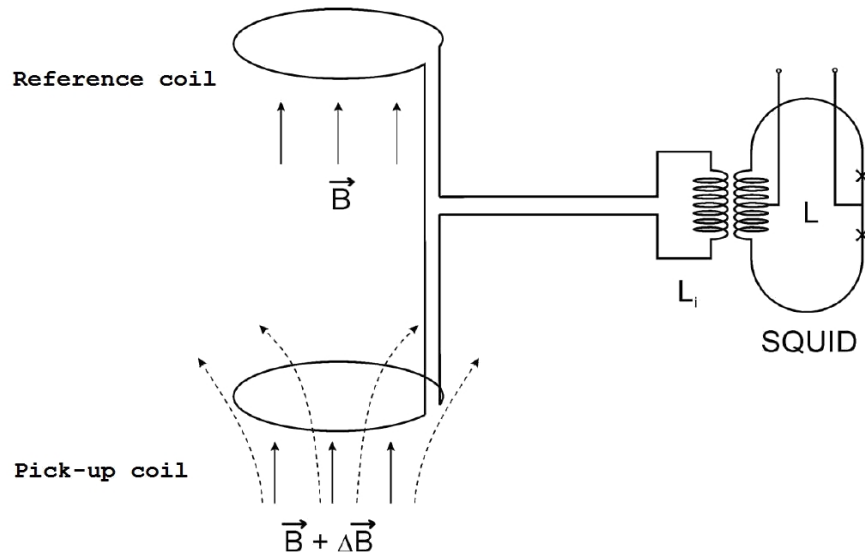


Figure 2.5: Schematic illustration of the coupling with a first order gradiometer, L_i inductance of the antenna and L inductance of the SQUID loop (Andrä and Nowak (2007))

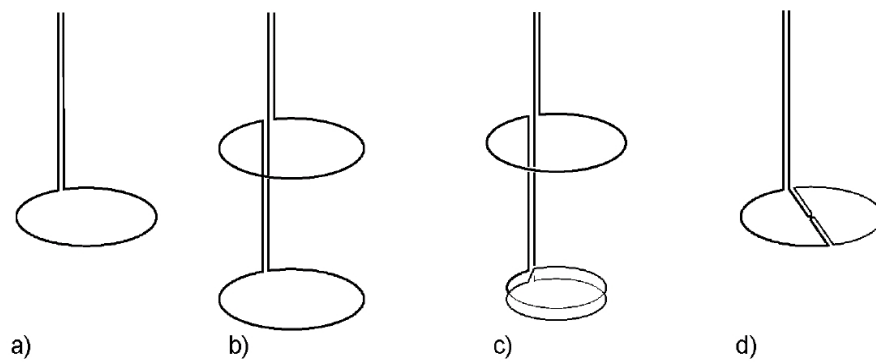


Figure 2.6: a) Magnetometer (detection of B_z) and different types of gradiometers: b) symmetric gradiometer of the first order (detection of $\Delta B_z / \Delta z$), c) asymmetric gradiometer of the first order (detection of $\Delta B_z / \Delta z$), and d) planar gradiometer of the first order (detection of $\Delta B_z / \Delta x$) (Andrä and Nowak (2007))

2.3.3 Cryostat-Dewars

In order to maintain the temperature below the critical temperature T_c , it is necessary to use a device that maintains a steady low-temperature environment and simultaneously fixes the positioning of the sensors. Dewars or cryostats are used. Criterion for a good cryostat is a proper isolation. Cryostats are almost entirely built of electrically non-conducting materials, such as glass and plastics, for three reasons:

- eliminating interference associated with radio frequency disturbances;
- reducing magnetic Nyquist noise associated with metallic enclosure;
- minimizing the helium evaporation rate.

Furthermore, the dewar is assembled so that the distance between the sensors (bottom of the dewar) and sources is as close as possible.

2.3.4 Magnetically Shielding Room

The amplitude of bio-magnetic signals is between femtotesla (fT) and picotesla (pT). Although SQUIDS sensors that are able to work in a not completely shielded environment exist, normally, in order to prevent external noise and artifacts, an MSR is used. There are different types of MSR, but generally the way how the MSR works can be summarized in active or passive shielding. In this work, MSRs with passive shielding are used. In order to shield the room against low frequency fields, layers of μ -metal, an alloy made of nickel and iron, are used. The μ -metal layers have such a high magnetic permeability that the MF lines prefer to flow through these metal layers instead of through the magnetically shielded room itself. The layer of aluminum is used to shield against the higher frequencies by means of eddy currents induced in the layer.

2.4 Equipment

2.4.1 MCG System

In the following paragraph the multichannel instrumentation is briefly described. The acquisitions are carried out in 4 different bio-magnetic systems (Table 2.1) ¹:

¹in the following list, the number of channels is related to the sensing sensors, the reference sensors are not counted

- 55-channel magnetometer system developed at the University of Ulm (Erne et al. (1998));
- 55-channel magnetometer system placed at the clinic of Hoyerswerda;
- 55-channel commercial gradiometer system developed by BMDsys GmbH and placed at the University of Jena (Figure 2.7);
- 168-channel vector-magnetometer system placed at the University of Jena and built by AtB (Pescara, Italy).

Since the above listed sensor systems have almost the same structure they will not be described singularly, but a general description will be done: What it is changing in the systems is the typology of sensing coils, their dimension and the number of channels.

A sensor system consists of a planar dewar, containing a complex structure with sensors distributed over two, three or more levels (a measurement level plus one, two or more reference levels). The first level, i.e., the primary measurement plane holds 55/168 SQUID sensors. The sensing elements are integrated magnetometers/gradiometers with a square shape of 12.7/15.5mm in diagonal. The sensors are uniformly distributed over the inner surface of the dewar, according to a hexagonal geometry, covering a circular surface of about 230/260mm in diameter. The measurement plane is 18mm from the outer dewar bottom. Additional SQUIDS are mounted on the second level and are used as reference channels. The second level (parallel to the first one) is circa 70/100mm far away from the measurement plane. On the third level there is a magnetometer or a set of magnetometers located 70mm from the reference plane to control the active shielding system. A fourth level can be also used (Table 2.2).

Table 2.1: Biomagnetic acquisition systems with name, location and number of channels

Name	Typology	Year	Channels	Sensors array	Location
ARGOS 55	M ¹	1998-2004	77	55	Ulm
ARGOS 55	M ¹	2005	77	55	Hoyerswerda
ARGOS 200	VM ²	from 2003	195	168	Jena
APOLLO CXS	G ³	from 2008	73	55	Jena

¹Magnetometer; ²Vector-Magnetometer; ³Gradiometer

All MCG systems operate in a shielded environment and according to the type of shielding there is a different shielding factor; the system shows different white noise levels on all channels. The on-line software-gradiometer set-up is performed by subtracting the background MF recorded by selected reference channels (on the second level and third level) from the signal of

Table 2.2: Biomagnetic system acquisitions: Dimensions

System Name	diameter- cm ¹	distance a-cm ²	distance b-cm	distance c-cm
ARGOS 50	23.0	7.0	14.0	n.a. ³
ARGOS 50	23.0	7.0	14.0	n.a.
ARGOS 200	23.0	9.8	19.6	25.4
APOLLO CXS	26.0	9.5	20.0	n.a.

¹with diameter is meant the circular planar surface of the sensor array

²with distance is meant the position of the first (a) second (b) and third (c) level of SQUID sensors in relation to the measurement plane

³ not available

each primary channel (in the first level). The patient handling set-up is made of non magnetic materials emulating the standard set-up for clinical cardiac electrophysiology.

The signal sensitivity is sufficient to allow the operator to have a first sight of the heart beats during the acquisition. The signals are then sampled at 8.2 kHz, digitally filtered and down sampled to a final sampling frequency of 1025 Hz and a bandwidth between DC and 250 Hz.

2.4.2 Ergometer

The exercise device is basically a supine bicycle ergometer (Figure 2.8), targeting compact size and limited weight for the purpose of quick installation on the measurement bed. The ergometer has been designed as a fully coaxial system, with a multiplying gearbox in order to achieve high inertia using a light flywheel. The transmission from pedals to flywheel consists of a two-stage planetary gearbox followed by a freewheeling joint to the flywheel. Each stage has a transfer ratio of 3, for a total multiplication ratio of 9. The flywheel has a perimetric cavity where a textile belt acts as brake. This belt is fixed at one end to the frame and is held at the other end, under tension, by a weight. In this way, it is possible to set the proper workload by adjusting the weight. By varying the weight, the operator can change the workload during the measurement, so that protocols with different load stages can be performed. The ergometer has been built making exclusive use of non-magnetic materials, the gears are out of nylon and their shafts are out of brass; frame, pedals, flywheel and mounting brackets are



Figure 2.7: Biomagnetic system at the University of Jena: View from the preparation room into the acquisition room with patient support and sensor system

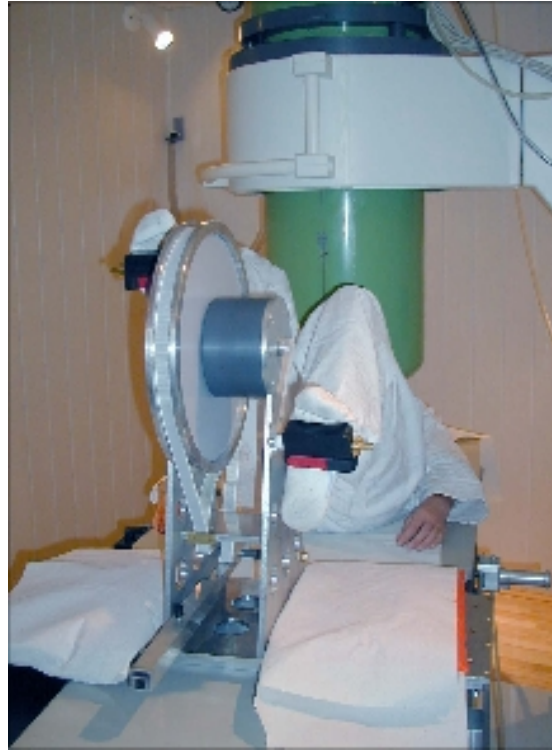


Figure 2.8: Ergometer used for stress acquisitions at the University of Ulm

made of aluminium, pedals' linings are made out of PVC, and the adjustable weight consists of a telescopic aluminium lever. Magnetic recordings performed with almost no load have shown no significant artifacts or noise introduced by the ergometer (Pasquarelli et al. (2002)).

A typical measurement protocol is described in section 2.6.1.

2.5 Patients

Seventy-three rest MCG examinations (65 healthy and 8 pathological) and 52 stress MCG (12 healthy ergometer SMCG and 40 pathological pharmacological SMCG) have been used. Eight patients out of 73 rest acquisitions are patients with an already implanted ICD. Twenty-five out of the remaining 65 acquisitions are used in the identification phase in order to find a unified threshold for the automatic selection of the heart related components (section 3.2.2) and the other 40 rest MCG together with the 12 ergometer SMCG are applied during validation.

For the pharmacological stress MCG (PSMCG), 15 patients were used as identification group and 25 in the validation phase.

All volunteers and patients have signed a written informed consent before undergoing MCG investigation, which has been approved by the Ethics Committee of the respective local hospital.

2.6 Acquisition Paradigma

2.6.1 Rest Data

The patient is led into the shielded room on a wheeled non-magnetic bed till his chest is positioned under the dewar bottom. At the beginning of the recording, the position of the patient in relation to the sensor array is calculated using a patient position unit (PPU), if any available. The data collection lasts between 3 and 5 minutes. The measurements are carried out mainly at the University of Ulm.

The MCG recordings for the eight ICD patients last 3 minutes and are carried out at the Biomagnetic Centre of the University of Jena under resting conditions using the 168 measuring channels vector-magnetometer (AtB, Pescara, Italy). The vertical component of the MF, calculated as vectorial sum of the three components, is considered: The final number of 56 channels is used in order to achieve comparability with the work of (Müller et al. (1999)). The ICD patients had all an idiosyncratic heart rhythm and those either with paced rhythm or atrial fibrillation are excluded. Two patients have been excluded from the data analysis, since the data recording failed: Due to interferences with ICD components, the biomagnetic signal once saturated whereas the second time the SNR was so small that was impossible to apply successfully the BSS methods.

2.6.2 Stress Magnetocardiographic Data

Ergometer stress testing

Twelve volunteers have undergone the examination protocol. The standard ergometer stress testing protocol starts with an up to 5 minutes lasting acquisition at rest. Then, the volunteer starts a warm-up stage of several minutes, which progressively reaches a steady exercise stage. According to the World Health Organization (WHO) scheme the initial workload is usually 50W and the increments are in steps of 25W every two minutes up to a final load of 125W to 150W depending on the degree of fitness. The heart activity gradually rises up to the target endpoint at 85% of age-predicted maximal heart beat rate, which is calculated by the formula:

$$f = 0.85 (200 - a) \text{ Beat/min} \quad (2.1)$$

where a is the life patient age in years.

At this point a second acquisition is performed while the exercise is still running with a duration of one to two minutes. The exercise is then discontinued and then a third recording at rest is started. Since abnormal heart wall motion normalizes rapidly after discontinuing the exercise, stress specific information must be acquired within the next one to two minutes.

The exercise is immediately stopped if any of the following conditions occurs:

- dyspnoea;
- angina;
- fatigue;
- SA-block or AV-block;
- ST-shift $< 0.2\text{mV}$;
- ventricular extra-systole;
- ventricular or supra-ventricular tachycardia.

Data are acquired over the entire heart relaxation time, for a total duration ranging between 2 and 5 minutes, according to the degree of fitness of the patient (Table 2.3).

Table 2.3: *Ergometer stress data acquisition: protocol*

Acquisition \ Phase	Phase			
	rest	warm-up	exercise	rest
Yes	x		x	x
No		x		

Pharmacological stress testing

PSMCG recordings (carried out in the hospital of Hoyerswerda) last either about 10 or 12 minutes using adenosine or dobutamine, respectively. During the stress test at least one experienced cardiologist continuously monitors the 12-lead ECG and has to decide about a premature termination of the stress-test according to the conditions mentioned above (section 2.6.2).

Pharmacological agents are used to intensify cardiac work or to cause coronary arterial vaso-dilatation in order to increase myocardial blood flow. Patients unable to undergo exercise testing for reasons such as de-conditioning, peripheral vascular disease, orthopedic disability, neurological disease, or concomitant illnesses can benefit from pharmacological stress testing.

Adrenergic agents such as dobutamine and adenosine are applied to challenge flow in stenosed vessels, and the functional consequences can be analyzed. The protocol recording for PSMCG

Table 2.4: Protocol of pharmacological stress data acquisition: In bold the acquisition intervals used in the data analysis

(a) Protocol for adenosine		
Time(s)	Phase	
<i>0-120</i>	Rest	
<i>120-540</i>	Adenosine Infusion	
	120-max	Rest
	max-520	Stress
<i>520-640</i>	Rest	
(b) Protocol for dobutamine		
Time(s)	Phase	
<i>0-120</i>	Rest	
<i>120</i>	First Dobutamine Infusion	
<i>240</i>	Second Dobutamine Infusion	
<i>360</i>	Third Dobutamine Infusion	
<i>480</i>	Fourth Dobutamine Infusion	
<i>480-720</i>	Rest	

varies according to the adrenergic agent. In case adenosine is used ($144 \mu\text{g}/\text{Kg}$ body weight), the drug is continually infused over 6-8 minutes (if the maximum rate in eq. 2.1 is not reached) or it is stopped if the maximum is reached (Table 2.4a). Dobutamine is infused intravenously over 2 minutes from $10 \text{ g}/\text{kg}/\text{min}$ to $40 \text{ g}/\text{kg}/\text{min}$. The infusion is stopped at any dose administered so far the 85% of the age-adjusted maximum heart rate is reached. The highest dose of dobutamine, however, is continued and supplemented with 0.5 mg of atropinsulfate, administered intravenously as a slow bolus, if less than 85% of the age-adjusted maximum heart rate is achieved (Table 2.4b).

Finally, the protocol is the following: rest MCG (around 2 minutes), MCG during pharmaco-

logical stress (injection of the adrenergic agents), second stage of rest (around 2 minutes). The nomenclature for the following paragraphs will be: rest acquisition (the first 2 minutes of the recording) and stress acquisition (second rest acquisition after infusion or part of the recording at maximum stress during the infusion if dobutamine or adenosine, are used, respectively).

2.7 Averaging procedure

2.7.1 Overview

Averaging of data (Rompelman and Ros (1986a,b); Jane et al. (1991); Craelius et al. (1986)) is one of the most used methods to determine the tendency of a data set and improve the SNR. In fact, it has been used for studying various kinds of biological signals, e.g., ECG, MCG, event-related potentials (ERP) and auditory brain stem responses (ABR).

In this section, a novel approach for averaging the data is presented. In the specific case the procedure is applied to the averaging of multichannel MCG recorded heart beats. Nevertheless, due to its intrinsic properties, this technique and all the consequences concerning SNR can be applied, with some suitable corrections, to any of the signals cited above. A broad variety of MCG analysis methods for the detection of the sundry heart beat properties and cardiovascular diseases requires a spatio-temporal averaging of cardiac signals. An important application is the detection of magnetic signals that are associated with ventricular arrhythmias in patients with ischemic heart disease or coronary heart disease (CHD). Such abnormalities, called late fields, appear in the MCG signal as low amplitude, high frequency deflections following the QRS (Erne et al. (1983); Stroink et al. (1989); Mäkijärvi et al. (1993); Achenbach et al. (1996); Montonen et al. (1995); Montonen (1995)). Signal averaging is further used in the MCG analysis of the intra-QRS fractionated activation, which indicates inhomogeneities of ventricular depolarization and therefore it is used as a tool for risk stratification (Endt et al. (1998); Oeff et al. (1995); Müller et al. (1999); Leder. et al. (2000)). Last, but not least, signal averaging is a prerequisite for all localization applications in biomagnetism, e.g. the localization of the accessory pathways (Uchikawa and Erne (1987)) in Wolf-Parkinson-White (WPW) syndrome patients (Fenici et al. (1989); Oeff et al. (1993); Weissmüller et al. (1992b)) and the localization of the origin of ventricular tachycardia (VT) from single ectopic beats of identical morphology (Weissmüller et al. (1992a); Moshage et al. (1995)). An overview of the different applications of the signal-averaged multichannel MCG is given in Stroink et al. (1998) (Stroink et al. (1998)).

Signal averaging is not trivial: In fact, the following requirements have to be fulfilled for temporal averaging to work effectively:

- The averaged data only represent the stationary part of the signal (in this case the heart beat), thus the signal of interest has to be repetitive and invariable;
- The signal of interest must be time-locked to a fiducial point (in general the R-peak, but in this work the Q-onset);
- The signal of interest and the noise must be independent and remain independent during the averaging (Cain et al. (1996)).

However, the problem is that signal averaging has to deal not only with the usual disturbances as white noise, non-white noise, and artifacts from the environment, but also with the biological variability of the signal in itself and with isolated signals, such as ectopic or premature beats in cardiology. Disturbances are also caused by respiration, digestion and small patient movements. These disturbances and artifacts cause a decrease of SNR during the averaging procedure and must be eliminated.

The first impression is that the optimal performances in averaging are obtained averaging *en bloc* the spatio-temporal data of the signal, but the experience shows that a disadvantage of this method is its low selectivity, i.e., QRS complexes of various amplitudes and shapes are averaged. Better results could be obtained by performing a *selected* averaging channel by channel using only the beats with better SNR. In fact, the noise sources could affect the sensors(, and a single channel as well) in different ways: Therefore an improvement of the SNR could occur by discharging, according to the estimated channel noise level, beats with the lowest SNR. This advantage compensates for the loss of strict coherence of the data. It is therefore appropriate to handle the averaging for each MCG channel separately.

2.7.2 Segmentation

Nomenclature

In averaging, the first preprocessing step is the choice of a trigger: In electroencephalography (EEG) and magnetoencephalography (MEG) this is realized by means of any trigger signal (e.g., auditory, visual, electromyographic) whereas in ECG and MCG by means of QRS detection.

In the remainder of the text, the following notation is used:

$S_i(t)$: measured output signal of i -th heart beat, containing noise components;

$A_i(t)$: heart beat signal;

$n(t)$: random noise from the environment, additive and uncorrelated with the heart beat;

$S(t)$: averaged heart beat signal.

Beat Detection from 3-Lead High Resolution (HRECG): Cardiac Beat Segmentation

The pre-detection and segmentation of the beats for the categorized clustering analysis (CCA) and averaging are based on either HRECG or on the magnetic signals with better SNR (in the following, this kind of signals will be called, in general, reference signals) ensuring, in this way, the detection of biological events (selection of activations eliminating disturbances and artifacts), that occur in all channels of the MCG simultaneously but with different intensity. During this phase, a rough estimation of suspected ventricular activations (not necessarily heart beats) is done: This means that all extrema higher than a determined threshold are detected. In order to avoid that the results are biased by a few big artifacts, the procedure described below is performed dividing the signal into time intervals, whose number depends on the recording time.

From the 3 reference channels ($i = 1, 2, 3$), all ventricular activations are detected using the second derivative of the signal amplitude $S_i(t)$ so to obtain a first guess of the beats number N_0 (eq. 2.2):

$$e(t) = \left(\sum_{i=1}^3 \frac{d^2 S_i(i)}{dt^2} \right)^2 \quad (2.2)$$

The quantity $e(t)$ is assumed to have its maxima during QRS. The N_0 local maxima are searched for values of $e(t_n) > 5e_{rms}$ where e_{rms} is the root mean square (RMS) value of $e(t)$. Hereby, N_0 ($0 < n \leq N_0$) defines the number of suspected ventricular activations (at this stage not necessarily heart beats). The average of the N_0 signals in a defined time range ($t_n \pm 150$) reveals the template $T_0(t)$ with a time duration of 300 ms (Figure 2.9).

Trigger Refinement

The definition of normal beats is implemented with 3 iterative trigger refinements. For each beat, a scanning range of $\pm 30ms$ is set and, subsequently, a deviation error $E(n)$ is calculated to get an optimum matching to the template beat $T_0(t)$. This provides a refurbished list of the beats activity positions. Then, a new improved beat template $T_1(t)$ is calculated, on the

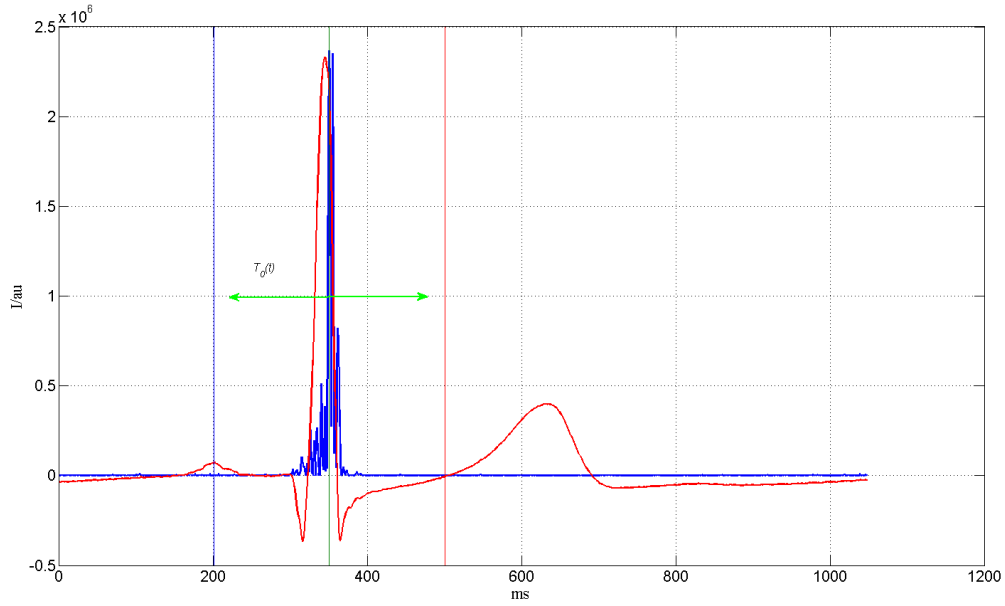


Figure 2.9: Graphical representation of the first steps of the beat detection procedure: In blue the quantity $e(t)$ is drawn, in red a cardiac heart beat $S(t)$ rescaled to $e(t)$. The two vertical lines represent the beginning and the end of the first template $T_0(t)$

basis not only of more precise fiducial points, but also of the noise level: In fact the segments where the optimum error exceeded the threshold (eq. 2.3) were eliminated:

$$E_{threshold} = \langle E(n) \rangle \pm 3E_{rms} \quad (2.3)$$

where E_{rms} is the standard deviation of $E(n)$ and $\langle E(n) \rangle$ its average. With this template, the procedure is repeated resulting in a third up-to-date template $T_2(t)$ for the final trigger refinement.

Rejection of Artifacts

First of all, three intuitive parameters are defined to determine which signal segments should be included in the cluster analysis. This procedure is executed to avoid performing the cluster analysis on those segments that are dominated by disturbances. In each epoch j and channel n these values are defined: the baseline drift d_n , the signal sweep a_n and the signal RMS r_n

(eq. 2.4).

$$\begin{aligned}
 r_n &= \sqrt{\frac{1}{t_{off} - t_{on}} \sum_{t=t_{on}}^{t_{off}} (S_{j,n}(t))^2} \\
 a_n &= \max(S_{j,n}(t)) - \min(S_{j,n}(t)) \\
 d_n &= |S_{on} - S_{off}|
 \end{aligned} \tag{2.4}$$

where S_{on} and S_{off} are the averaged amplitudes of the first and the last 60 ms of the current beat. Beats with these huge values can be eliminated *a priori*. The value of RMS is calculated three times in three different time intervals analyzing the phases in the heart beat where the SNR is quite low: t_{on} and t_{off} are the starting and the ending points in these three gaps. The used intervals are: the interval between T-end and P-onset, the interval between Q-onset and P-end, and finally the beginning of the ST segment.

Then, the average and the standard deviation over all beats are performed in order to get a threshold for each parameter (eq. 2.5):

$$\begin{aligned}
 r_{thr} &= \langle r_n \rangle + 3\sigma_r \\
 a_{thr} &= \langle a_n \rangle + 3\sigma_a \\
 d_{thr} &= \langle d_n \rangle + 3\sigma_d
 \end{aligned} \tag{2.5}$$

The beats with values above the thresholds are eliminated: A graphical view is shown in Figure 2.10 where the red vertical lines correspond to beats that are excluded and the green ones to those put in the average process.

The categorized cluster analysis is used to get a one-dimensional scale in analogy to the noise amplitude.

2.7.3 Cluster Analysis

Preliminary note

Many papers have been published to overcome the problem of non-stationary in biological signals and many efforts have been made to obtain an optimal averaging method to increase the SNR using only *selected* data segments (Hoke et al. (1984); Riedel et al. (1999); Mühler and von Specht (1999, 1996)). For data sets dominated by noise, an estimation of the noise amplitude is straightforward and can be used to improve the averaging process, as proposed by Mühler (Mühler and von Specht (1999, 1996)). The Mühler's case is, however, very singular: Generally

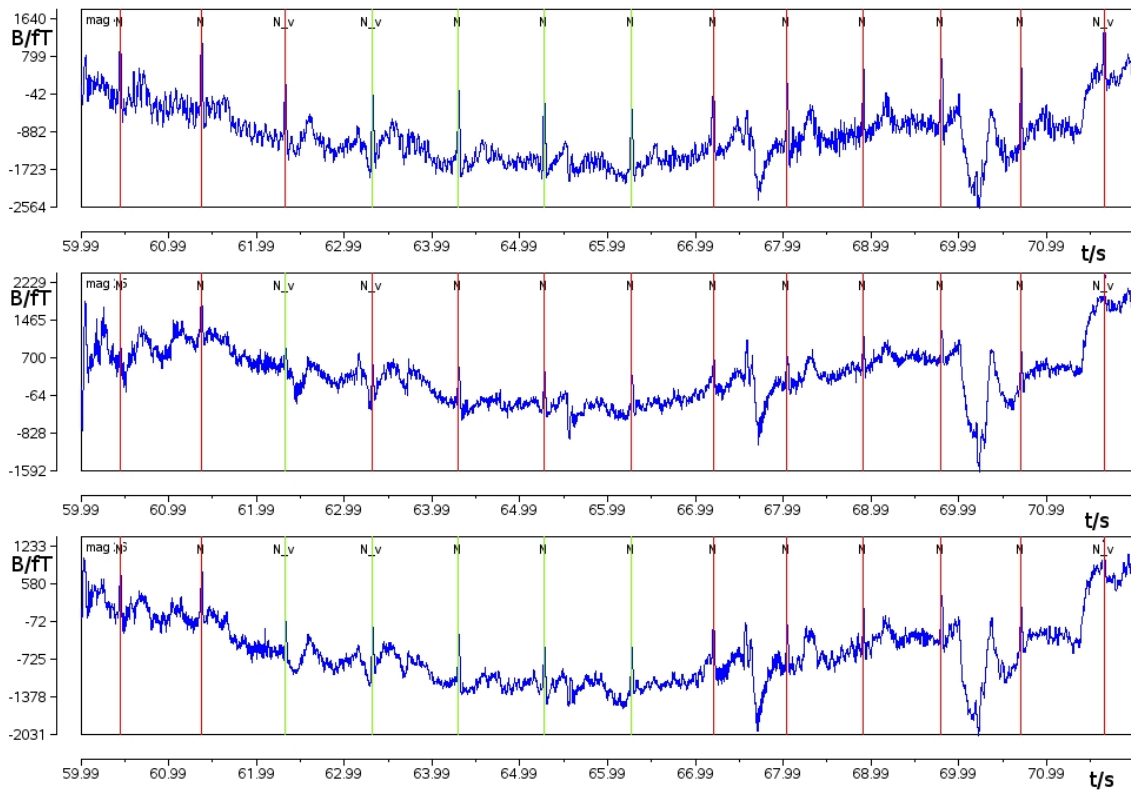


Figure 2.10: Time series of the heart beat signal in 3 out of the 55 channels: The markers in green correspond to the beat suitable for the average, the red ones to the beats that are not used since too noisy, or with a big drift

the recorded biological signals are perhaps of insufficient quality but surely not dominated by noise. In this case, especially in cardiology, an estimation of the amplitude of the noise is impracticable.

With cluster analysis, a workaround for this situation becomes feasible.

Categorized Cluster Analysis

Cluster analysis is a well-known procedure used in partitioning observations into subsets or "clusters", such that those within each cluster are more closely related to each other than those belonging to different clusters. Here, the clustering analysis is used in somewhat of an improper way and a hierarchical procedure is only applied to generate a dendrogram that assembles all elements in a single tree, associating to each element an increasing dissimilarity level (Erne et al. (1987)). In this way, starting from a distance (= dissimilarity) matrix a 1-dimensional dissimilarity scale is generated that can be used to govern the averaging process.

Hierarchical Cluster Analysis (HCA) produces a series of overlapping groups or clusters on different levels ranging from separate individual data segments (heart beats) to one single cluster. In order to obtain this unique tree the following steps are needed: As a prerequisite an upper-diagonal distance matrix D (defined 1 - correlation function between two beats) of size Z^2 (where Z is the total number of beats, each beat at the beginning is a one-element cluster) has to be built.

$$D = 1 - \frac{\sum_{t=1}^L S_{i,n}(t) S_{j,n}(t)}{\sum_{t=1}^L (S_{i,n}(t))^2 \sum_{t=1}^L (S_{j,n}(t))^2} \quad (2.6)$$

where n is the MCG channel under process, i and j two any beats and L the length of the segment of interest. The elements of the distance matrix D represent the dissimilarity of the

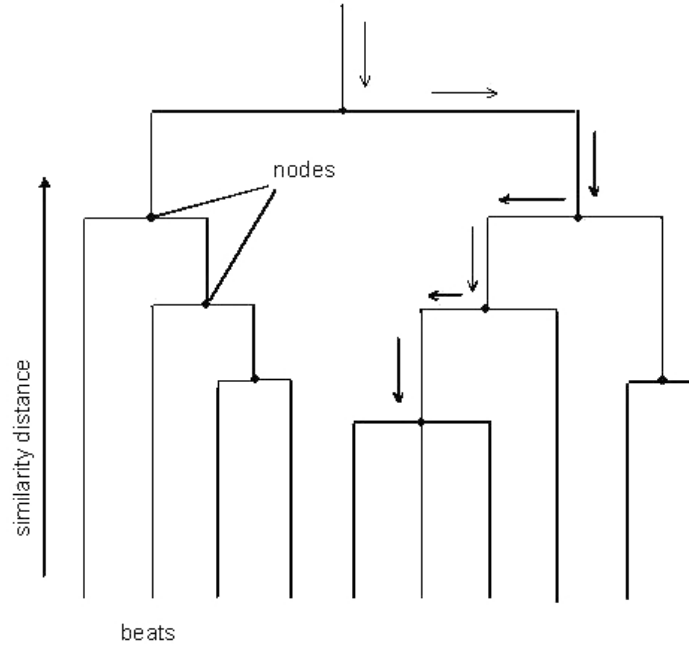


Figure 2.11: Schematic illustration of a dendrogram which is the graphical representation of the cluster analysis. Following the arrows at each node, the largest group of beats with the smallest similarity distance is found and thus the starting point for function SNR. The horizontal axis represents the observations (beats), the vertical axis gives the distance (or dissimilarity measure)

beats on the basis of the dissimilarity of the time courses of the beats. By means of the distance matrix D , the agglomerative clustering method produces a hierarchical tree starting with single beats, and then, at each of $Z - 1$ stages, merging two clusters to form a larger cluster, so as to have, in the end, a 1-dimensional description of the quality of the signal. This process is represented by a so-called dendrogram that shows at which distance the clusters merge (see

Figure 2.11).

Among the different methodologies used to determine at which level the clusters should merge, the Average Group Linkage Method (AGLM) is used for its computational efficiency as well as its robustness against the noisiness. Single linkage and complete linkage are relatively much more susceptible to noise as they only calculate a single distance (either minimum or maximum) when comparing clusters². At each stage the joined closest clusters form a new group and a new distance matrix D' is computed for the reduced number of clusters. The end of the clustering process is only reached when one single cluster is left. Following the path that sets the direction with more beats (follow the arrows in the dendrogram in Figure 2.11), a sequence of beats is defined with monotonically increasing "noise" (actually dissimilarity, but, as mentioned before, the "noise" is summarized to all biological variability, disturbances and noise).

Theoretical SNR improvement for white noise

Consider first the well-known case of coherent averaging. Hereby, no biological beat alteration and no biological noise are assumed, so that the noise has the following properties:

- Additive and uncorrelated with the signal;
- Stationary;
- Normally distributed with zero mean and variance σ^2 .

The signal $A_i(t)$ is assumed to have:

- Independent and identically distributed samples so that it is invariant with the time.

$$S_i(t) = A_i(t) + n_i(t) \quad (2.8)$$

Coherent averaging can be expressed by

$$S(t) = \frac{1}{N} \sum_{i=1}^N A_i(t) + \frac{1}{N} \sum_{i=1}^N n_i(t) = A(t) + \frac{1}{N} \sum_{i=1}^N n_i(t) \quad (2.9)$$

²The method of Average Group Linkage Method is based on the average distance among the objects. The linkage function specifying the distance between two any clusters is computed as the distance between the average values (the mean vectors or centroids) of the two clusters. Mathematically the linkage function - the distance between clusters X and Y - is described by the following expression:

$$L(X, Y) = \rho(\bar{x}\bar{y}) \quad (2.7)$$

where \bar{x} and \bar{y} are the mean vectors of the first and the second clusters, respectively and X and Y are two sets of objects (clusters).

In order to estimate the SNR, it is necessary to estimate the statistics of any sample and then of a sample average. In a sequence of N samples $S_i(t)$ the mean μ and the variance σ^2 of any of them are by definition:

$$\mu = E[S_i(t)] = A(t) \quad (2.10)$$

and

$$\sigma^2 = \text{Var}[S_i(t)] \quad (2.11)$$

Consider, now the statistics of the averaged signal $S(t)$.

Denote the mean of the average μ_{avg} and the standard deviation σ_{avg} . Since $A_i(t)$ and $n_i(t)$ are stationary, $\mu_{avg} = \mu$ and $\text{Var}[S(t)] = \sigma_{avg}^2 = \frac{\sigma^2}{N}$, $\sigma_{avg} = \frac{\sigma}{\sqrt{N}}$. Before the averaging procedure the variance was $\text{Var}[S_i(t)] = \text{Var}[n_i(t)]$, whereas after the averaging procedure the variance has been reduced of a factor N , and the amplitude of SNR improved of a factor of \sqrt{N} , as expected.

In section 3.1, a mathematical extension of Mühler's approach (Mühler and von Specht (1999, 1996)) that utilizes this sequence is described. The extension is necessary because in the original Mühler's work at any step only one segment is added to the average; on the contrary in this work the segment/segments to be added to the average is/are either a single segment (the cluster is constituted by one epoch) or a cluster of segments (more epochs form a cluster).

2.8 Blind Source Separation

2.8.1 Introduction

The term Blind Source Separation (BSS) refers to a wide class of problems in signal and image processing, where one needs to extract the underlying sources from a set of mixtures without knowing anything about the sources. This method is called blind, because little information is available, i.e., both the mixture and the sources are unknown.

In recent years, BSS techniques based on Independent Component Analysis (ICA) have been applied to several different fields and to biomedical applications. Independent Component Analysis is a particular branch of BSS that aims to separate a combined data set into independent components. In the following sections the terms BSS and ICA will be used without distinction, although the forementioned difference has to be addressed.

The independence assumption means that the joint *probability density function* (PDF) is

the product of all densities for all the sources.

$$P(S) = \prod (p_i) \quad (2.12)$$

where (p_i) is the PDF of the source i and $P(S)$ is the joint density function.

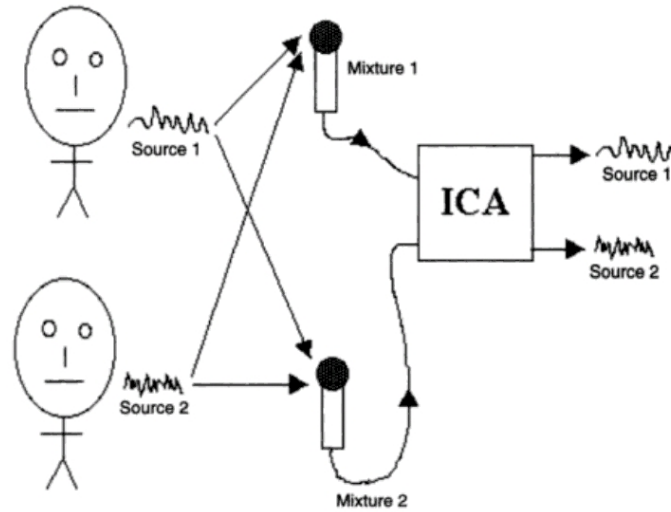


Figure 2.12: *Cocktail party example: Two persons are talking simultaneously in a room (like at a cocktail party), a third person is trying to follow one of the discussions. The human brain can handle this sort of auditory source separation problem, but it is a very tricky problem in digital signal processing. In case the number of microphones is equal or larger than the people speaking, ICA is able to extract the source signals from any set of two or more measured signal mixtures (Stone (2004))*

The most common example for illustrating ICA refers to the so-called cocktail party problem (Figure 2.12): Image a cocktail party where there are a number of people speaking in the same room. Assume further that there are several microphones in different positions, so that each records a combination of the speech signals with slightly different weights. In this situation a BSS is required, since the aim is the retrieval of the different sound sources from the recordings without any *a priori* information. ICA is the technique able to do it if there are at least as many microphones in the room as there are different simultaneous sound sources.

In this work BSS/ICA is applied to MCG data. The support that ICA can give to the clinical practice in this field is manifold: Fetal MCG (fMCG) extraction from maternal MCG, analysis of atrial fibrillation (AF), MCG denoising and removal of ICD artifacts.

In this chapter, a brief overview of BSS algorithms is presented addressing their differences. Although many algorithms are available, they can be grouped into four approaches (Figure 2.13):

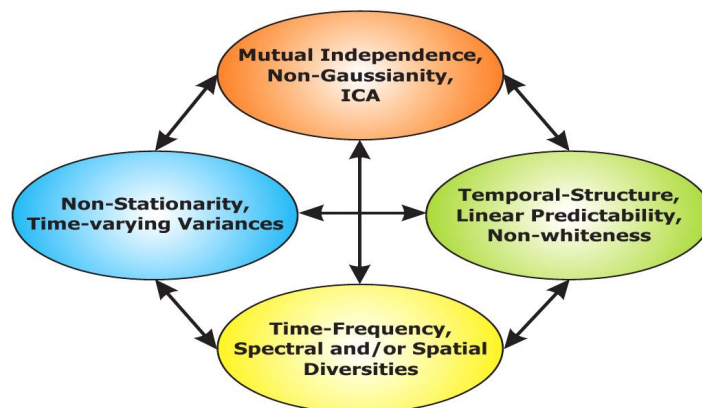


Figure 2.13: The four basic approaches of blind source separation; each approach exploits a particular property of the source: ICA (orange) exploits the independence among sources using the mutual independence; the methods based on the second order use the temporal structure of the data (green); in case the data are not stationary the time-varying variance is used if it does not change fast (blue); the fourth approach exploits the various diversities (yellow). The arrows indicate the possibility of combining or integrating the all above approaches in order to separate or extract sources with various statistical properties and to reduce the influence of noise and undesirable interferences (Cichocki and Amari (2002))

- The most important approach and also the most widely used is based on the principle of independence among the sources. In this case a cost function that estimates the independence or the non-Gaussianity of the data is minimized. When the sources are assumed to be independent the use of High Order Statistics (HOS) is fundamental for resolving the problem of BSS. Example of this approach is Fast Independent Component Analysis (fastICA).
- If the sources have a temporal structure, then each source has no vanishing temporal autocorrelation matrix, and less restrictive conditions than independence can be used: It is sufficient to estimate the Second Order Statistics (SOS) for finding the sources. Molgedey and Schulder (1994) and Ziehe et al. (2000) (Molgedey and Schulder (1994); Ziehe et al. (2000)) used for example, autocorrelation functions to separate temporal correlated signals (Second order blind identification-SOBI, TDSEP).
- A third possible criterion for performing ICA is to utilize the non-stationarity (NS) of the source signals and SOS. This is typically achieved by inspecting the variances of the sources (Matsuoka et al. (1995)). If they vary slowly, it is possible to separate sources with Gaussian marginals and equal autocorrelations, which is not possible with any other method: The NS information based methods allow the separation of colored Gaussian

sources with identical power spectra shape. However, they can not separate sources with identical non stationary property.

- The fourth approach exploits the various diversities (different characteristics) of signals; typically time, frequency, or more generally joint-space time frequency diversity. The signals can be separated easily if they do not overlap in either -time (TDMA), -frequency (FDMA) or time frequency domain. More sophisticated algorithms foresee a combination of two or more approaches.

An alternative way of dividing the different BSS methods is examining how the sources are found: whether evaluating directly the *data* or just using some *statistics* made on them. In the former, successive linear transformations are applied to the data until an independence criterion is maximized. In the latter, the information on the data is summarized into a smaller set of statistics (i.e., cumulant or auto correlation matrix): The mixture is searched using the information available on the matrices without analyzing the data themselves. It is possible to have algorithms combining the two approaches, as well.

In this thesis five out all the possible BBS methods are presented:

- fICA: Data based approach; it looks for sources as independent as possible maximizing some non-gaussian criterion;
- TDSEP: Statistics (temporal structure of the data) based approach;
- JADE: Statistics (cumulant matrices) based approach;
- Shifted Block Blind Separation (SHIBBS): Combination of statistics and data based approach;
- SVD: Statistics (covariance matrix) based approach.

For further information refer to (Cichocki and Amari (2002); Hyvärinen et al. (2001); Jolliffe (1986); Stone (2004)).

2.8.2 Singular Value Decomposition

Singular Value Decomposition is a technique used to solve sets of linear algebraic equations and has found application in many fields of biomedical engineering. Singular Value Decomposition/Principal Component Analysis (PCA) reduces the data dimension by finding a few orthogonal linear combinations of the original variables (with known characteristics) with the largest variance retaining as much information as possible from the original data. The observed data matrix (zero-mean) $X = [x_1, x_2, x_3 \dots x_m]$, x_i with $i = 0, i \leq n$, where n is the

time samples and m the number of sensors, can be written (eq. 2.13) as the product of an $n \times m$ column-orthogonal matrix D , an $m \times m$ diagonal matrix L with positive or zero elements (singular values), and the transpose of a $m \times m$ orthogonal matrix U (the Eigenvector matrix) (Deprettere (1988)).

$$X = DLU^T \quad (2.13)$$

The order of the eigenvalues is according to the variance of the signal, with the highest value in the upper left index of the L matrix. The signals associated to the high variance are deemed more important than those with low variance.

A procedure for calculating the SVD is to first calculate the Eigenvector matrix U^T and the Eigenvalues L by diagonalizing the covariance matrix $C_x = X^T X$. The easiest approach is to use the Eigenvalue Decomposition (EVD) since (eq. 2.14):

$$X^T X = UL^2U^T \quad (2.14)$$

where L^2 is the Eigenvalues matrix. D can then be calculated as (eq. 2.15):

$$D = XUL^{-1} \quad (2.15)$$

Since the eigenvalues are in descending order, the last components in the matrix D correspond to the signals that give negligible information and for this reason are rejected. In fact the signal information is mostly concentrated within a certain number of singular values with related singular vectors due to the strong inter beat correlation among MCG cycles when compared with the other sources. As first step of noise reduction the eigenvalues that exceed the below formula 2.16 are excluded.

$$\frac{\sum_{i=1}^{\lambda_{max}} \lambda_i}{\sum_{i=1}^N \lambda_i} > 0.95 \quad (2.16)$$

where λ_{max} is the last eigenvalue to be taken into account.

2.8.3 Independent Component Analysis

Overview

Independent Component Analysis (Comon (1994); Bell and Sejnowski (1995); Hyvärinen et al. (2001); Hyvärinen (1999)) is a technique for separating a combined data set into independent components. Generally the generative model can be written as eq. 2.17.

$$X = f\{S\} + N \quad (2.17)$$

where X is the observed zero-mean data, f a any unknown function applied to the sources S and N the additive noise that is corrupting the measurement X .

However, if ICA is applied to the MF produced by the heart, the foregoing model can be simplified; in fact in this case the observed data are those coming from the heart and the transmission through the mixing medium (lungs, fat, skin etc) can be assumed to be instantaneous and the observed signals (at the measurements points) are only considered a linear combination of (attenuated) sources. For this reason the eq. 2.17 can be replaced by:

$$X = AS + N \quad (2.18)$$

where A is the weights matrix.

Another assumption normally done in order to facilitate the problem solution computation is to define the model as noiseless (eq. 2.19); this precondition is actually less realistic than the first one, since it is assumed that there is no sensor noise. Anyway defining the noise as a source allows for a simplified ICA model and still gives good results.

Furthermore, the statistics of the mixing matrix A does not change with time, i.e., the assumption of stationarity of the mixing matrix: This means that the physics of the mixing of the sources as measured by the sensors is not changing during the recording. This assumption can be sometimes a little bit too restrictive, but in case of MCG measurements still applicable.

$$X = AS \quad (2.19)$$

In order to recover the sources, it is necessary that the number of sources is equal or smaller than the number of observations, although in the last years some algorithms for the under-determined case have been developed with the assumption that all sources have sparse distribution (De Lathauwer et al. (2003)). The number of sources is assumed to be equal to the number of observations, even though from a biomedical signal analysis perspective this is less likely. For this reason many researchers apply data-reduction techniques to the data (during the whitening process) prior to ICA although this may be ill advised in certain situations, where the SNR is very low.

The goal of ICA is to calculate the original sources S from the mixture (Figure 2.14): Thus, to find a de-mixing matrix $W \approx A^{-1}$ that gives eq. 2.20.

$$\hat{S} = WX \quad (2.20)$$

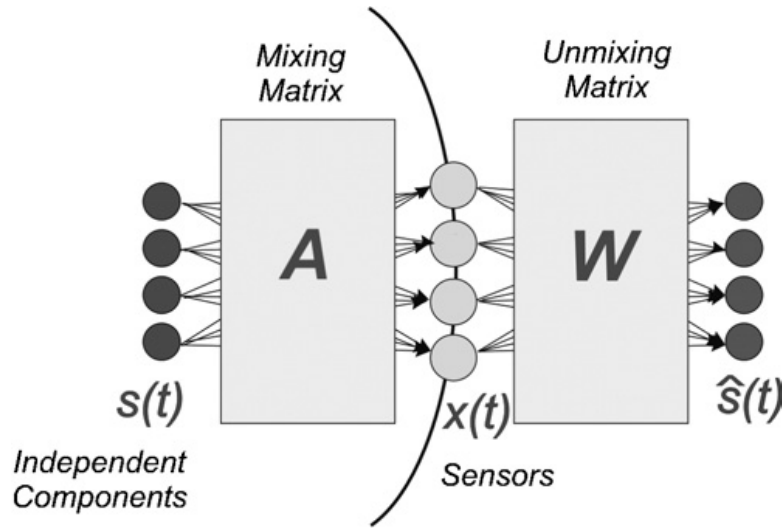


Figure 2.14: General ICA model: The matrix S represents m independent sources, the constant matrix $A [m \times m]$ the linear mixing of the sources, and $X [m \times n]$, with $m \leq n$ a linear mixture of the sources, i.e., the observations. ICA produces an unmixing matrix W , which unmixes the measurements in order to yield an estimation of the found components $\hat{s}(t)$ (James and Hesse (2005))

Both the unmixing matrix W and the estimated sources \hat{S} are found from the observations matrix X ; unfortunately without some *a priori* information it is not possible to estimate uniquely the original sources signals. However, it is possible estimate them up to certain indeterminacies:

- arbitrary scaling (eq. 2.21): Since the mixing matrix A and the source S are unknown it is always possible that a source has an amplitude α that can be canceled out from a scale factor of the matrix A (i is the number of sources).

$$X = \sum_i \left(\frac{1}{\alpha_i} \mathbf{a}_i \right) (s_i \alpha_i) \quad (2.21)$$

- order of the sources (eq. 2.22): It is not possible to determine the order of the ICA components (disadvantage respect to SVD) since a permutation matrix P and its inverse can always be added to the model so that the observations remain the same.

$$X = AP^{-1}PS \quad (2.22)$$

- delay of the estimated sources.

These indeterminacies preserve, anyway, the sources waveform and only influence their amplitude and order. In order to overcome these inconveniences in general the sources are assumed to be with zero-mean and one-variance so that the amplitude of the signal is irrelevant.

The order of the independent components still remains ambiguous; for this reason numerous efforts are made in order to automatically find the sources of interest discarding the other ones, as in this thesis. In case the sources have some *a priori* information and some specific statistical properties it is possible using an autoregressive model to extract the sources of interest: This field is called Blind Source Extraction (BSE).

In order to simplify the computation of W and to diminish the number of unknowns, a preprocessing is necessary: the whitening or sphering of the data. A variable is said to be *white* if its elements are uncorrelated and its variance is 1. Whitening can be seen as a process of decorrelation followed by a suitable scaling and the EVD can be used for achieving the result (eq. 2.23 and eq. 2.24):

$$C_y = E \{ Y Y^T \} = I \quad (2.23)$$

where E indicates the expectation, U the orthogonal matrix of Eigenvectors and L^2 the diagonal matrix of its Eigenvalues.

$$C_x = E \{ X X^T \} = U L^2 U^T \quad (2.24)$$

Whitening is then performed by eq. 2.25 or eq. 2.26:

$$Y = U L^{-1} U^T X = M X \quad (2.25)$$

or

$$Y = U L^{-1} U^T A S = \tilde{A} S \quad (2.26)$$

The purpose of whitening resides in the fact that the new mixing matrix \tilde{A} is orthogonal (unmixing matrix $F = \tilde{A}^T$): The number of parameters to be estimated is not m^2 anymore (see the dimension of the A matrix), but only $m(m-1)/2$ (Hyvärinen (2000)).

The procedure of whitening is the same for all the used BSS.

Fast Independent Component Analysis (FICA)

Hyvärinen has introduced a family of algorithms that are grouped under the name of *fixed-point algorithms*. Since the details of this algorithm are discussed in Hyvärinen et al. (2001) (Hyvärinen et al. (2001)), only a brief summary of this method is introduced here.

Let the differential entropy H of a random vector $\mathbf{y} = (y_1, y_2, y_3, \dots, y_n)$ with PDF $p(\cdot)$ be defined as

$$H(\mathbf{y}) = - \int d\mathbf{y} p(\mathbf{y}) \ln(\mathbf{y}) \quad (2.27)$$

The neg-entropy J can be interpreted as a measurement of non-gaussianity and can be defined as:

$$J(\mathbf{y}) = H(\mathbf{y}_g) - H(\mathbf{y}) \quad (2.28)$$

where \mathbf{y}_g is a gaussian random variable of the same covariance matrix as \mathbf{y} . Neg-entropy is always non-negative and it is zero if and only if \mathbf{y} has a gaussian distribution. Another approach for ICA estimation is inspired to the information theory by minimizing the mutual information. It can be proved that there is a strong relationship between mutual information and neg-entropy as shown in eq. 2.29. The mutual information I among the n scalar random variables y_i is a natural measure of the dependence among random variables that can be defined as

$$I(y_1, y_2, y_3, \dots, y_n) = \mathbf{J}(\mathbf{y}) - \sum_i \mathbf{J}(y_i) \quad (2.29)$$

where

$$J(y_i) = H(y_{ig}) - H(y_i) \quad (2.30)$$

since y_i is a *scalar* random variable.

The ICA of a random vector \mathbf{y} can now be defined as the invertible transformation $S = FY$ chosen in such a way that $I(s_1, s_2, s_3, \dots, s_n)$ is minimized. The new de-mixing matrix F is found by optimizing a cost function which decreases if the estimated sources become more independent. Since several different cost functions can be used for performing ICA (e.g. kurtosis, neg-entropy, etc), different methods to calculate F exist.

For finding the independent components different types of functions that approximate the neg-entropy can be used. The most general form of these approximations is any non linear function that does not grow so fast (i.e. the exponential, the hyperbolic tangent). In practice, however, there are criteria to be followed:

- the computational simplicity: The polynomial function is faster to compute than the hyperbolic tangent;
- the order in which the components are found (in case one by one estimation is used) depends on the type of function used: An ordinary method of optimization tends to first find maxima that have large basins of attraction.

The iterative solution for each vector subsequently is :

$$\vec{f}^+ = E \left\{ \vec{y} g \left(\vec{f}^T \vec{y} \right) \right\} - E \left\{ \vec{y} g' \left(\vec{f}^T \vec{y} \right) \right\} \vec{f} \quad (2.31)$$

where g is any suitable non-quadratic contrast function, with g' its derivative. The choice for the contrast function falls on the following contrast functions:

$$g_1(u) = \frac{1}{a_1} \log \cosh(a_1 u), \quad g'_1(u) = \tanh(a_1 u) \quad (2.32)$$

$$\begin{aligned} g_2(u) &= -\frac{1}{a_2} e^{-a_2 u^2/2}, & g'_2(u) &= u e^{-a_2 u^2/2} \\ g_3(u) &= -\frac{1}{4} u^4, & g'_3(u) &= u^3 \end{aligned} \quad (2.33)$$

where $1 \leq a \leq 2$.

The first function is a good general-purpose contrast function, whereas the second one has to be applied when the robustness and the distribution of the components are highly super-gaussian and the third one is generally used for estimating sub-gaussian components.

After every iteration step the new vector of the un-mixing matrix needs to be normalized and, for each vector (except the first), orthogonalized with respect to the previously calculated vectors (2.34 and 2.35).

$$\vec{f}_{p+1} = \vec{f}_{p+1} - \sum \vec{f}_{p+1}^T \vec{f}_j \vec{f}_j \quad (2.34)$$

$$\vec{f}_{p+1} \rightarrow \vec{f}_{p+1} / \sqrt{\vec{f}_{p+1}^T \vec{f}_{p+1}} \quad (2.35)$$

After calculating all the unmixed data, the task is to identify properly the components.

Ideally, all data available should be used, but this is often not a good idea because the computations may become too demanding. The averages can be estimated using a smaller sample, whose size may have a considerable effect on the accuracy of the final estimates.

TDSEP

The TDSEP (Ziehe et al. (2000)) algorithm only uses second order information in the form of time-delayed covariance matrices (see eq. 2.36). In this way, the unmixing matrix W and the independent components S result from the simultaneous diagonalization of these matrices taking care that they are positive definite (this is not always guaranteed for all time delays). The time lags $\tau_1 \dots \tau_{N_m}$ are chosen so that the selected time instants maximally carry different information. The optimal choice is to use time delays in a way that the signals have strong autocorrelations at the selected time-lags and small cross-correlation. For example, if a 10 Hz tone and a 20 Hz tone have to be separated, the time lags $\tau_1 = 1/f_1 = 0.1$ seconds and $\tau_2 = 1/f_2 = 0.05$ seconds (Gomez-Herrero and Huupponen (2004)) have to be chosen.

For those selected lags, the autocorrelations of the two source signals are maximal in absolute value and the cross correlations are minimal yielding two almost completely diagonal covariance matrices. However, the optimal choice for time delays is, in general, unknown. The performance of TDSEP can decrease drastically if the wrong time delays are chosen. For overcoming this problem many time delays are used that provide a good performance, but not optimal.

Two different sets ($N_m = 100$ for ICD patients and $N_m = 13$ for rest and stress acquisitions) of time-delayed correlation matrices are used that at most correspond to the properties of the signal (i.e., noise, disturbances and cardiac signal characteristics). The generalized cost function to be minimized is eq. 2.36.

$$T(K)_{ij} = \sum_{i \neq j} (y_i(t) y_j(t))^2 + \sum_{k=0}^N \sum_{i \neq j} (y_i(t) y_j(t + \tau_k))^2 \quad (2.36)$$

The matrices for ICD patients have the following time delays:

$$\tau_0 = 1, \quad \tau_{N_m-1} = 5600, \quad \tau_{N_m-2} = 4500, \quad \tau_{N_m-3} = 3000, \quad \tau_{N_m-4} = 2000, \quad \tau_{N_m-5} = 1200,$$

and the remaining ones are calculated as:

$$\tau_i = \tau_{i-1} + 3, \quad \forall i = 0, \quad i < N_m - 5$$

For stress and rest measurements the time-delayed covariance matrices are set up with 13 different values: following 1, 5, 10, 50, 100, 150, 200, 300, 500, 700, 900, 1.200, 1.500. These values are chosen because they are the time-delays that at most correspond to the signal auto terms.

This method is more stable than using a unique delay because in that case the delay parameter τ should be chosen carefully in order to have two matrices that maximally carry different information. After the pre-whitening step, any time delayed correlation matrix of the transformed signal should be approximately a diagonal matrix up to a transformation matrix Q . The rotation matrix Q is computed either by means of a simultaneous Jacobi diagonalization (Cardoso and Souloumiac (1996)) of these matrices (see eq. 2.37) where $T_k(\phi_k)$ represents an elementary rotation or by taking a linear combination (for example the average) of these covariance matrices (see eq. 2.38) and after applying standard EVD (eq. 2.14).

$$Q = \prod_k T_k(\phi_k) \quad (2.37)$$

$$\bar{T} = \frac{1}{N} \sum_{k=1}^N T_i \quad (2.38)$$

The concatenation of the whitening matrix M and the rotation matrix Q yields an estimation of the mixing matrix: $A = M^{-1}Q$ or of the un-mixing matrix $W = Q^T M$.

JADE

The JADE algorithm, developed by Cardoso (1999), presents a substantial difference in comparison with the fICA algorithm. In this method the unmixed data are not found considering the whole data set (whitened data) Y but some statistics calculated on them. In this case statistics is given by the cumulant matrices: All information contained in the measure can be calculated by operations on cumulants, i.e. variance and kurtosis are the second and fourth cumulants. A side effect of this algorithm is in the estimation of the whole set of fourth-order cross-cumulants that requires the storage of n^4 cumulants matrices (the number of fourth-order cumulants grows as $O(n^4)$) and this can be computationally prohibitive in case the number of observations is high.

The JADE contrast function is the sum of squared fourth order cross cumulants defined as:

$$\phi^{JADE}(Y)^{def} = \sum_{ijkl \neq iikl} \left(\hat{C}_{ijkl}^Y \right)^2 \quad (2.39)$$

where the notation indicates a sum over all the quadruples $(ijkl)$ of indexes with $i \neq j$. Then a joint diagonalization using the Jacobi technique is performed so that a matrix rotation Q that makes the cumulants as diagonal as possible (the sum of the elements *Off* diagonal has to be minimized) is found

$$Q = \arg \min \sum_i \text{Off}(Q^T \hat{C}_i^Y Q) \quad (2.40)$$

and hereby the mixing matrix

$$A = QM^{-1} \quad (2.41)$$

In calculating the joint diagonalization (Cardoso and Souloumiac (1996)), the givens angles at each step can be computed in closed form even in case of possibly complex matrices.

SHIBBS

The SHIBBS algorithm has an intermediate character between the all data based algorithms, as fICA, and the all statistics based algorithm, as JADE. The set of cumulant matrices to

be estimated is not anymore the maximal set which contains $O(n^2)$ matrices, but only n : iteratively SHIBBS recomputes a number of $O(n^3)$ matrices. The SHIBBS criterion is defined as:

$$\phi^{SH}(Y)^{def} = \sum_{ijkl \neq iikk} \left(\hat{C}_{ijkl}^Y \right)^2 \quad (2.42)$$

A set of m cumulants matrix $\left\{ \hat{C}^Y(M_m) | 1 \leq p \leq m \right\}$ is estimated and a joint diagonalizer Q of it (eq. 2.40) is calculated. If $Q \approx I$ the algorithm stops and the mixing matrix is (eq. 2.41), otherwise, the whitened data Y are rotated using the rotation matrix $Q : Y = Q^T Y$ and a new set of cumulant matrices C using the new transformed data set with the respective joint diagonalizer Q calculated.

2.8.4 Overfitting: Bumps and spikes

One problem with ICA that has recently been addressed is over-learning or over-fitting that can occur in the ICA algorithms, especially when the independent sources underlie temporal dependencies (Hyvärinen et al. (1999)). Over-learning can lead to spikes or bumps in the computed sources, which have no significance to the data being examined and may be defined artifacts. Over-learning in ICA algorithms is caused by either the insufficient number of samples if compared to the observations or to the considerable amount of noise present. There are two methods for solving this problem, one is to apply a reduction of the observation points (applying before the PCA, for example), the other one is to increase the sample size: A rule of the thumb is having a sample size at least the same size as the unmixing matrix.

2.8.5 Singular Value Decomposition vs Independent Component Analysis

The main difference between SVD and ICA is that the former method finds source signals that are gaussian and uncorrelated whereas the latter is able to retrieve signals that are non-gaussian and independent. For a better understanding please refer to Figure 2.15: Here a geometrical interpretation of the difference between uncorrelatedness (SVD) and independence (ICA) is shown. In case two signals are gaussian it is enough to make them uncorrelated, since in case of gaussian signals uncorrelatedness is equal to independence.

Two random zero-mean variables x and b are said to be *uncorrelated* if they satisfy the following relation:

$$C_{xb} = E\{xb\} = E\{x\}\{b\} = 0 \quad (2.43)$$

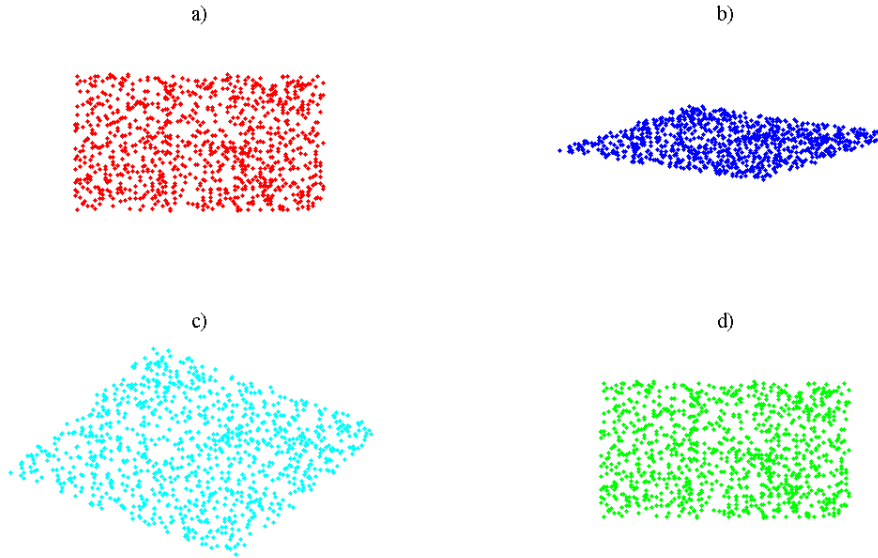


Figure 2.15: Geometrical interpretation of the difference between ICA and SVD: a) Original random sources, b) sources after a linear mixture, c) after the process of uncorrelatness, d) sources after application of ICA

where $E\{x\}$ and $E\{b\}$ are the expected values of the variable x and b , respectively and C_{xb} their cross-correlation. On the contrary two random zero-mean variables x and b are said to be *independent* if they satisfy the following relation:

$$E\{x^p b^q\} = E\{x^p\} E\{b^q\} = 0 \quad (2.44)$$

where p and q are two any natural numbers. Note that in case $p = q = 1$ this formula is equal to eq. 2.43.

Summarizing, the uncorrelatedness is a special case of independence where the relation between the expectations is linear. Thus, ICA is more restrictive since the sources have to be independent, not only orthogonal.

2.8.6 Finding the cardiac signals

Overview

The order of the unmixed data/sources can not be determined *a priori*. Therefore, a visual inspection of the source matrix S , for the identification of the noise related and cardiac related components, is necessary. However, this kind of procedure is not desirable in the clinical use,

where a user-independent tool is needed. Here, different methods for automatically detecting the components representing artifacts and disturbances from those containing heart information are described. These methods are:

- A statistical method with *no a priori* knowledge: kurtosis. In this way the unmixed data with no deterministic contribution are detected;
- A statistical method with *a priori* knowledge: correlation and reference channels. Using this method based on the *a priori* knowledge on the properties of the signal the unmixed data related to the components are detected;
- The power-spectra. In this way the *a priori* known spectral contribution of the noise is examined.

Kurtosis

The kurtosis is the fourth order cumulant. For a zero-mean signal s , the kurtosis is defined as:

$$Kurt(s) = E(s^4) - 3[E(s^2)]^2 \quad (2.45)$$

The gaussian noise/continuous noise has a value close to zero, whereas the time series with spikes have a value of kurtosis different from 0³.

The main reason for choosing kurtosis is its simplicity. In fact, computationally, kurtosis can be estimated by using the fourth moment of the sample data. However, it also has some drawbacks. The main problem is the sensitivity to outliers or abrupt changes: Its value can strongly depend on only a few observations in the distribution tails, which may be erroneous or irrelevant observations. This means that unmixed data with abrupt changes and artifacts cannot be differentiated in MCG measurements by using this method. In section 3.2.2 the use of an histogram will be introduced as a workaround and a threshold to be used in the validation phase will be provided.

Correlation

The identification of heart related components among the remaining unmixed data has been performed by taking advantage of the reference data (HRECG or MCG) and the derived trigger

³Distributions with zero excess kurtosis are called mesokurtic, with positive excess kurtosis leptokurtic and with negative excess kurtosis platykurtic

points list. Three different correlation methods have been compared in order to find the most suitable for our problem.

The sources/unmixed data have been found using the TDSEP algorithm followed by joint diagonalization. In general the number of unmixed data related to the cardiac activity is circa 7.

1. The cross-correlation of the averaged odd and even beats in each unmixed data has been calculated (CM1). First of all, the mean signals $\bar{S}_{even}(t)$ and $\bar{S}_{odd}(t)$ of the $N/2$ even and $N/2$ odd beats respectively (according to the trigger points list) have been computed:

$$\bar{S}_{even}(t) = \frac{2}{N} \sum_{i=0}^N S_{2i}(t), t_1 < t < t_2 \quad (2.46)$$

and

$$\bar{S}_{odd}(t) = \frac{2}{N} \sum_{i=0}^N S_{2i+1}(t), t_1 < t < t_2 \quad (2.47)$$

Then the cross-correlation c between them is calculated by:

$$c = \frac{\sum_{t=t_1}^{t_2} \bar{S}_{even}(t) \bar{S}_{odd}(t)}{\sqrt{\sum_{t=t_1}^{t_2} \bar{S}_{even}^2(t)} \sqrt{\sum_{t=t_1}^{t_2} \bar{S}_{odd}^2(t)}} \quad (2.48)$$

2. The template $\bar{S}(t)$ (eq. 2.49), built for each channel averaging all the time instants in correspondence of the QRS complexes, has been scanned in correspondence of each beat yielding the following value of the correlation \bar{c} (CM2):

$$\bar{S}(t) = \frac{1}{N} \sum_{i=0}^N S_i(t), t_1 < t < t_2 \quad (2.49)$$

$$\bar{c} = \frac{1}{N} \sum_{i=0}^N \frac{\sum_{t=t_1}^{t_2} \bar{S}(t) S_i(t)}{\sqrt{\sum_{t=t_1}^{t_2} \bar{S}^2(t)} \sqrt{\sum_{t=t_1}^{t_2} S_i^2(t)}} \quad (2.50)$$

3. The cross correlation of odd and even beats in each unmixed data is evaluated in order to reckon the value of correlation for that channel (eq. 2.51) (CM3):

$$\bar{c} = \frac{1}{N} \sum_{i=0}^N \frac{\sum_{t=t_1}^{t_2} S_{2i}(t) S_{2i+1}(t)}{\sqrt{\sum_{t=t_1}^{t_2} S_{2i}^2(t)} \sqrt{\sum_{t=t_1}^{t_2} S_{2i+1}^2(t)}} \quad (2.51)$$

The chosen range in all cases has been 180 ms (in correspondence of the QRS complex), i.e., t_1 is 60 ms before and t_2 is 120 ms after the R-peak.

In section 3.2.2 the three methods will be compared and the most suitable one will be used for providing a threshold to be applied in the validation phase.

FFT

In the last step, the remaining components have been FFT transformed and those with a maximum power spectrum P_{max} between 49 and 51 Hz are filtered to eliminate the residual power line interference (Figure 2.16). The procedure is as follow: The power spectrum, calcu-

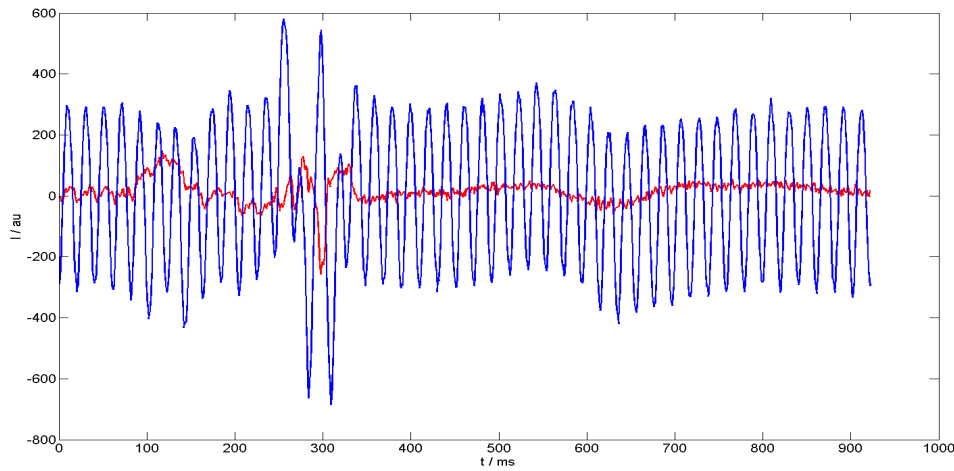


Figure 2.16: Averaged unmixed data before (in blue) and after the application of the 50 Hz filter (red)

lated into the interval of interest (49-51 Hz) P_{pl} , has been compared to the total one P_t . In case the ratio $\frac{P_{pl}}{P_t}$ is bigger than a determined value (set to 0.06), that component is defined to be a good pretended for the net filtering.

Furthermore, in SMCG, in addition to the noise, unexpected disturbances and artifacts related to the movements of the patient occur: These movements are connected not only to the ergometer vibrations, but to patient muscular movements as well. For this reason, an alternative way for eliminating these disturbances is the use of FFT: The components with a maximum in the power spectrum between 8 and 10 Hz (Figure 2.17), related to the high frequency ergometer disturbances, are eliminated (Müller et al. (2006)). The power spectrum is recalculated after the PL-filtering and the value stored at each frequency. In case the maximum value, calculated as in eq. 2.52 is in the range of 8-10 Hz, that component is rejected.

$$P_{max} = \max Pow_k, Pow_k = \sqrt{A_k^2 + B_k^2} \quad (2.52)$$

where A_k and B_k are the coefficients of the FFT.

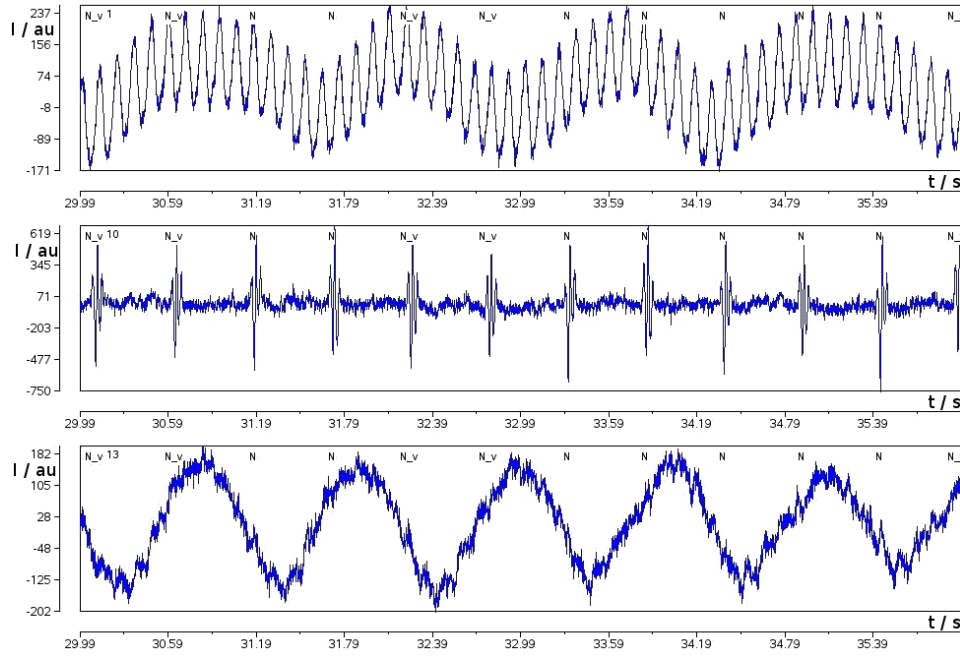


Figure 2.17: Three unmixed data/sources with different values of frequency: The first picture represents the ergometer noise with a frequency peak of 8.5Hz modulated with a lower frequency signal, the second one corresponding to the QRS complex circa 35 Hz and the last one circa 1Hz. The labels N and N_v correspond to the QRS activity

2.8.7 Reconstruction

Using the rules in section 3.2.2, the rows of the matrix S_* related to noises and disturbances were set to 0 and a cleaned signal X_R reconstructed.

$$X_R = WS_* = W \begin{pmatrix} s_{1,1} & s_{1,2} & \dots & s_{1,n} \\ 0 & 0 & \dots & 0 \\ s_{3,1} & s_{3,2} & \dots & s_{3,n} \\ 0 & 0 & \dots & 0 \\ \vdots & \vdots & \vdots & \vdots \\ s_{m,1} & s_{m,2} & \dots & s_{m,n} \end{pmatrix} \quad (2.53)$$

2.8.8 ICs validations

The manual classification of all extracted components is performed by an expert investigator for each dataset and for each sensor configuration; two signal categories (cardiac activity and noise) are used, and the number N_{man} of components belonging to each category is calculated.

Then, the automatic procedure is used, and the number N_{aut} of components classified for each signal category is obtained; the number N_{corr} of components that are correctly identified is evaluated comparing N_{aut} with N_{man} . For each signal category, two numerical indexes are used to quantify the performance of the automatic method with respect to the investigator categorization: A first index is the percentage of found sources (FS), which represents the number of components that are correctly classified (true positive) ⁴ -TP- that is defined as

$$FS = 100 \left[\frac{N_{corr}}{N_{man}} \right] \quad (2.54)$$

A second index based on the percentage of incorrectly classified sources (ICS), which corresponds to false positives ⁵ (FP) is given by

$$ICS = 100 \left[\frac{N_{aut} - N_{corr}}{N_{aut}} \right] \quad (2.55)$$

The third value to be estimated is the number of heart related components that are identify as noise related: False Negative (FN).

Using these three values, the sensitivity and the specificity of the methods can be calculated.

The sensitivity is the fraction (in %) of the true matches that actually are corrected predicted as matches by the pattern. If the pattern is too stringent (to avoid noise and disturbances), then too few of the true matches will be identified by it.

The specificity is the fraction of the sequences predicted as matches that really are true matches. If the pattern is too inclusive (to catch as many as possible), then much noise will also be falsely identified by it.

The specificity is computed as $TP / (TP + FP)$ where TP is true positive and FP is false positive. The sensitivity is computed as $TP / (TP + FN)$ where TP is true positive and FN is false negative ⁶. These two values are the most widely used statistics used to describe a diagnostic test.

⁴components that are correctly classified in the automatic recognition

⁵components that are identified heart related but they are not

⁶in the medical context (diagnosis), specificity is defined differently = $TN / (FP + TN)$

Chapter 3

Results

3.1 SNR improvement in averaged data using categorized data analysis

3.1.1 Theoretical explanation

The clustering procedure is performed for each MCG-channel separately since the noise influences the cardiac signal differently according to the sensor position. Thus, for each channel, the maximum SNR improvement is reached. Of course, the number of averaged beats differs from channel to channel and depends on the local noise level.

Since the raw cardiac signal recorded by MCG is of poor quality, but it is generally not ruled by noise, an evaluation of the noise is impossible; for this reason the SNR estimation and its improvement is precluded (section 2.7.3). The theoretical proof to obtain the optimum SNR is given in the next section (eq. 3.13).

The standard SNR improvement (section 2.7.3) is not valid in reality since the noise is often non-stationary (Willemsen et al. (1999)). In fact, it cannot be assumed for a typical MCG recording that all biological heart signals are identical and that the noise is normally distributed for each heart beat with the same variance: during the acquisition the subject can move, a door can be closed, a train can go by, causing non-stationarity. In this case, the signal model for coherent averaging is:

$$S_i(t) = A_i(t) + \sigma_i n_i(t) \quad (3.1)$$

where $A_i(t)$ is the signal of interest, which is assumed to have an invariant morphology and to be uncorrelated with $n_i(t)$; σ_i is the noise level in the i_{th} interval (single-event related data or

block of similar data: clusters), generally with $\sigma_i \neq \sigma_j, \forall i, j$, and $n_i(t)$ that can be assumed to have zero mean and unity variance, without losing generality. It is also assumed that in each interval (cluster or cluster constituted by a single element) the noise level is stationary and independent from another cluster. Due to biological alterations of the heart beat, artifacts and biological noise (respiration, digestion, little movements etc.), the optimum SNR is reached by averaging only certain heart beats (Figure 3.1). The optimum choice of heart beats has to be found by selection processes that optimize the SNR. The selection process is done in this case

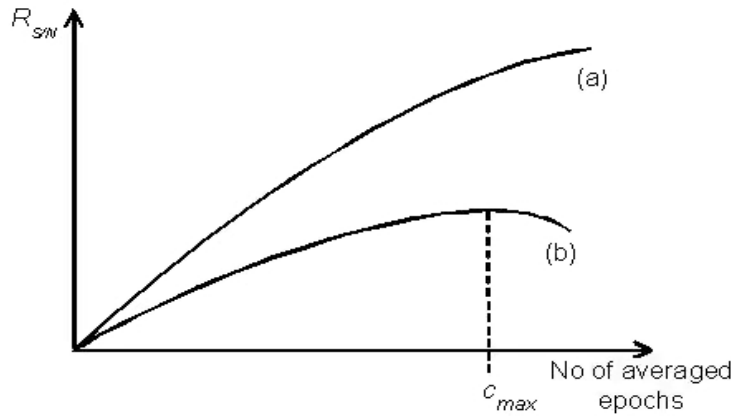


Figure 3.1: Schematic illustration of the SNR function $R(S/N)$. The values in the ordinate represent the ratio (R) between the signal (S) and the noise (N) according to the number of epochs: (a) the function $R(S/N)$ grows with the square root of the epochs/clusters, reaching its maximum at the extreme case of all clusters used (single-element cluster). This happens in case identical signals and stationary, normally distributed noise are used; (b) For non stationary noise, the function $R(S/N)$ can have its maximum either at the maximum number of epochs (single-element cluster)(a) or at c_{max} : number of epochs/clusters, the maximum SNR is achieved

by means of the CCA: The data segments to be averaged are ordered according to their noise level: $\sigma_i < \sigma_j \forall i, j$. Thus, the optimum SNR is now reached by:

- sorting the time segments according to the noise level;
- finding the criterion according to groups of time segments have to be averaged to reach the optimum SNR.

Consider the statistics of the averaged signal: The improvement is seen in the decreasing of

the variance when comparing a single event with an averaged one over N events.

$$S(t) = \frac{1}{N} \sum_{i=1}^N A_i(t) + \frac{1}{N} \sum_{i=1}^N \sigma_i n_i(t) = A(t) + \frac{1}{N} \sum_{i=1}^N \sigma_i n_i(t) \quad (3.2)$$

where S is the observed signal, N the total number of samples, A the signal of interest, σ the noise level in the $i - th$ interval.

Since $A(t)$ is deterministic, all variance is assumed to be contained in the noise.

$$Var[S_i(t)] = \sigma_{avg}^2 = E \left[\left(\frac{1}{N} \sum_{i=1}^N \sigma_i n_i(t) \right)^2 \right] = \quad (3.3)$$

$$E \left[\left(\frac{1}{N} \sum_{i=1}^N \sigma_i n_i(t) \right) \left(\frac{1}{N} \sum_{j=1}^N \sigma_j n_j(t) \right) \right] = E \left[\left(\frac{1}{N^2} \sum_{i=1}^N \sum_{j=1}^N \sigma_i n_i(t) \sigma_j n_j(t) \right) \right]$$

Since N is a constant:

$$\frac{1}{N^2} \sum_{i=1}^N \sum_{j=1}^N E[\sigma_i n_i(t) \sigma_j n_j(t)] = \frac{1}{N^2} \sum_{i=1}^N E[\sigma_i^2 n_i(t)^2] + \frac{1}{N^2} \sum_{i=1}^N \sum_{i \neq j}^N E[\sigma_i n_i(t) \sigma_j n_j(t)]$$

As the variance is assumed to be piecewise constant over time:

$$\frac{1}{N^2} \sum_{i=1}^N \sigma_i^2 E[n_i(t)^2] + \frac{1}{N^2} \sum_{i=1}^N \sum_{i \neq j}^N \sigma_i \sigma_j E[n_i(t) n_j(t)] = \quad (3.4)$$

The variance of the noise is in σ , so it is possible to write:

$$\frac{1}{N^2} \sum_{i=1}^N \sigma_i^2 E[n_i(t)^2] = \frac{1}{N^2} \sum_{i=1}^N \sigma_i^2 \quad (3.5)$$

Now from the hypothesis $\sigma_i < \sigma_j \forall i, j$, exists a point x such that, adding a further block of data-segments, the SNR does not improve anymore, but becomes worse: i.e, the variance till the block $x + 1$ is higher than the variance till block x .

$$\frac{\sum_{i=0}^{x+1} \sigma_i^2}{(x+1)^2} > \frac{\sum_{i=0}^x \sigma_i^2}{x^2} \quad (3.6)$$

The left part of the inequality 3.6 can be divided into two parts: The former is the variance till the block x and the latter is the variance at the block $x + 1$

$$\frac{\sum_{i=0}^x \sigma_i^2 + \sigma_{x+1}^2}{(x^2 + 2x + 1)} > \frac{\sum_{i=0}^x \sigma_i^2}{x^2} \quad (3.7)$$

Developing the expression:

$$x^2 \sum_{i=0}^x \sigma_i^2 + x^2 \sigma_{x+1}^2 > x^2 \sum_{i=0}^x \sigma_i^2 + 2x \sum_{i=0}^x \sigma_i^2 + \sum_{i=0}^x \sigma_i^2 \quad (3.8)$$

$$x^2 \sigma_{x+1}^2 > 2x \sum_{i=0}^x \sigma_i^2 + \sum_{i=0}^x \sigma_i^2 \quad (3.9)$$

$$\sigma_{x+1}^2 > \frac{2x+1}{x^2} \sum_{i=0}^x \sigma_i^2 = \frac{2x+1}{x} \frac{\sum_{i=0}^x \sigma_i^2}{x} \quad (3.10)$$

Since x is the number of data groups, the existence conditions $x \neq 0$ and $x \neq -1$ are always verified. The inequality can be so rewritten in this way:

$$\sigma_{x+1}^2 > \frac{2x+1}{x} \sigma_{avg}^2 \quad (3.11)$$

where $\sigma_{avg}^2 = \frac{\sum_{i=0}^x \sigma_i^2}{x}$ can be defined as the noise level until the previous node.

Since $x \gg 1$,

$$\frac{2x+1}{x} \approx 2 \quad (3.12)$$

therefore

$$\sigma_{x+1}^2 > 2\sigma_{avg}^2 \quad (3.13)$$

Finally, as long as the beat noise level is less than twice the mean noise level of the previous node, an improvement of the SNR is reached, otherwise it is necessary to stop as the data are not good candidates for averaging (Di Pietro Paolo et al. (2005)).

3.1.2 Examples

Figure 3.2 shows two spatio temporal dendrograms based on the averaged data: Figure 3.2a shows a typical dendrogram of data from a subject with homogeneous noise level and low variability among the beats. The dendrogram is almost symmetric: the number of beats belonging to the main two branches is very similar (146 vs 150). On the contrary Figure 3.2b shows an example of data with different noise levels and with higher variability (when compared to Figure 3.2a): In this case the two main branches have a different number of beats (49 vs 127).

An example of results obtained averaging over a few beats the two different branches in Figure 3.2b is given in Figure 3.3. Figure 3.3a shows the average calculated on 4 beats from the left branch of the dendrogram, whereas Figure 3.3b shows the average of 4 beats from the right branch. The resulting figures show a different shape: Figure 3.3a has got a T-wave

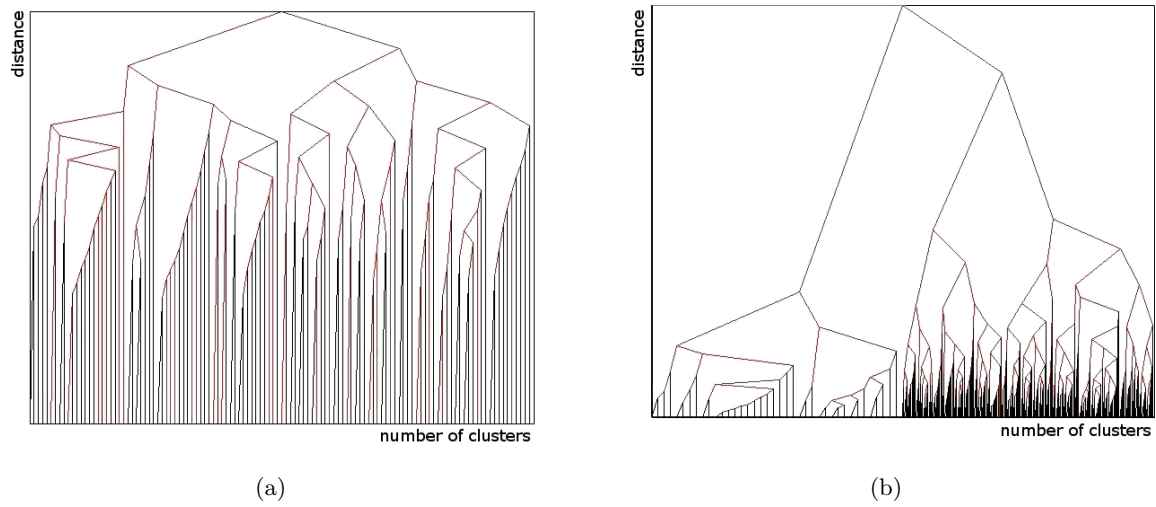
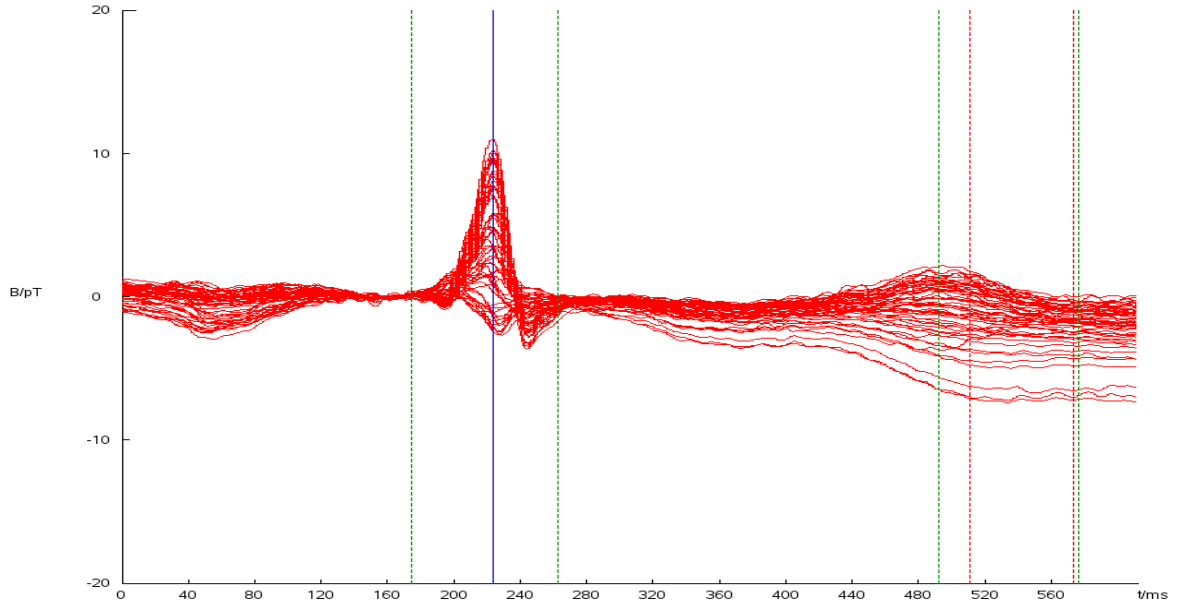


Figure 3.2: Two representative dendrograms of two patients with different characteristics are shown. The knots indicate where two clusters or group of clusters merge: a) Dendrogram of a measurement where the noise is homogeneous and there is not so much variability among the beats: The dendrogram is in fact almost symmetric; b) Dendrogram coming from a measurement where the beats have a higher level of variability: It is possible to see two main branches, one that contains almost all beats and the other one containing the beats with either more variability or with different shape

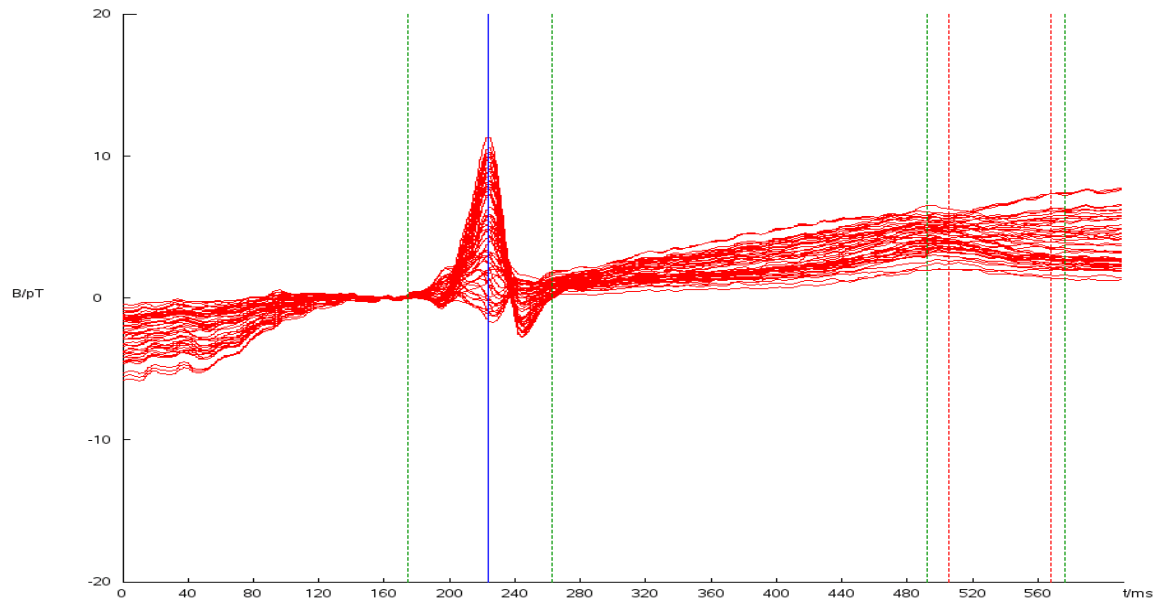
with higher amplitude and different baseline when compared to Figure 3.3b. This difference in baseline can be caused by the different influence of the breath on the sensors placed in different positions.

Figure 3.4 shows the raw data in 2 out of the 55 channels of an acquisition recorded in a moderate shielding environment: The first row reveals a channel with low SNR whereas in the second row a channel with higher SNR (when compared to the figure in the first row) is shown. These two representative MCG channels are then averaged (Figure 3.5) using either classical averaging (red line) or averaging preceded by the cluster analysis (blue line). In Figure 3.5a a channel with low SNR is displayed (compare to the first row in Figure 3.4): Although during the process of averaging with the cluster analysis only 118 beats out of 273 recorded activations are averaged, the signal amplitude is higher than in the classical procedure (thus averaging all activations). In case the SNR is high the signal amplitude after averaging, with or without the application of the CCA, is very similar: the two signals almost overlap. This result can be explained pointing out that in this second case the condition 3.13 is not fulfilled (see Figure 3.5b).

This procedure of averaging has been tested in some hundred MCG measurements of patients



(a)



(b)

Figure 3.3: Two representative overlay plots of 56 averaged signals from the same data set, but with different noise characteristics: a) average calculated over 4 beats shown in the Figure 3.2b, using the left smaller branch b) average calculated over 4 out of the beats shown in the Figure 3.2b using the right bigger branch. The vertical green lines show the markers calculated on the averaged signals: Q-onset, R-peak, Q-end, T-wave, and T-end are visible

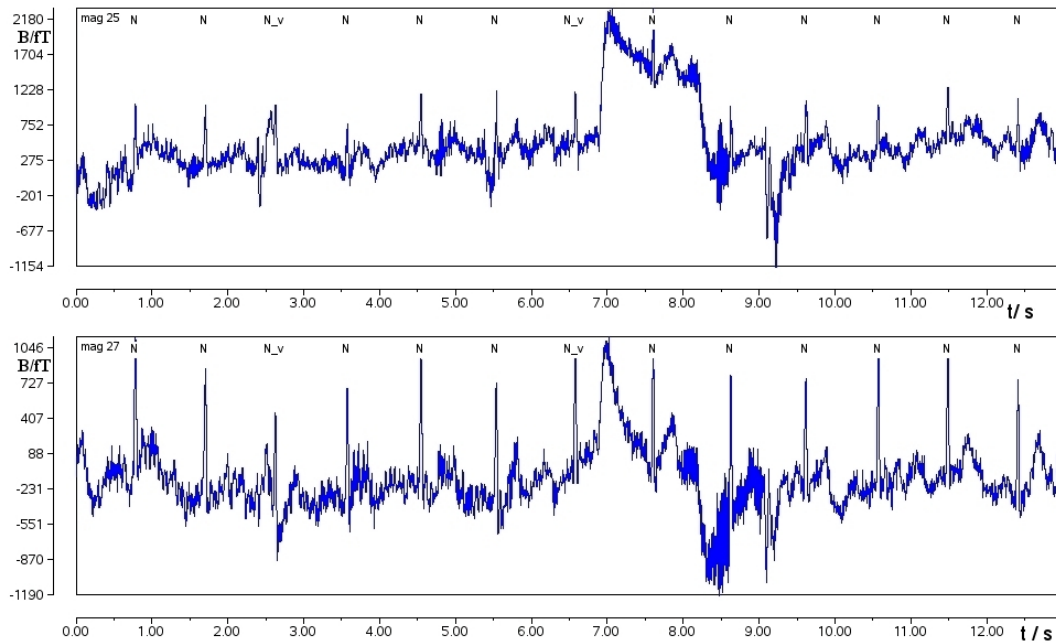


Figure 3.4: Raw data of an examination in moderate shielding room: in the first row a channel with low SNR, in the second row a channel with high SNR. The label N stands for Normal beats, the label N_v for normal visual beats

and healthy subjects providing satisfactory results and execution time-performances (less than 2 seconds in a 5 minutes acquisition). As the procedure is done channel by channel, the algorithm becomes scalable and can be parallelized for a multiprocessor system, drastically reducing the computation time.

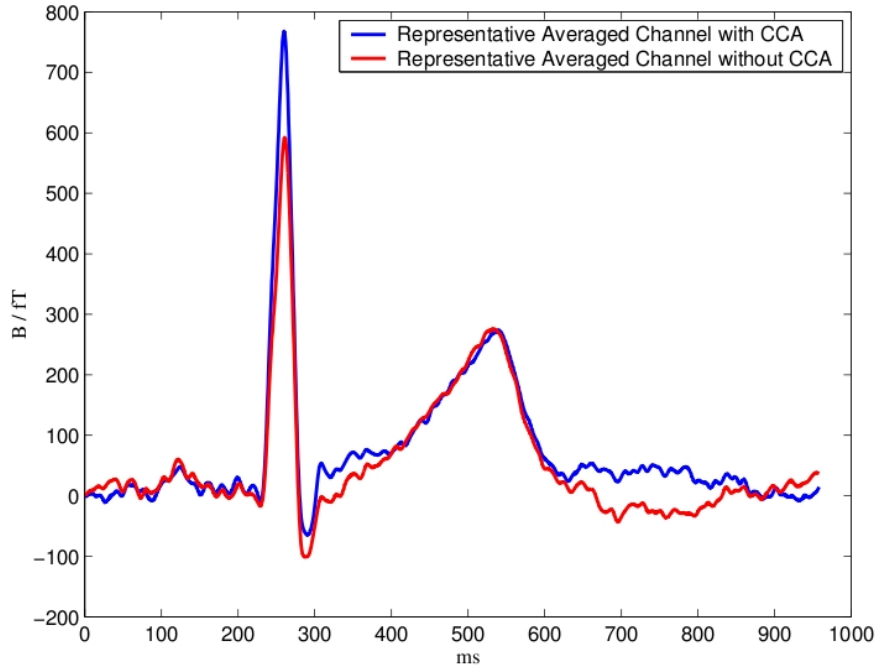
3.2 Noise Reduction using Blind Source Separation

3.2.1 Choosing the optimal BSS algorithm

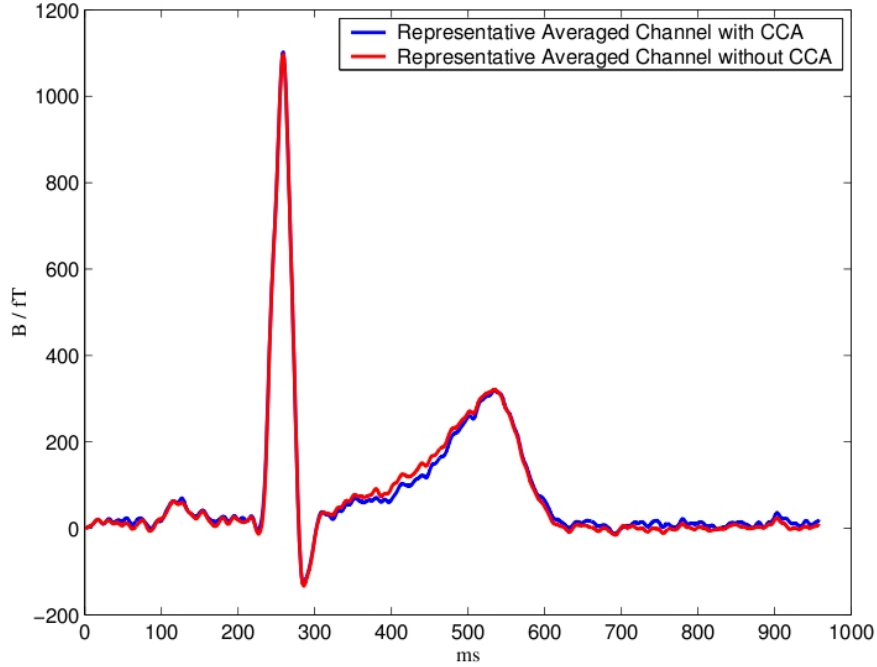
Five BSS methods are compared using nine examinations having different SNR: Two acquisitions are carried out at the University of Jena with a gradiometer system and moderate shielding, four of them at the hospital of Hoyerswerda using a magnetometer system and three at the University of Ulm with a magnetometer system (see section 2.3).

The manual classification of all extracted components is performed by an expert investigator for each data set and each sensor configuration (one or two groups). Two different signal categories for this first test are used and the number of cardiac components calculated.

Table 3.1 shows the results. Among the methods, the algorithm that gives the worst results is TDSEP-EVD: It is impossible to separate noise and heart signal in all examinations. The other



(a)



(b)

Figure 3.5: Two representative averaged channels with (blue line) and without cluster analysis (red line): a) Channel with low SNR: the signal amplitude after the selection procedure (118 beats out of 273) is greater than in the conventional averaging (all 274 beats); b) Channel with high SNR is shown: using all beats or a subset of them does not make almost any difference

methods perform better: They could differentiate between noise and heart related components with similar results (first and second column in the Table 3.1). The number of sources is different, depending on the noise level in the acquisitions: If an acquisition with low SNR is analyzed the number of components is lower than in one with high SNR.

The third and fourth columns show the computational load results: "1 Group" means that all 55 sensors are used simultaneously, "2 Groups" that the sensors are divided into two groups and two unmixed data and sources are calculated separately. Among the methods the best results are achieved by TDSEP followed by joint diagonalization (TDSEP-JD). For further information see section 3.3.

The typology of sources got using either HOS (Higher-Order Statistics) or SOS (Second-Order Statistics) is different: Applying the first family of algorithms it is possible to separate the cardiac sources into their components: the atrial and ventricular activity (Figure 3.6). On the contrary, the differentiation between the two activities is not always reached in the methods based on SOS although a good separation between heart components and noise is shown: In fact, it is still possible to find the activity of the T-wave, but not that of the P-wave.

The aim of this work is not feature extraction, but noise reduction: This means that, although the best performances from a point of view of separation are given by HOS methods, importance is given to the computational load as well. In fact, in this procedure, components of heart origin are not required to be separated from each other exactly, because they are mixed again by back projection after removing artifact-related components. Furthermore, with the same procedure, it is possible to filter off the noise also in wider sense, improving the relative amount of any types of useful information in the signal.

Finally, TDSEP-JD is preferred. This method is compared with a standard de-noising algorithm such as SVD in case of rest measurement.

In section 3.2.2 methods for the automatic detection of hearth activity are described and the optimal threshold in case of rest MCG is determined.

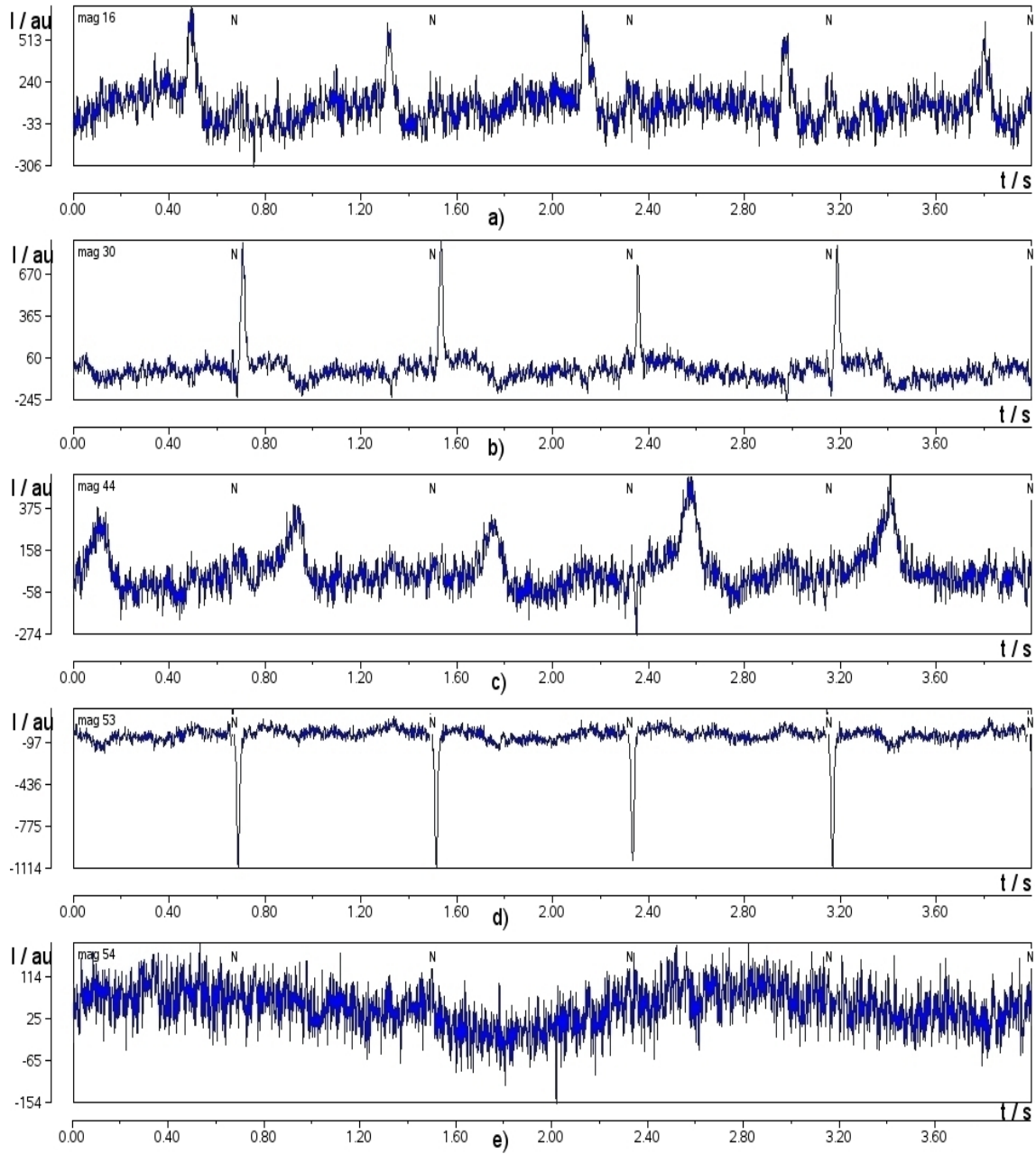


Figure 3.6: Five out 55 sources detected by fICA from a 300s measurement (The label N is in correspondence of the QRS-complexes): There are different kinds of sources related to the cardiac activity: In the first panel the P-wave is clearly visible, in the second and fourth panels the QRS-complex, in the third panel the unmixed data related to T-wave. In the last panel, gaussian noise. The number on the left in each panel corresponds to the channel where the source was found

Table 3.1: Number of components and time necessary to get the unmixed data in 9 patients using five BSS algorithms: *G* means that the measurement is performed with a gradiometer system, *M* a magnetometer system is used. One group: All the channels are used simultaneously; two groups: The channels are divided into two groups

	1 Group	2 Groups	1 Group	2 Groups
	Number of Components		Time (hh:mm:ss)	
Subject 1- M				
JADE	10	21	01:45:57	00:02:47
fICA	14	19	00:55:21	00:08:29
TDSEP-EVD	No good separation			
TDSEP-JD	11	17	00:00:55	00:00:25
SHIBBS	10	20	01:27:20	00:02:41
Subject 2 - G				
JADE	2	3	01:30:14	00:02:47
fICA	2	2	00:16:06	00:02:44
TDSEP-EVD	3	No good separation		
TDSEP-JD	3	3	00:00:52s	00:00:20
SHIBBS	2	2	03:31:50	00:08:20
Subject 3 - G				
JADE	3	3	01:28:33	00:01:51
fICA	1	5	00:13:16	00:02:33
TDSEP-EVD	No good separation			
TDSEP-JD	3	2	00:00:48	00:00:20
SHIBBS	3	3	00:03:46	00:01:09
Subject 4 - M				
JADE	8	15	00:55:48	00:05:07
fICA	7	13	00:16:23	00:01:45
TDSEP-EVD	No good separation			
TDSEP-JD	9	14	00:00:23	00:00:12
SHIBBS	9	15	00:32:15	00:04:31
Continued on next page				

Table 3.1 – continued from previous page

	Number of Components		Time (hh:mm:ss)	
Subject 5 - M				
JADE	9	16	01:53:12	00:04:24
fICA	8	14	00:09:17	00:01:58
TDSEP-EVD	No good separation			
TDSEP-JD	8	13	00:00:21	00:00:11
SHIBBS	9	14	00:31:58	00:04:19
Subject 6 - M				
JADE	17	28	02:20:14	00:02:33
fICA	15	26	00:33:41	00:06:20
TDSEP-EVD	No good separation			
TDSEP-JD	13	25	00:00:53	00:00:27
SHIBBS	16	27	00:39:36	00:04:43
Subject 7 - M				
JADE	6	13	01:51:43	00:03:38
fICA	6	17	00:10:43	00:04:38
TDSEP-EVD	No good separation			
TDSEP-JD	6	13	00:00:57	00:00:33
SHIBBS	5	12	00:52:28	00:20:19
Subject 8 - M				
JADE	11	18	03:46:23	00:01:14
fICA	8	14	00:12:59	00:02:12
TDSEP-EVD	No good separation			
TDSEP-JD	11	15	00:00:18	00:00:11
SHIBBS	12	18	00:34:07	00:00:58
Subject 9 - M				
JADE	13	24	02:04:29	00:02:38
fICA	12	21	00:53:12	00:05:53
TDSEP-EVD	No good separation			
TDSEP-JD	11	20	00:00:43	00:00:23
Continued on next page				

Table 3.1 – continued from previous page

	Number of Components		Time (hh:mm:ss)	
SHIBBS	15	26	00:41:14	00:03:33

3.2.2 Identification Phase-Finding the cardiac components

Kurtosis

In order to overcome the problem of outliers the value of kurtosis is calculated on time intervals of ten seconds in each unmixed data. The number of intervals depends on the length of the unmixed data (time acquisition). The kurtosis values calculated in each period are given as input to a histogram procedure where the number of bins is between 8 and 20, according to the acquisition time.

The histogram is here used as a form of data binning, that is a pre-processing technique applied to reduce the effects of minor observation errors: In fact the averaged value of kurtosis (calculated over the intervals) is substituted by the most frequent one.

In the Table 3.2 is shown that, by using the histogram, the kurtosis values are less biased by artifacts that instead appear a few times in the unmixed data.

Table 3.2: Kurtosis in five different sources computed with (second column) and without (first column) histogram

Sources	Kurtosis	Kurtosis + Histogram
Heart-1	11.20	11.26
Noise	94.11	0.23
Heart-2	90.41	37.70
Noise	20.36	9.35
Gaussian Noise	0.11	0.13

The value of kurtosis for the unmixed data related to the heart (Figure 3.7a and c) and to the continuous noise (Figure 3.7e) remains leptokurtic and mesokurtic, respectively, apart from the fact that the histogram is used for computing the kurtosis value or all data samples are used. This occurs as in these sources the value of the 4th order moment remains *constant*

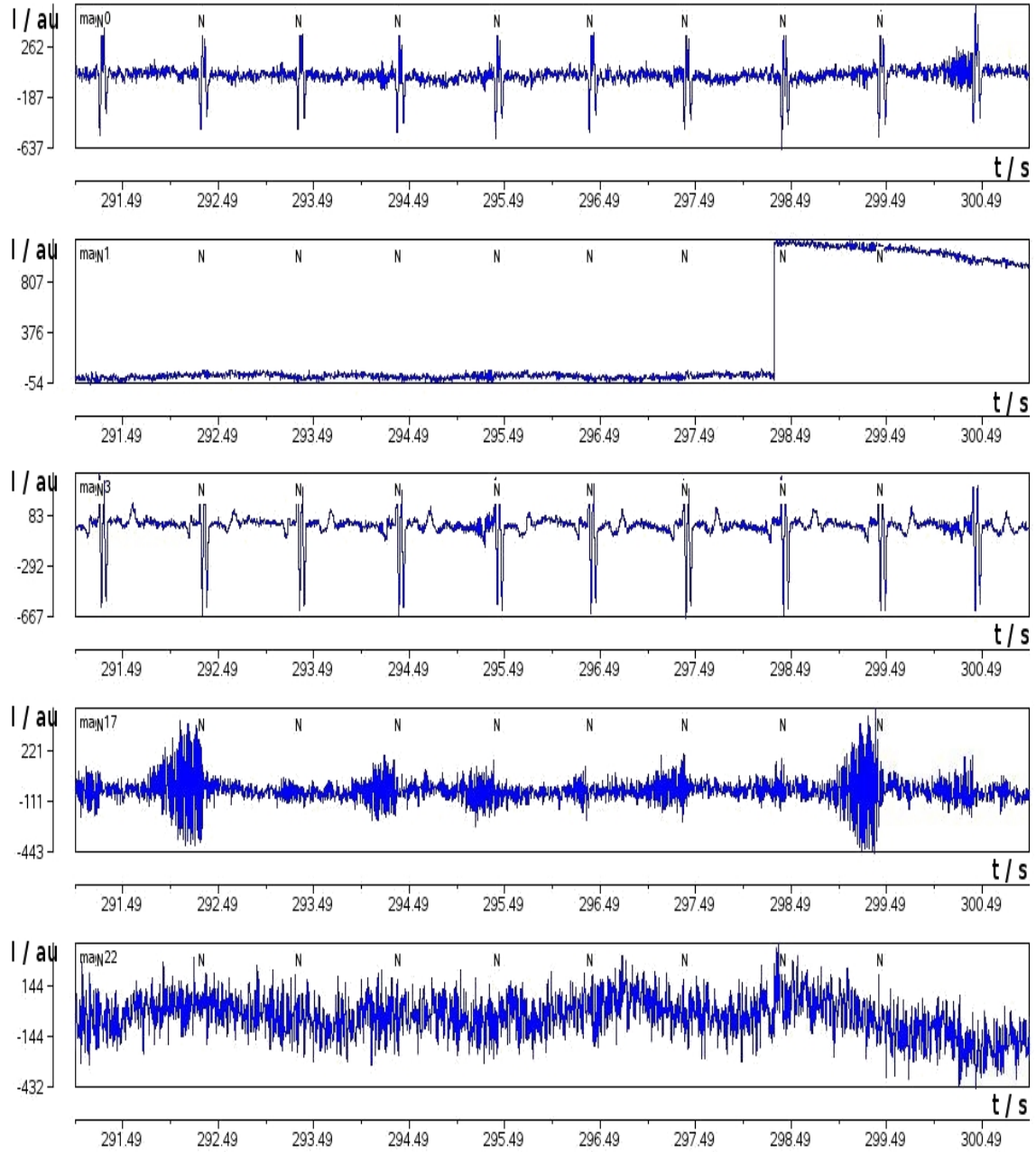


Figure 3.7: Sources with different values of kurtosis: a) and c) Heart related components; b) and d) non gaussian distribution noise; e) continuous noise

over the time intervals. In the first source of noise (Figure 3.7b) (kurtosis 94.11 and 0.23 using the procedure without and with histogram, respectively) the drawback of the usual kurtosis is clear: Its high value without the histogram procedure is given by the abrupt artifact occurred around the 298th second since the value of kurtosis (94.11) has been calculated using a normal average procedure instead of using the histogram result.

Twenty-five examinations of volunteers have been used to determine the kurtosis threshold (KT) which may discriminate continuous noise from the other components, after the application of SVD or TDSEP-JD. Using the values displayed in Figure 3.8 two thresholds have been defined for kurtosis, after eliminating those values lower or greater than $avg \pm 2\sigma$ (σ is the standard deviation (SD) and avg the mean value, calculated over the examinations). The values are then validated in the 40 remaining patients.

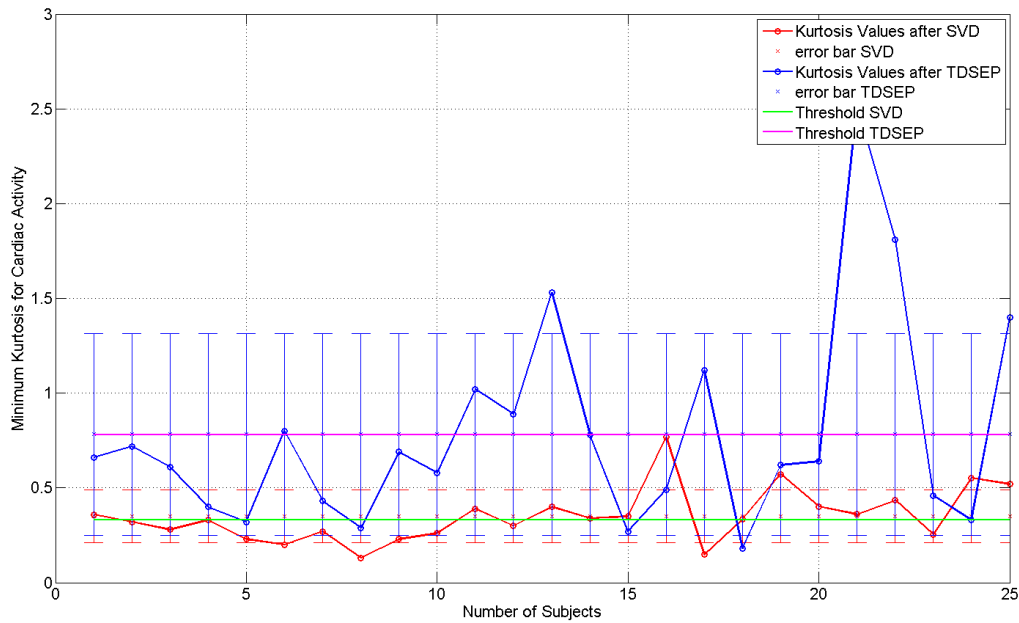


Figure 3.8: Minimum kurtosis value related to cardiac activity in 25 volunteers: The red color is related to the kurtosis values after computing SVD and its error bars, the blue color to the kurtosis values after computing TDSEP and its error bar, the magenta color is TK_{TDSEP} , the green color TK_{SVD}

The thresholds are 0.33 for SVD (TK_{SVD}) and 0.78 for TDSEP (TK_{TDSEP}): The unmixed data having a modulus of Kurtosis below these thresholds are defined as *continuous* noise.

Correlation

The methods described in section 2.8.6 are applied to eight examinations in order to verify which of them is more suited for a user-independent noise reduction.

In Figure 3.9 an example of unmixed data related to the cardiac activity with the corresponding correlation values is shown.

All three methods (CM1, CM2, CM3) succeed in the recognition of cardiac sources, but among them CM1 has demonstrated to be the best indicator for heart activity in the unmixed channels. In fact the correlation values obtained with this algorithm on the unmixed data, after the application of TDSEP-JD, have the minimum σ across the examinations when compared to CM2 and CM3. The SD σ in the three methods CM1, CM2 and CM3 is 0.01, 0.14 and 0.15, respectively (i.e., the SD derived by the application of either CM2 or CM3 is 10 times higher than applying CM1). Due to their elevated variability, CM2 and CM3 are not good pretender for determining a threshold.

A summary of the values obtained is displayed in Table 3.3.

Table 3.3: Minimum value of correlation with cardiac activity in the sources: CM1 (avg = 0.99 and $\sigma = 0.01$), CM2 (avg = 0.61 and $\sigma = 0.14$), CM3 (avg = 0.51 and $\sigma = 0.15$). The correlation values with CM1 have lower variability (10 times lower) than the ones obtained by CM2 and CM3. The subject 4 is highlighted since this examination is used for the Figure 3.9

Examinations	CM1	CM2	CM3
Subject 1	0.998	0.741	0.741
Subject 2	0.995	0.784	0.718
Subject 3	0.996	0.626	0.556
Subject 4	0.981	0.594	0.400
Subject 5	0.993	0.383	0.505
Subject 6	0.966	0.580	0.380
Subject 7	0.993	0.680	0.392
Subject 8	0.992	0.460	0.370

The bigger stability of the first algorithm (CM1) when compared to CM2 and CM3 is due to the values of correlation, calculated on the averaged beats: Using averaged beats a part of the variability that depends on the noise vanishes.

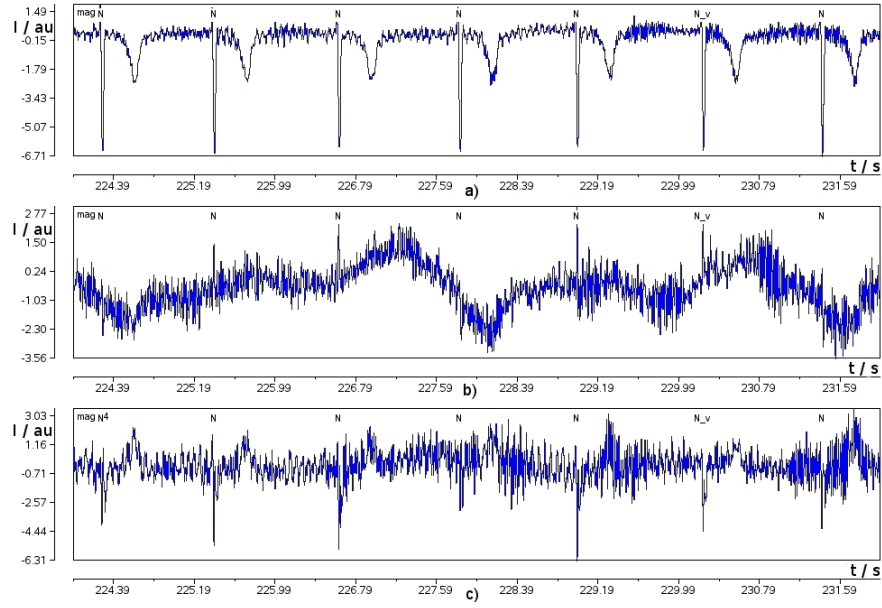


Figure 3.9: Cardiac sources of the subject 4 in Table 3.3 with different correlations in an examination carried out in noisy environment: a) Correlation value: 1.00 b) Correlation value: 0.981 (this is the minimum correlation value associated with cardiac activity) and c) Correlation value: 0.994

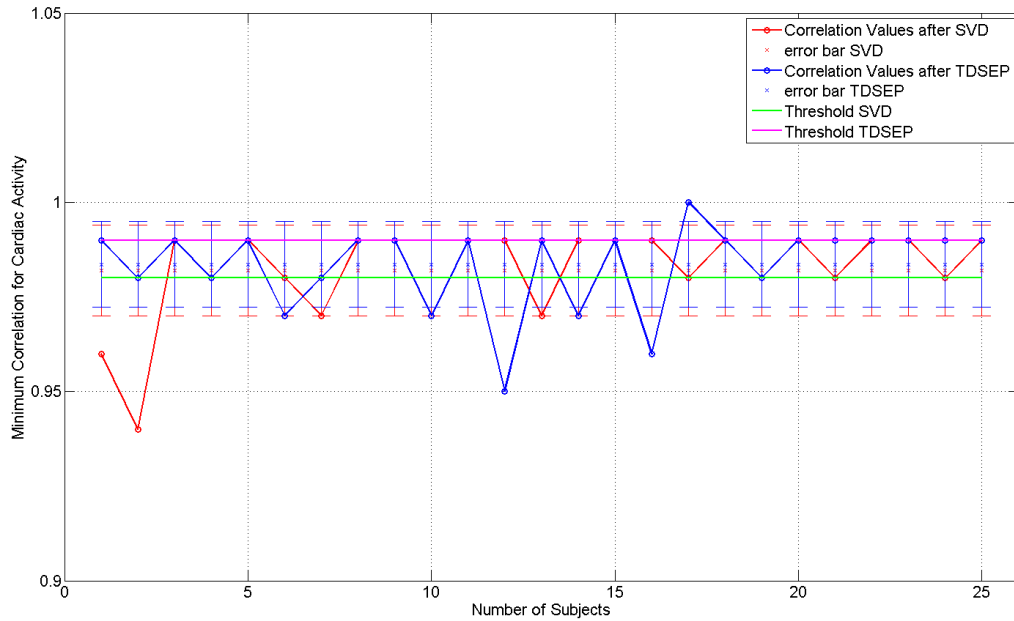


Figure 3.10: Minimum correlation value related to cardiac activity in 25 volunteers: The red curve is related to the correlation value after computing SVD and its error bar, the blue curve to the correlation value after computing TDSEP and its error bar, the magenta curve to the CT_{tdsep} , the green curve to the CT_{svd}

The twenty-five examinations analyzed in paragraph 2.8.6 are used to determine the correlation threshold (CT) which can discriminate the cardiac activity from the remaining components after the application of kurtosis. The CT will be then validated in the 40 remaining patients.

Using the identification group (Figure 3.10) the CTs, $CT_{tdesp} = 0.99$ (TDSEP) and $CT_{svd} = 0.982$ (SVD), are calculated using the same procedure as in the definition of KT_{SVD} and KT_{TDSEP} . If the correlation in a source is less than CT, that source has been removed since it is defined to contain more noise than cardiac activity.

Fifteen CHD patients that have undergone pharmacological stress MCG, are also used for determining the correlation and kurtosis thresholds. Two different thresholds are estimated for each methodology (one to be applied during rest and the other one during stress) for a total of 8 values. Among these values, only the two correlation thresholds CT_{rest} and CT_{stress} , after the application of TDSEP can be used.

The value of kurtosis (Figure 3.11 and Figure 3.12) cannot be applied to the validation data since the value of SD in all cases is very high, in a case even higher than the average (Table 3.4, average = 1.59 vs SD = 1.60).

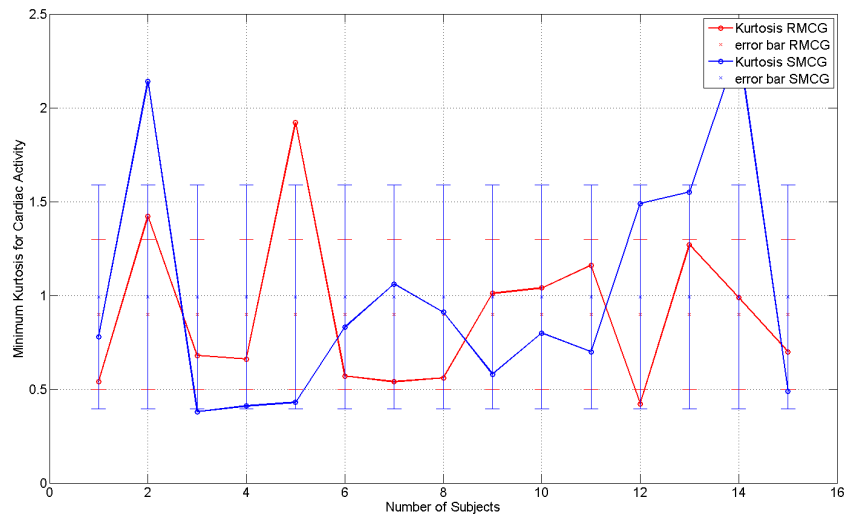


Figure 3.11: Minimum kurtosis value (with error bar) related to the cardiac activity after the application of SVD in 15 patients: The red line is related to the kurtosis value at rest, the blue one to the kurtosis value after stress. The values of SD (error bars) are high, especially when considering the stress case (0.58 vs 0.40)

The values of CT for SVD cannot be defined since the correlation of the last heart-related

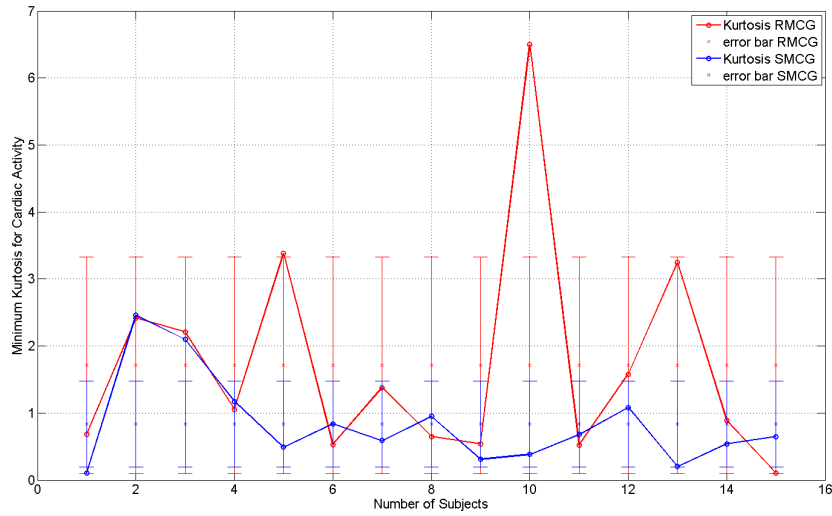


Figure 3.12: Minimum kurtosis value (with error bar) related to the cardiac activity after the application of TDSEP in 15 patients: The red line is related to the kurtosis value at rest, the blue one to the kurtosis value after stress. The values of SD (error bars) are high, in case of rest MCG even higher than the mean value

Table 3.4: Kurtosis thresholds in PSMCG with SDs

Methods	TDSEP-rest	TDSEP-stress	SVD-rest	SVD-stress
Average	1.59	0.82	0.86	1.01
SD	1.60	0.63	0.41	0.58

components had a large variance, especially when the variance in the stress phase (0.22 and 0.35, rest and stress respectively) was estimated (Figure 3.13).

On the contrary when TDSEP-JD is applied, the value of correlation in the last cardiac-related component is much more reliable: The value of SD is 0.025 during rest and 0.013 under stress so that it is possible to calculate a unified threshold for the validation. The values of correlation are different during rest and under stress: $CT_{t-rest} = 0.973$ and $CT_{t-stress} = 0.987$, respectively (Figure 3.14).

After having found the components to be rejected, the cleaned signals are calculated according to section 2.8.7.

The different thresholds ($KT_{svd}, KT_{tdsep}, CT_{svd}, CT_{tdsep}, CT_{t-rest}, CT_{t-stress}$) are then applied to the remaining data sets: rest MCG, stress MCG and patients with already ICD implanted.

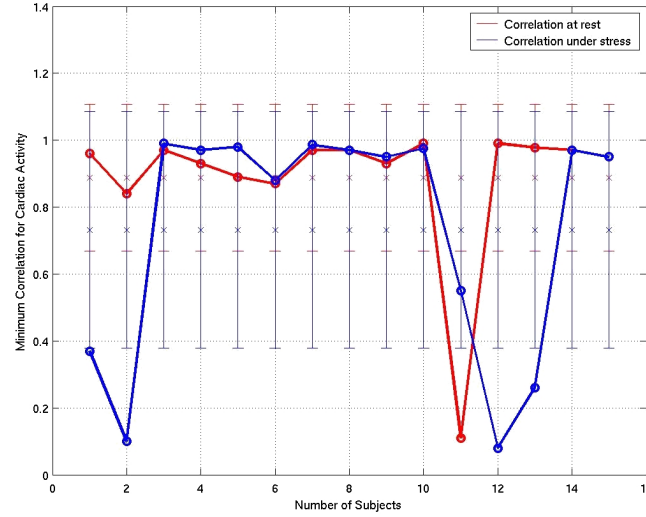


Figure 3.13: Minimum Correlation value (with error bar) related to the cardiac activity after the application of SVD in 15 volunteers: The red line is related to the correlation value at rest, the blue one to the correlation value during stress. The values of SD (error bars) are high, especially when considering the stress case (0.35)

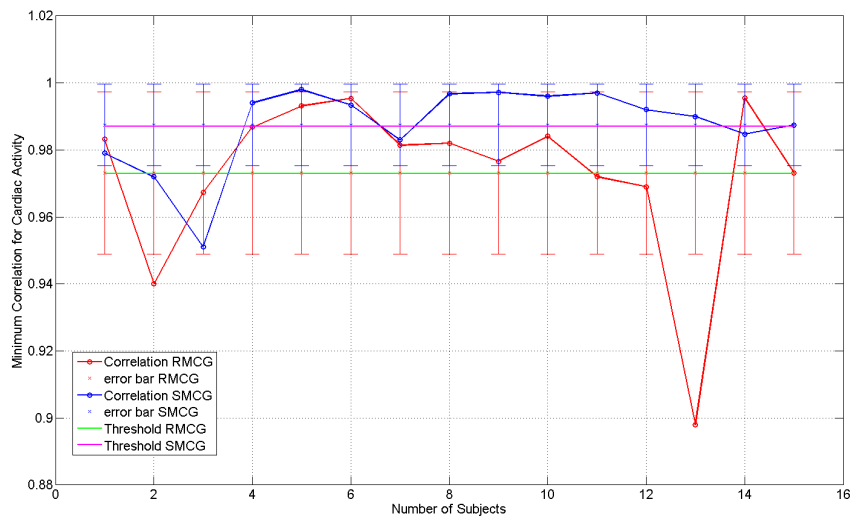


Figure 3.14: Minimum Correlation value related to cardiac activity in 15 volunteers with error bar after the application of TDSEP: The red curve is related to the correlation value at rest, the blue one to the correlation value during stress. The values of SD are much lower than in SVD (see Figure 3.13): 0.025 and 0.013 at rest and during stress, respectively

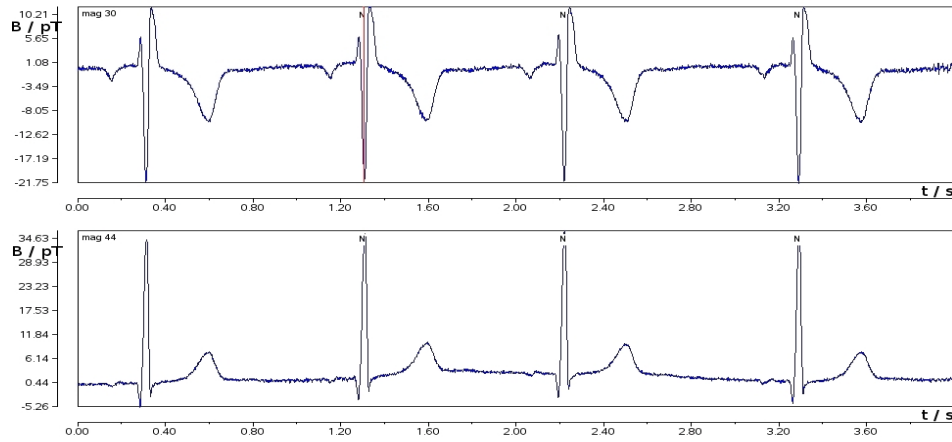
3.2.3 Validation Phase-Cleaned data

Rest Data

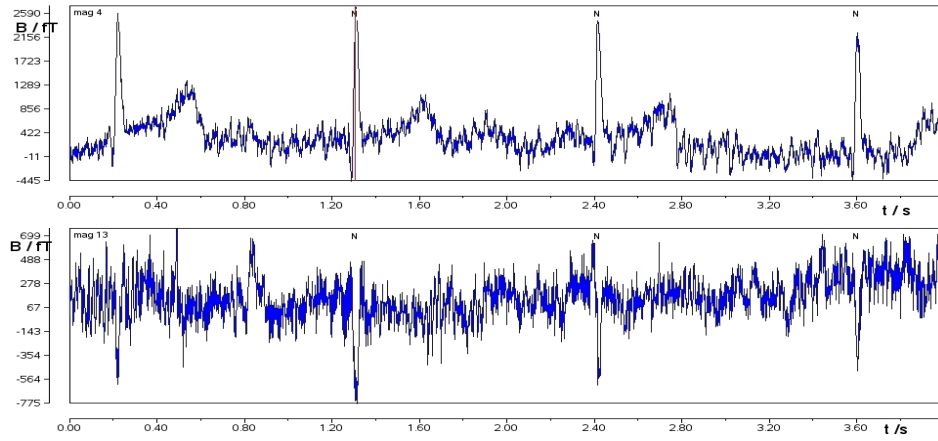
SVD and TDSEP are applied to the residual 40 RMCG. An example for each typology of data is given. To display the results of the different separation techniques, the following scheme is used (Di Pietro Paolo et al. (2006a)):

- The two channels with maximum and minimum amplitude at R-peak in two data sets with different SNR and their related spatio temporal representation using the MF with related color bar (Figure 3.15),
- Three selected unmixed data determined applying SVD: noise, component with high correlation and one component with a special disturbance or feature related to the examination (Figure 3.16a: acquisition with low SNR; Figure 3.16b: acquisition with high SNR),
- Three selected unmixed data estimated applying TDSEP: noise, component with high correlation and one component with a special disturbance or feature related to the examination (Figure 3.17a: acquisition with low SNR; and 3.17b: acquisition with high SNR),
- The two cleaned channels with maximum and minimum amplitude at R-peak using the SVD algorithm: Figure 3.18a shows the results of the denoising process in an examination with low SNR (compare to Figure 3.15b). Figure 3.18b shows the results of noise reduction in the examination with high SNR (compare to Figure 3.15a),
- The two cleaned channels with maximum and minimum amplitude at R-peak using the TDSEP algorithm: Figure 3.19a shows the results of the denoising process in an examination with high SNR (compare to Figure 3.15 a). Figure 3.19b shows the results of noise reduction in the examination with low SNR (compare to Figure 3.15 b).

The separation into noise and cardiac components in RMCG works well both for SVD and TDSEP-JD according to the percentage of automatically recognized sources: In fact, the correlation threshold CT_{SVD} determined using SVD (0.982) is successful (FC) with a percentage of 92%. This percentage is calculated as the ratio between the automatically recognized heart related components (TP) and all the heart related components (visual inspection) multiplied then by 100 (see section 2.8.8).



(a)



(b)

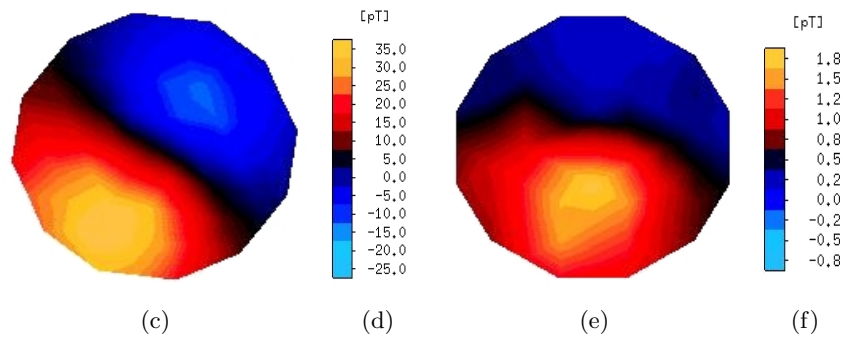


Figure 3.15: Time display of the two channels with maximum (upper row) and minimum amplitude (lower row) at R-peak: a) signal with high SNR; b) signal with low SNR; c) Spatio-Temporal representation of the averaged 55 channels in Figure 3.15a: The MF map corresponds to the time instant Q-max (i.e. red line in Figure 3.15a); d) color bar of the MF amplitude related to Figure c); e) MF map corresponding to the time instant Q-max (i.e. red line in Figure 3.15b); f) color bar of the MF amplitude related to Figure e). Note that the MF amplitude in the signal with high SNR is 10 times higher than the MF in the signal with low SNR

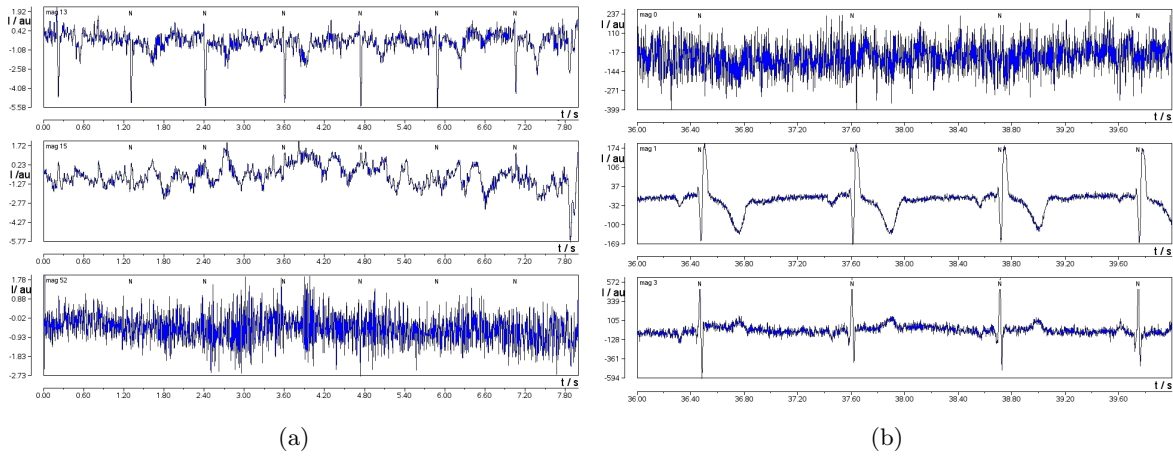


Figure 3.16: Three out of the 55 sources using SVD in two examinations a) unmixed data coming from a measurement with low SNR. Upper row: cardiac signal; middle panel: sources with both cardiac and noise signals; lower panel: gaussian noise b) unmixed data coming from a measurement with high SNR. Upper row: gaussian noise; middle panel: cardiac signal; lower panel: cardiac signal

In 24 out of the 40 validation measurements 1 up to 4 components are not recognized, but the unmixed data are more related to the noise than to the cardiac signal (very low SNR); on the contrary the components with only cardiac components (high SNR) are always detected.

Concerning $TK_{svd} = 0.33$, the threshold has a success rate (FC) of 91%. In determining this percentage only the FN defined as heart related components exchanged with noise have been included, since kurtosis can only differentiate between continuous noise and signals with distribution different from the gaussian one. In the second stage of the denoising process the FP (noise confused with heart cardiac signal) can be easily detected by using the correlation matching routine. Considering both methods together (kurtosis before for eliminating the continuous noise followed by CM1 for detecting the cardiac sources), the method has a successful rate of 88%. This percentage depends on the fact that the 91% successful rate using kurtosis and 92% successful rate using correlation do not always have the same population.

The results concerning the automatic recognition of cardiac components obtained with TD-SEP for the RMCG are better than with SVD in terms of automatic separation. The kurtosis value for eliminating the continuous noise $TK_{tdsep} = 0.78$ (using only the FN) is successful in 98.0% of cases: As in the case of kurtosis, the false positive (FP) can be easily eliminated with the method based on the correlation. The correlation threshold produces good results in the 97% of cases. Joining the two methods a 93% success rate has been reached. The sensitivity and specificity (section 2.8.8) are also used. The kurtosis method has got a good sensitivity,

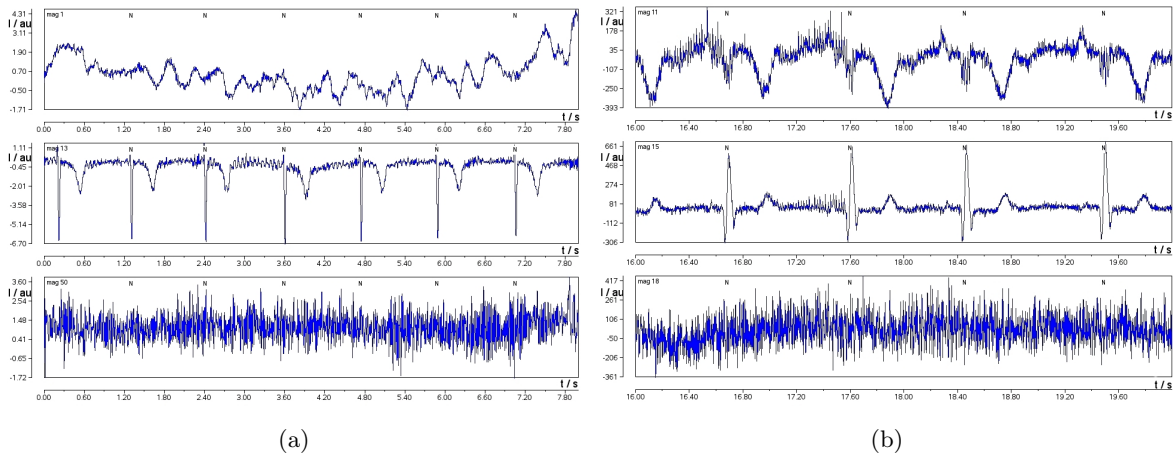


Figure 3.17: Three out of the 55 sources using TDSEP in two examinations a) unmixed data coming from a measurement with low SNR. Upper row: disturbances; middle panel: cardiac signal; lower panel: gaussian noise; b) unmixed data coming from a measurement with high SNR. Upper row: cardiac signal (T-wave); middle panel: cardiac signal (R-peak); lower panel: gaussian noise

but not a good specificity especially with TDSEP-JD since kurtosis can only be used for recognizing continuous noise related components with a distribution very close to the gaussian one: artifacts, non-gaussian noise and cardiac components cannot be identified. If only components with cardiac activity are used, kurtosis has shown to be very sensitive (100% in both cases, SVD and TDSEP): In fact only a few sources related to the cardiac signal are misinterpreted: 1 and 7, respectively. Problems occur in the unmixed data both heart and noise related: In this case the sensitivity decreases (84% in case of SVD and 96% for TDSEP) in terms of number of components 65 vs 45. The method based on the correlation provides good sensitivity and specificity. In fact it differentiates noise related components and cardiac related with good results (100% sensitivity if components with only cardiac components are considered). A summary of the results is in the Tables 3.5 and 3.6. SVD outperforms TDSEP in case

Table 3.5: Sensitivity and specificity for Kurtosis: (C) The sensitivity is computed on cardiac related components, (M) the sensitivity is computed on mixed related components

	SVD (%)	TDSEP (%)
Specificity	74	63
Sensitivity (C)	100	100
Sensitivity (M)	84	96

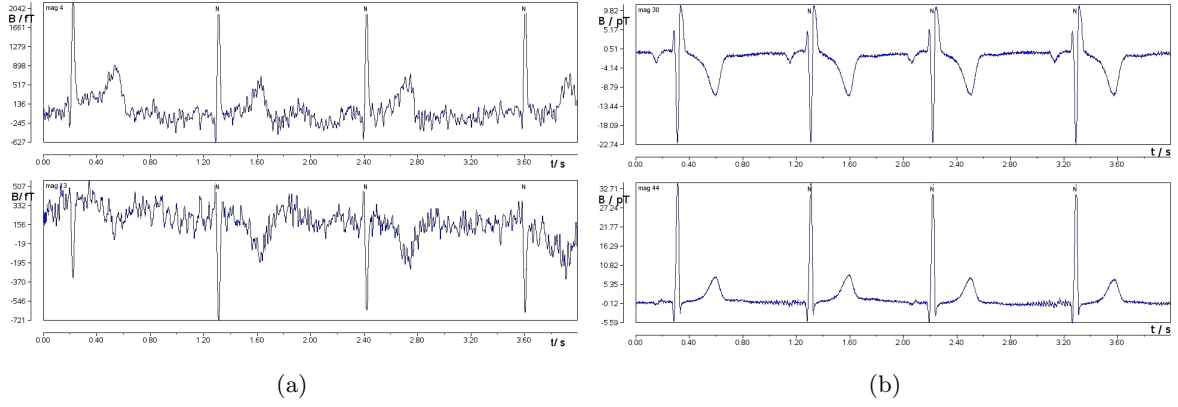


Figure 3.18: a) Cleaned signals (SVD) in an examination with low SNR (compare to Figure 3.15b) b) Cleaned signals (SVD) in an examination with high SNR (compare to Figure 3.15a)

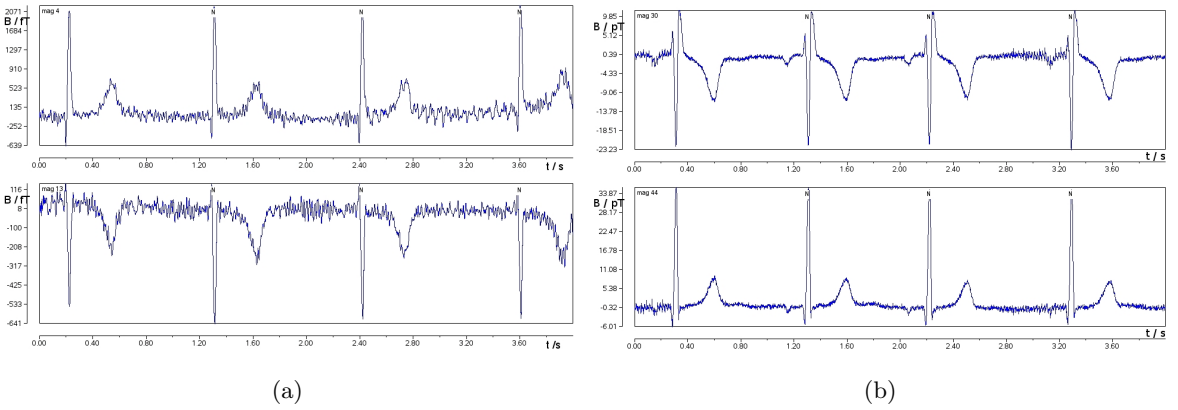


Figure 3.19: a) Cleaned signals (TDSEP) in an examinations with low SNR (compare to Figure 3.15b) b) Cleaned signals (TDSEP) in an examination with high SNR (compare to Figure 3.15a)

Table 3.6: Sensitivity and specificity for correlation: (C) The sensitivity is computed on cardiac related components, (M) the sensitivity is computed on mixed related components

	SVD (%)	TDSEP (%)
Specificity	97	100
Sensitivity (C)	100	100
Sensitivity (M)	96	77

of measurements with high SNR, on the contrary if the acquisition has a low SNR TDSEP performs better. This result can be explained evaluating the number of cardiac components not correctly classified using kurtosis (1 for SVD and 10 for TDSEP).

Pharmacological Stress MCG

The two thresholds $CT_{t_{rest}}$ and $CT_{t_{stress}}$ estimated by the application of TDSEP-JD on the identification population are applied to the 25 CHD patients. The goodness of the methods is estimated using the sensitivity and the specificity after the automatic recognition of the heart related components (Di Pietro Paolo et al. (2006c)). Table 3.7 shows that the specificity of the correlation method is very high (100% in both cases, rest and stress measurements), the sensitivity, if the components with low SNR are considered, is 89% at rest and 90% under stress.

Table 3.7: Sensitivity and specificity for Correlation at rest and during stress

	TDSEP rest (%)	TDSEP stress (%)
Specificity	100	100
sensitivity (M)	89	90

Examples of data cleaning in RMCG and SMCG are shown in Figures 3.20 and 3.21. Both

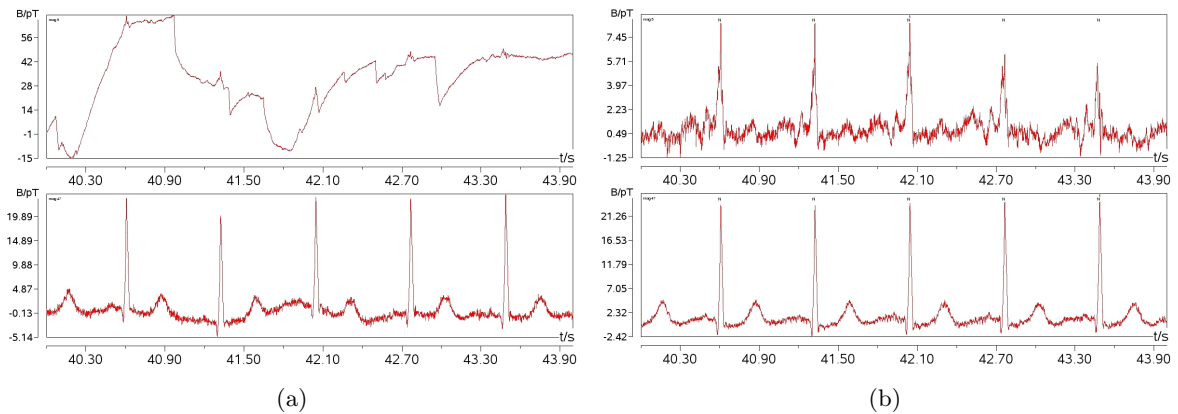


Figure 3.20: a) Raw RMCG: in the upper panel a channel with low SNR: Patients artifacts and drifts are displayed; the lower panel displays the channel with maximum amplitude b) Cleaned RMCG signal using TDSEP: the disturbances in 3.20a (upper panel) are vanished, in the channel with maximum amplitude an improvement of the SNR is evident

figures show 4 seconds of raw data in a rest and under stress measurement before a) and after b) application of TDSEP: The channels represented in the pictures portray a signal with large disturbances and a channel with the maximum of amplitude of the QRS-complex. After the application of TDSEP the noise, especially in the channel with lower SNR (compare Figure 3.20a upper panel with the corresponding panel in Figure 3.20b) has greatly decreased (circa a factor of 10): The disturbances caused by artifacts, large drifts etc are almost disappeared so that it has been possible to depict the heart cardiac signal. In SMCG, TDSEP has introduced some noise in the channel with higher SNR (compare Figure 3.21a lower panel with the corresponding panel in Figure 3.21b).

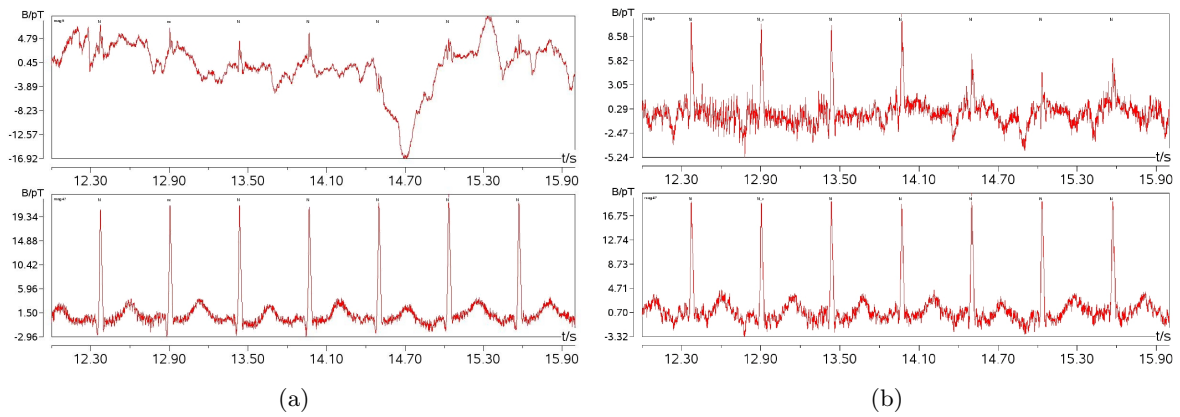
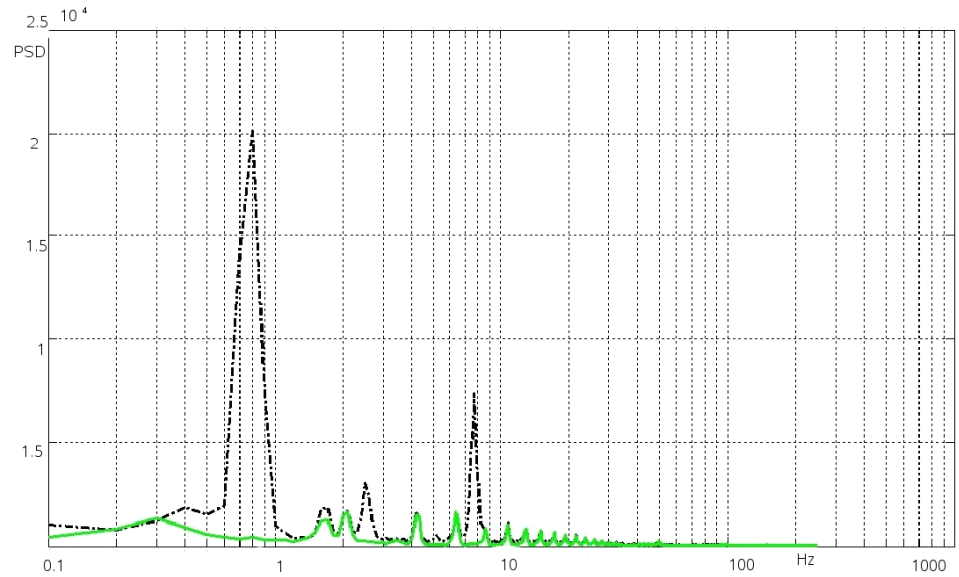


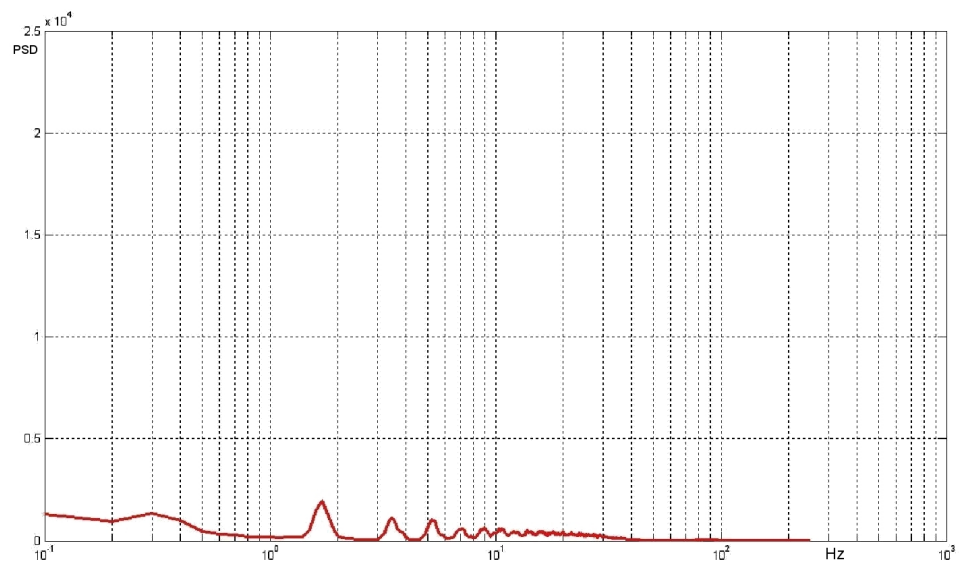
Figure 3.21: a) Raw SMCG: in the upper panel a channel with low SNR: Patients artifacts, drifts are displayed; the lower panel displays the channel with maximum amplitude b) Cleaned SMCG signal using TDSEP: the disturbances in 3.21a (upper panel) are vanished, in the channel with maximum amplitude the application of TDSEP caused a droop of the SNR

Ergometer Stress MCG

The value of threshold $CT_{tdsep} = 0.99$ has a success rate of 95.0%. The elimination of ergonomic disturbances around 8-10 Hz gives good results using the FFT transformed sources. Figure 3.22a shows the power spectrum of a channel before and after the application of TDSEP. The black dots represent the power spectrum of a channel dominated by two disturbances at high frequency (around 8-10 Hz) and at low frequency (around 1 Hz). The green curve represents the power spectrum of the same channel after the application of TDSEP: The disturbances at high and low frequencies disappear Di Pietro Paolo et al. (2006b). To have a direct comparison, the Figure 3.22b shows the power spectrum of the same channel but at rest.



(a)



(b)

Figure 3.22: a) Spectrum of SMCG data before (green) and after (black dots) ICA cleaning in the channel with maximum R-peak amplitude. The arrow indicates the vanishing of the peak between 8 and 9 Hz and below 1 Hz b) Spectrum of rest measurement (rescaled for direct comparison to (a))

In order to quantify the performances of the four algorithms for stress measurements, the RMS before and after the application of the BSS methods are computed on the averaged magnetic signals in the segment [Q-onset-30ms, Q-onset] since in this region, under normal condition, the signal amplitude is very low: It is not used as region the Tend-P-onset segment since, especially in measurements under stress, the two waves can overlap.

Table 3.8 shows the percentage of noise reduction: The analysis with ergometer disturbances shows that all BSS methods give a significant SNR improvement (although the results in terms of SNR and morphology of the cleaned signals are different) compared to the SNR before the application of these methods. Singular Value Decomposition is not included since it fails in all subjects: it could not separate the disturbances coming from the ergometer and the cardiac activity (Figure 3.23c). Figure 3.23 shows an example of denoising: The drawings are based on the data of the subject no. 9, highlighted in Table 3.8. Fast ICA using as contrast function 2.32 gives the worse results in terms of noise reduction (Table 3.8). When compared to the other methods, fICA results in a deformed QRS wave, and furthermore power-line disturbances appear. The other BSS methods (TDSEP-JD, SHIBBS and JADE) have better results and similar each other: The only difference is in the reconstruction of the T-wave. Using SHIBBS and JADE some information of the repolarization phase are lost (see the difference in the T-wave amplitude among JADE, SHIBBS and TDSEP-JD).

Table 3.8: Percentage of noise reduction in the 12 subjects: The label "No" for subject 8 means that for that subject data the algorithm did not converge. The highlighted column indicates the noise reduction values for the data drawn in Figure 3.23

Subject	1	2	3	4	5	6	7	8	9	10	11	12
	(%)	(%)	(%)	(%)	(%)	(%)	(%)	(%)	(%)	(%)	(%)	(%)
fICA	86	78	50	93	96	83	90	73	88	96	92	96
JADE	87	95	95	98	97	93	91	No	93	98	95	99
SHIBBS	90	95	93	98	94	89	92	79	94	98	94	98
TDSEP	96	97	97	98	91	95	96	84	96	99	97	99

Figure 3.24 displays the results of noise reduction in 3 out of the 55 channels of subject no. 9 (Table 3.8): In Figure 3.24a a channel with very low SNR is shown, Figure 3.24b displays the channel with maximum positive R-peak and Figure 3.24c displays the channel with the

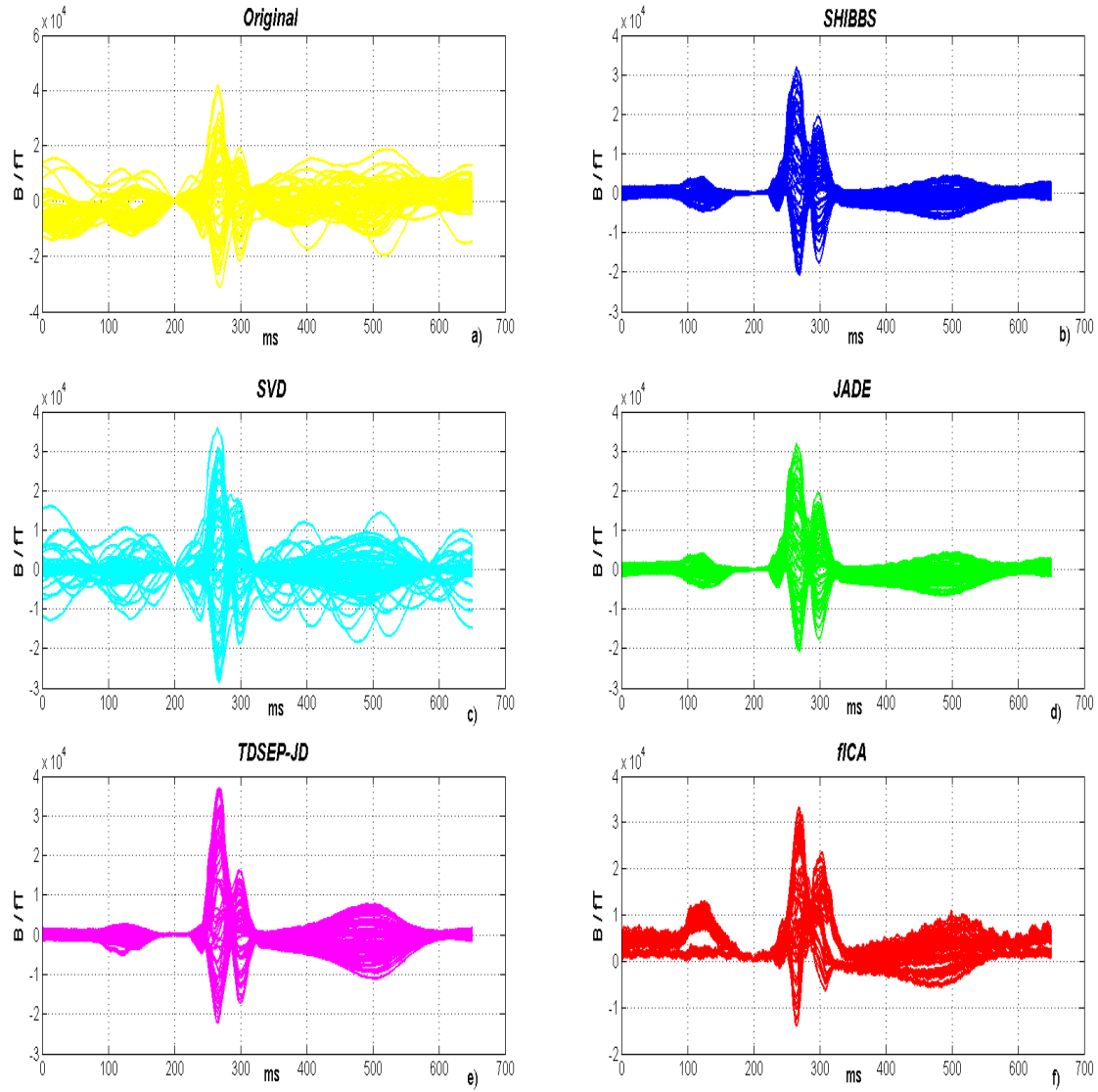


Figure 3.23: Differences in noise reduction in an ergometer SMCG (patient no. 9) using a overlay display: a) Averaged stress measurement with ergometer movement; b) Averaged stress examination after the application of SHIBBS: Note the lower amplitude of T-wave when compared to Figure e); c) Averaged stress examination after the application of SVD: The high frequency disturbances are still present; d) Averaged stress examination after the application of JADE: Note the lower amplitude of T-wave when compared to Figure e); e) Averaged stress examination after the application of TDSEP, f) Averaged stress examination after the application of fICA (using as contrast function the hyperbolic tangent): In this case not only the T-wave has a lower amplitude, but the noise level is higher and power-line noise has been introduced

maximum negative R-peak.

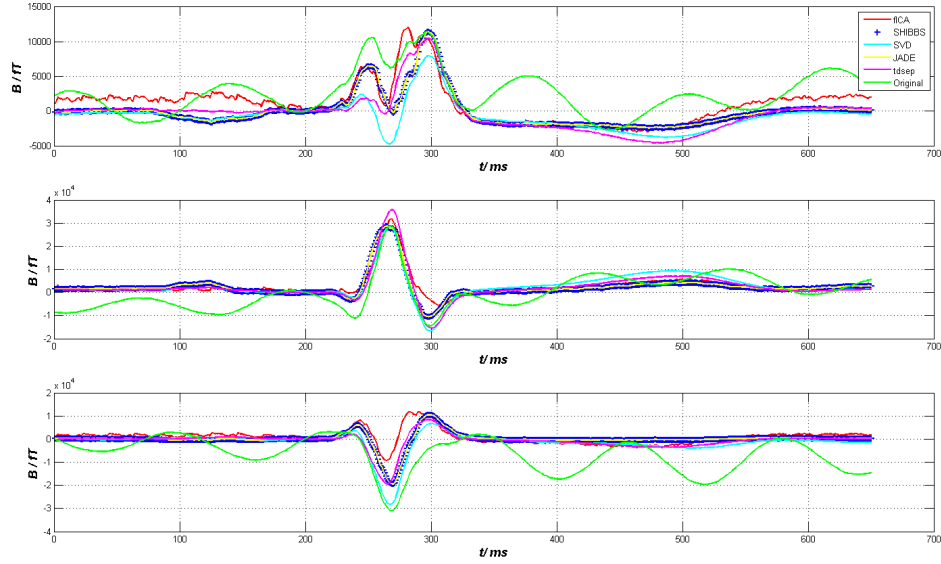


Figure 3.24: Differences in noise reduction in an ergometer stress data set in 3 out of the 55 channels. The original averaged raw measurement (green) is compared with the results of the cleaning procedure by applying the BSS and SVD (cyan) methods: a) channel with low SNR); b) channel with maximum positive R-peak; c) channel with maximum negative R-peak

Data from patients with Implanted Cardiac Device

Until now, it has not been possible to perform biomagnetic measurements in patients with ICDs. In fact, the presence of this device in the thorax (normally located inside the chest on the left shoulder) of the patient leads to very strong interferences (Figure 3.25), that are orders of magnitude larger than the biomagnetic signal of the heart. For this reason, ICDs and pacemakers are among the exclusion criteria for studies concerning MCG. Contrarily to the other data typology (rest and stress data), the CM1 and KT procedures failed in separating between ICD disturbances and cardiac signals. For this reason visual inspection of the averaged unmixed data S is used to discriminate between noise and signal of interest (Figure 3.26). For selecting the un-mixed channels to be used for heart signal recovery, averaging of the time intervals corresponding to the heart beats has to be performed. In order to obtain the averaged un-mixed data, the HRECG data are recorded simultaneously. The details of the averaging process are described in section 3.1.

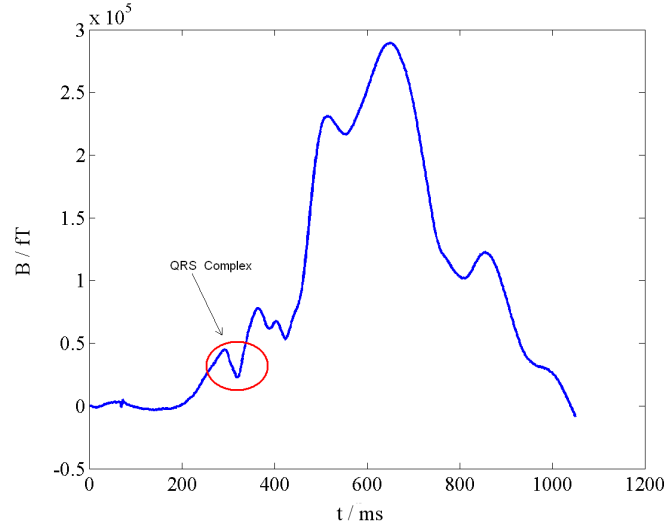


Figure 3.25: Representative channel showing the interferences caused by the batteries contained in the ICD

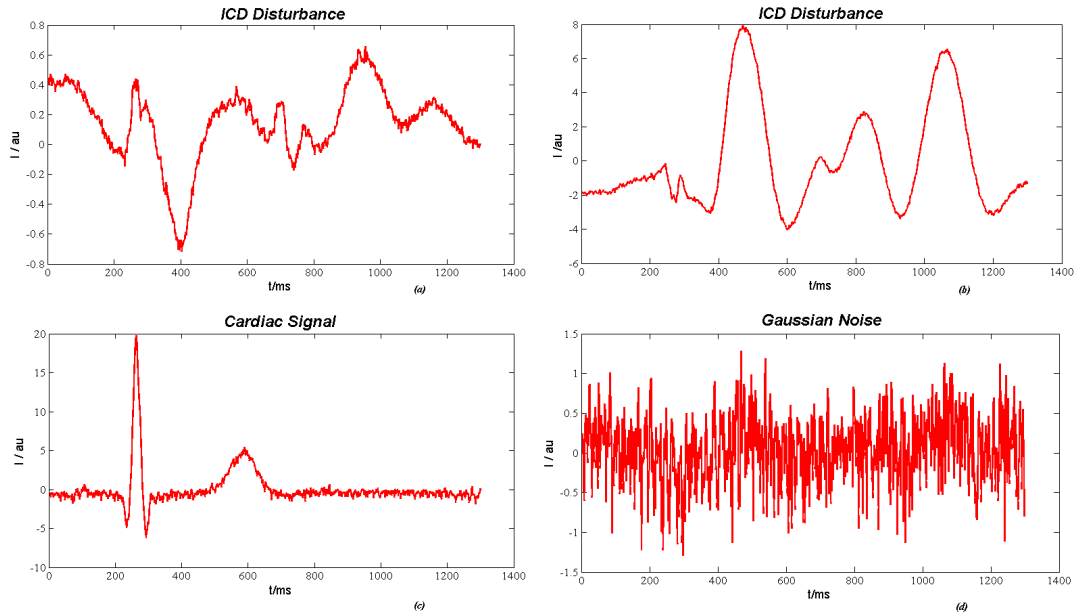
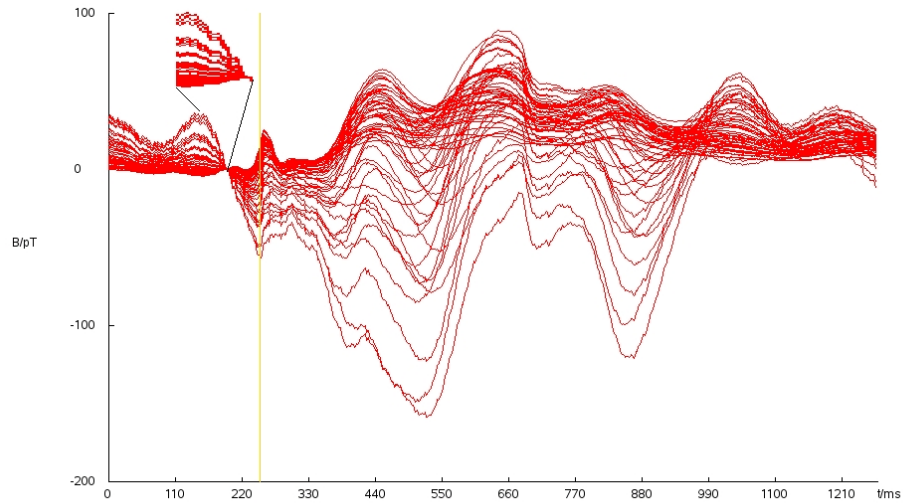
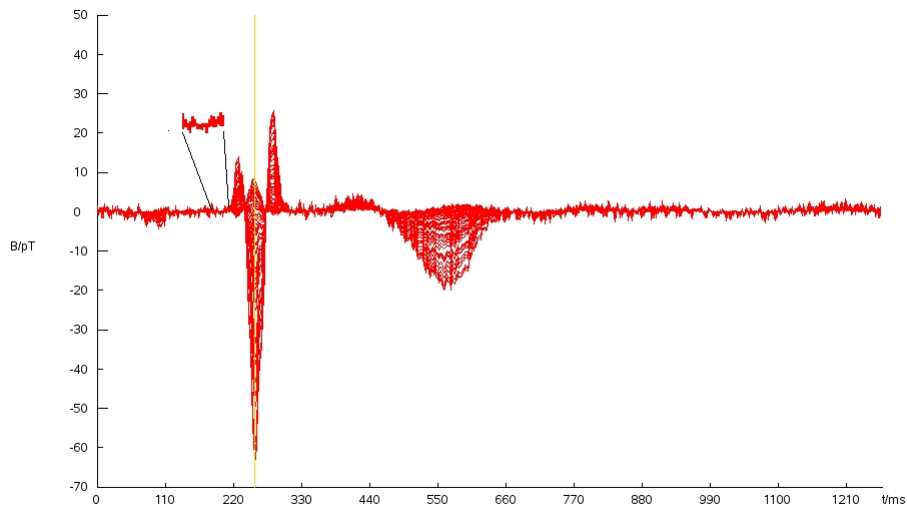


Figure 3.26: Average time signal display of 4 out of the 56 unmixed data components from measurement of patient number six: a) and b) sources representing ICD disturbances, c) the main heart related component d) gaussian noise

In order to quantify the performances of the six algorithms, the RMS before and after the application of BSS is used (see section 3.2.3)(Figure 3.27). Figure 3.27 shows the averaged signal



(a)



(b)

Figure 3.27: Averaged signal before and after the application of TDSEP-Joint: Note the difference in the interval $[Q\text{-onset}-30, Q\text{-onset}]$ between the two averaged signals: The interval of interest is zoomed

of the patient in Figure 1.3 before and after application of TDSEP-JD; the zoom in the pictures represents the interval where the RMS is calculated. As expected, SVD is hardly capable of separating ICD disturbances and cardiac signal, that is why the method is not included in Table 3.9. TDSEP-EVD cannot separate the cardiac source from the ICD disturbances in 4 out of 6 cases; contrarily TDSEP-JD performs the best so to yield a cleaned signal applicable

Table 3.9: Percentage of noise reduction in the 6 subjects: The label No indicates those algorithms where the separation was not successful

Subject	1	2	3	4	5	6
	(%)	(%)	(%)	(%)	(%)	(%)
fICA	88	No	78	No	56	26
JADE	27	83	92	94	50	No
SHIBBS	No	88	92	97	61	58
TDSEP-Joint	87	98	98	92	94	60
TDSEP-EVD	No	95	No	95	No	No

to QRS-fragmentation.

The BSS methods based on higher order statistics (fastICA, JADE and SHIBBS) fall in the middle in terms of separation successful rate: They have worse results in terms of noise reduction than TDSEP-JD in all subjects but two cases where SHIBBS and fICA perform slightly better (97% versus 92% and 88% versus 87% in the considered interval, respectively); on the contrary the successful rate in terms of reconstructed signal after noise reduction is higher than in TDSEP-EVD. The sensor arrangement of the patient number 6 after the application of TDSEP-Joint is shown in Figure 3.28: The disturbances related to the ICD disappear (compare to Figure 1.3). Figure 3.29 shows the results of the application of TDSEP-JD in the six patients analyzing a representative channel: The low frequencies disturbances caused by ICD (in green in the pictures) diminish in all patients although in some channels it is impossible to extract the T-wave (Di Pietro Paolo et al. (2009)). Nevertheless, the reconstructed heart signal is to our opinion good enough for performing QRS-fragmentation analysis (Di Pietro Paolo et al. (2008))(Figure 3.30).

3.3 Computation time

The problem of most BSS methods, in application on data sets with many sensors and a long recording time, is the computation time (CpT): In fact, especially in methods based on HOS the computational load raises exponentially with the number of acquisition points. Since nowadays, it is common that the workstations used to analyze the data have two or more CPUs, physical or logical, it was possible to optimize the different components and makes it possible the use of paralyzed and scalable algorithms in order to exploit the presence of these additional

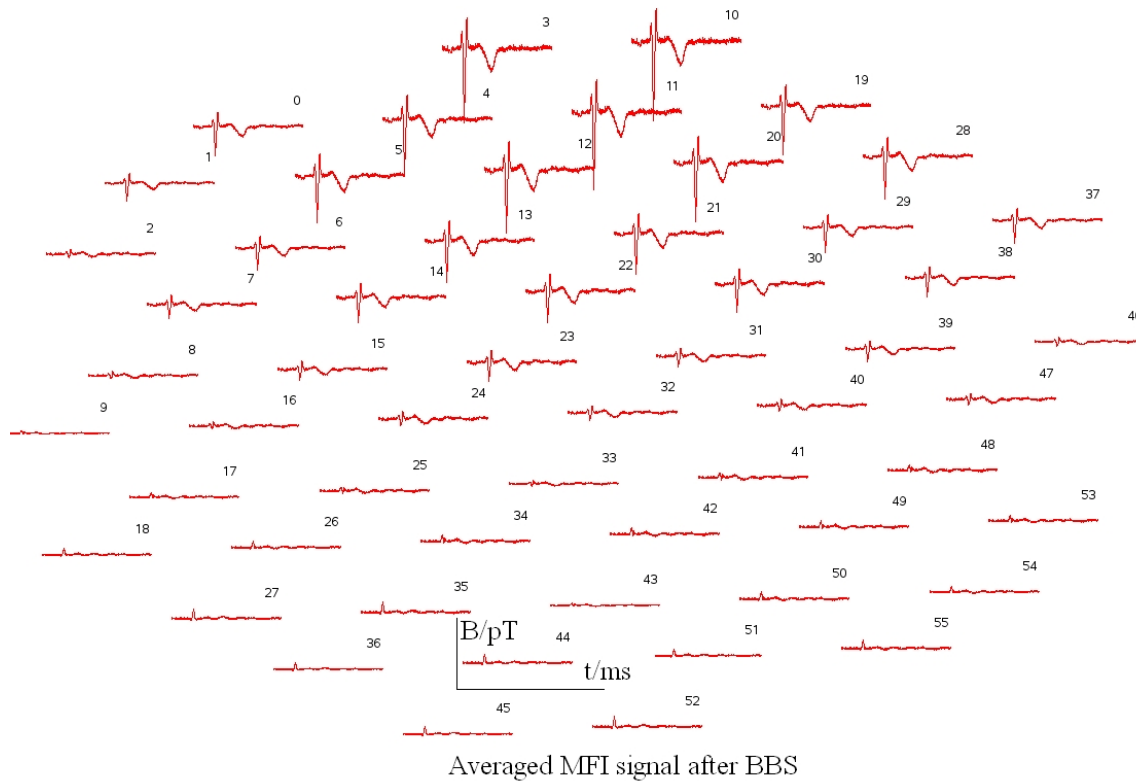


Figure 3.28: *Averaged Signal: sensors arrangement*

processors. In order to use these features, the data are divided into 2 groups (not in case of ICD patients) homogeneously distributed over the sensor area. Then the BSS methods are independently applied at each group so that two unmixing matrices and two sources matrices are calculated separately. The computational load has been measured on a four processors AMD Opteron (2 GHz and 3.5 GB RAM). The routines are written in C++ language and compiled using gcc.

The methods show very different results: Those based on SOS have better performances than HOS methods: For one sensor group the convergence speed has been of the order of some minutes (3-5 minutes) whereas that of JADE and SHIBBS of the order of hours (2-3 hours) (ICD patients). Fast ICA shows, from this point of view, intermediate CpT. The performances of the algorithms depend on the number of observation (number of channels) especially in the JADE and SHIBBS algorithms since, in those cases, the number of calculations to be performed grows exponentially with the number of channels.

Tables 3.10 and 3.11 show the results of the algorithms application in a 100s and 300s

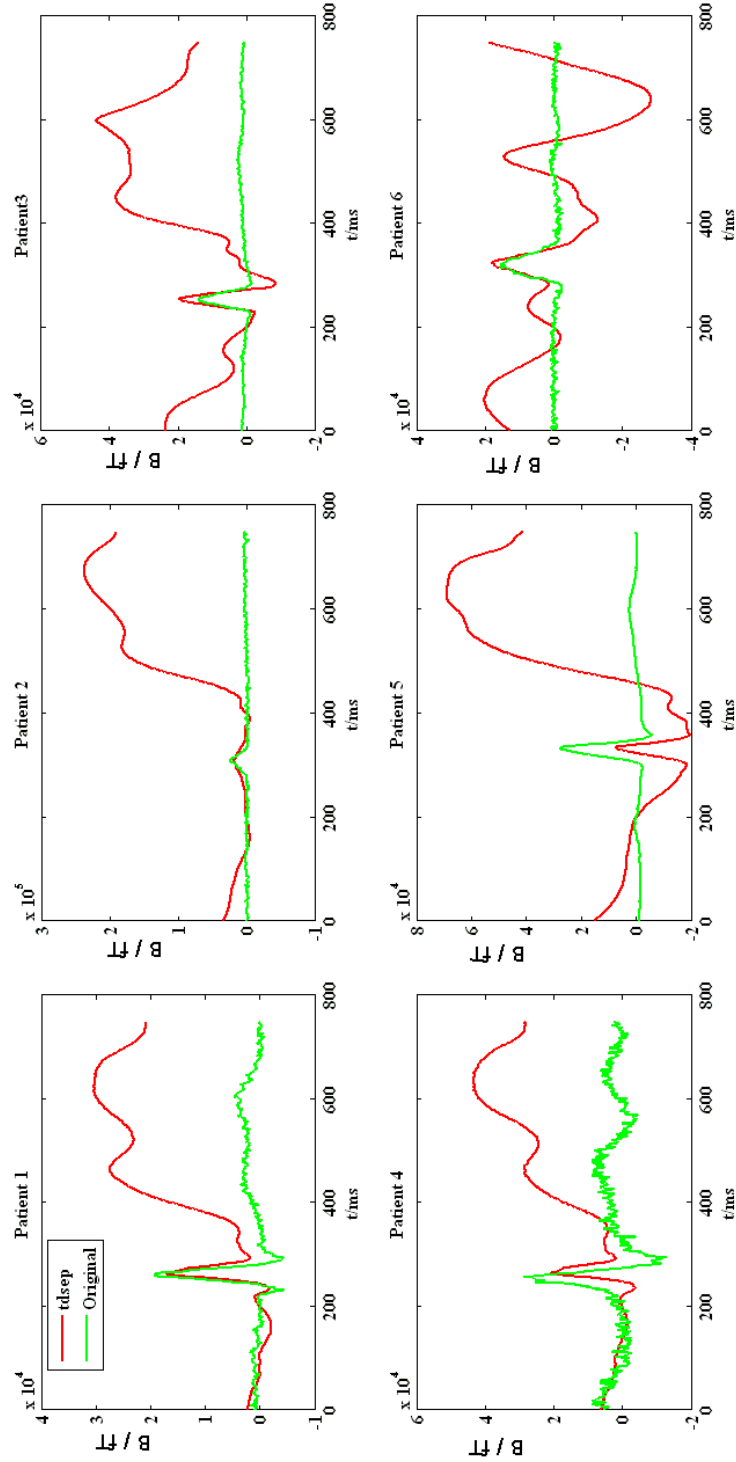


Figure 3.29: Averaged Signals: In green are shown the cleaned signals, in red the signals with ICD interferences: the disturbances caused by the ICD disappear

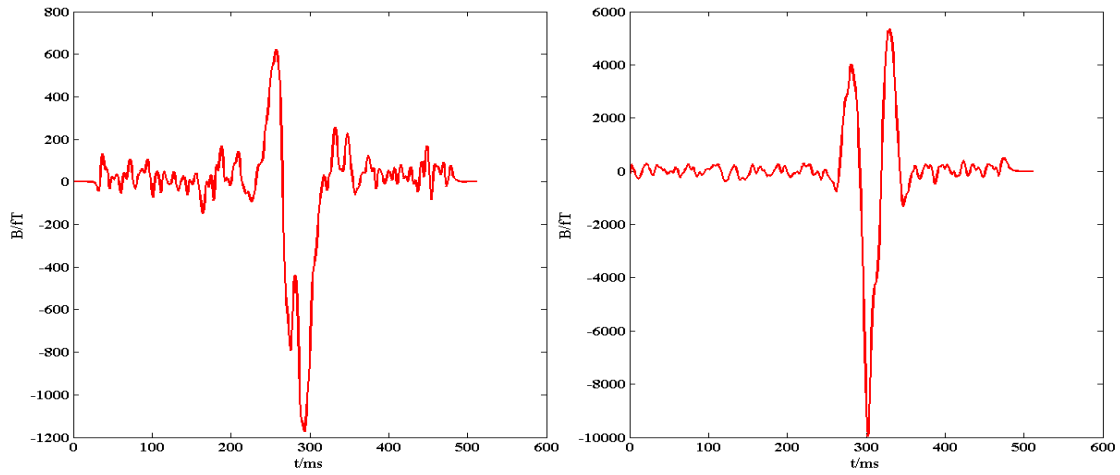


Figure 3.30: Illustration of QRS fragmentation in two patients: a) QRS fragmentation of a shocked patient, b) QRS fragmentation of a patients that did not shock: Note the difference in the fragmentation level into the two cases

Table 3.10: Computation time of 5 algorithms: SVD and TDSEP have lower CpT compared to HOS methods. FICA show intermediate CpT. SHIBBS and JADE need more than one hour for extracting the sources

	SVD	TDSEP	SHIBBS	JADE	fICA
	(mm:ss.cc)	(mm:ss.cc)	(mm:ss.cc)	(mm:ss.cc)	(mm:ss.cc)
1 processor	00:05.78	01:16.32	> 1 hour	> 1 hour	06:43.77
2 processor	00:03.17	00:39.79	> 1 hour	> 1 hour	06:23.08
4 processor	00:01.93	00:22.69	> 1 hour	> 1 hour	06:46.78

Table 3.11: Computation time of the 5 algorithms: see table 3.10. In this case a 300s examination is used: The computational time is circa tripled when compared to the results of the 100s measurement

	SVD	TDSEP	SHIBBS	JADE	fICA
	(mm:ss.cc)	(mm:ss.cc)	(mm:ss.cc)	(mm:ss.cc)	(mm:ss.cc)
1 processor	00:18.70	03:45.87	> 1 hour	> 1 hour	06:43.77
2 processor	00:03.17	01:54.69	> 1 hour	> 1 hour	06:23.08
4 processor	00:01.93	01:03.84	> 1 hour	> 1 hour	06:46.78

Table 3.12: Computation time of the two algorithms, note that a 5 min measurement (300 s) is performed within 2 min

	SVD	TDSEP	SHIBBS	JADE	fICA
	(mm:ss.cc)	(mm:ss.cc)	(mm:ss.cc)	(mm:ss.cc)	(mm:ss.cc)
1 processor	00:10.38	01:51.09	38:52.58	10:27.17	06:36.52
2 processor	00:05.38	00:55.06	19:38.46	07:04.00	03:36.38
4 processor	00:03.37	00:30.04	11:50.89	05:17.04	02:18.69

Table 3.13: Computation time of the 5 algorithms with different processors. SVD and TDSEP had the better results. HOS methods, specially the ones based on the cumulants have dramatically reduced the computational load when comparing this results with the one in table 3.11

	SVD	TDSEP	SHIBBS	JADE	fICA
	(mm:ss.cc)	(mm:ss.cc)	(mm:ss.cc)	(mm:ss.cc)	(mm:ss.cc)
1 processor	00:03.38	00:37.93	11:54.98	03:31.68	02:15.57
2 processor	00:01.85	00:18.22	06:54.54	01:53.22	01:18.96
4 processor	00:01.25	00:09.95	06:21.63	02:07.21	01:22.37

examination, respectively. Since the parallelization in the HOS methods is related to the division into 2 groups, the time necessary for unmixing the data is very similar when comparing 1, 2 or four processors.

Tables 3.13 and 3.12 show the results of the algorithms application in a 100s and 300s examination. In these tables the sensors are divided into two groups. Also in this case the algorithm with lowest CpT is SVD, followed by TDSEP-JD. Contrarily at what expected, the JADE algorithm gives better results than SHIBBS, although the number of cumulant matrices is higher. The fact that the computational load in the HOS methods is increasing when the number of processor is four is due to the fact that the algorithms are threaded considering the division in group. TDSEP has been parallelized calculating independently from each other the delayed matrices.

Chapter 4

Discussion

The most used method for increasing the SNR of the MCG signals (as well as for most of biological signals: ECG, EEG, MEG, ABR) is the classical technique of EA in time domain. However, many requirements must be fulfilled to obtain the well-known improvement of the SNR with the square root of the number of samples: In reality, the stationarity is often violated and many efforts have been made for obtaining an *optimum* method. The work of Hoke et al. (1984) (Hoke et al. (1984)) showed how the highest SNR could be obtained if the inverse power of the noise σ_i^2 of one epoch was assigned as weighting w_i to sweep the signal, but it is possible that when the σ_i are determined from the same data-set as the signal $S(t)$, this estimator, which included σ_i , is not bias free, and the signal could be underestimated (Lutkenhoner et al. (1985)). Furthermore, Mühler and von Specht (1999, 1996) (Mühler and von Specht (1999, 1996)) proved how the maximum SNR could be obtained ordering the epochs according to their noise level; however this could be done only if a good measurement of noise is possible. As mentioned in section 2.7.3 in case of MCG this estimation was faulty, for this reason a workaround to the noise calculation was applied.

In this work, an alternative method for averaging MCG signals was presented: Using established ventricular activation detection techniques applied on the reference data, disturbances and artifacts that appeared in the MCG channels with different amplitudes were eliminated. Two methods were used to take care of the effects of noise instability (non-stationarity, variability etc.) on SNR: The former one was the common method to reject the beats exceeding a certain level of parameters classified as artifacts from the averaging process, the latter was the CCA that was used to sort the beats according to their estimated global noise including biological variability and the non-stationarity of the noise. Categorized cluster analysis was

applied in an improper way and it was used to generate a dendrogram that assembled all elements in a single tree, associating to each element an increasing dissimilarity starting with low-noise beats (- more similar beats) and then adding, at each step, a different block of beats or cluster. The resulting curve, representing the SNR (as a function of the number of samples, in this case one beat or a group of similar beats), could be modeled as in Figure 3.1, curve b. Due to the non-stationarity of the signal the SNR function did not behave like in Figure 3.1 curve a, where the well-know SNR was shown (SNR increased with the square root of the number of samples), but by averaging more and more clusters, the dependency reached a maximum in Figure 3.1, curve b. This behavior was explained mathematically in section 3.1 where the known derivation of the SNR after the average was extended in order to consider the non-stationarity of the noise, or better a piecewise stationarity.

In fact, analyzing the noise level in each MCG channel and in each cluster of beats added, the goal of optimum SNR was reached whenever the condition in eq. 3.13 was verified; i.e., if the increase of noise power (represented in this case by the signal variance in each "block"), caused by the inclusion of a new cluster, overbalanced the increase of the denominator caused by raising the number of blocks by one, then a maximum could be obtained (eq. 3.6). In other words, a maximum was reached if the variance calculated at the "block" $x + 1$ was at least twice the averaged variance calculated till the "block" x .

The main problem was that the procedure of a coherent or quasi-coherent averaging technique worked well if the noise level was small enough so that the fiducial points (in general a point in the QRS complex), as a synchronization reference, could be correctly estimated. As the locking to these fiducial points was not always exact, jitters of the signal, related to these points, occurred and introduced, in the averaging procedure, a low pass filter with a time constant $\tau = \frac{1}{\sigma}$ where σ was the square root of the jitter variance.

Furthermore, in case the SNR was very low, the fiducial points to be estimated were not exactly positioned, leading to an incorrect average. For this reason a preprocessing (BSS methods) for reducing the noise level was necessary before the average procedure.

As already mentioned BSS methods were already successfully applied in MEG and EEG recording. Since, especially in neurophysiology, time series and not observations from a certain distribution are treated, an attractive framework is the simultaneously diagonalization of appropriately defined matrices: in case of TDSEP-JD these matrices are time-delayed correlation matrices. In fact using TDSEP-JD it was possible to solve the problem of the inadequate

separation of more than one Gaussian signal, present in the ICA methods (Ziehe et al. (2000)).

The results in chapter 3.2, where TDSEP-JD outperformed the other methods, confirmed the statement aforementioned: In fact the electrophysiology in the heart involves several sources (cells) that are rather related by a temporal pattern than independent.

Many efforts were devoted to artifact cancellation and to make it an automatic procedure. Despite the large number of existing methods (see section 1.2) used for artifacts removal, few algorithms were tested with a sufficient number of subjects and exhaustive studies were made only on simulated/synthetic data.

Although a comprehensive study on the application of ICA to EEG/MEG noise and artifacts rejection has been carried out extensively, there was no general approach for ECG/MCG. Thus a systematic BSS noise reduction procedure was still missing and an adequate number of subjects had still to be enrolled.

In fact He et al. (2006) (He et al. (2006)), that applied kurtosis and a method based on the variance for detecting the continuous noise and artifacts in the ECG data, only used 10 data set from healthy subjects. Furthermore, the paper did not analyze the case of RR-interval less than 1 s and non periodic signals. In that situation problems could rise since the interval for the variance-based method was fix, and it did not depend on the RR-interval of the subject under examination.

In this thesis this problem was avoided using as reference for the calculation of the correlation the reference data (ECG/MCG data): In this way the variability and the length of the RR-interval were taken into account.

Moreover, in comparison to the other studies aforementioned, where the number of real data set estimated was very limited, here a higher number of examinations was analyzed.

In this thesis 5 BSS algorithms were first applied to 9 RMCG examinations in order to find the method to be the best in terms of cardiac signal separation and computation time. They were based on different assumptions: SOS methods (TDSEP-EVD and TDSEP-JD) were able to separate the observations that had a temporal structure even in presence of gaussian sources, whereas the other three methods (based on HOS) were able to separate sources without temporal structure, but independent and with at most one gaussian source. Another substantial difference among the algorithms was the number of parameters that had to be optimized to obtain good separation in terms of performances. Achieving a good separation was highly dependent on tuning the many parameters. Temporal Decorrelation Source Separation had

several parameters to be set: The time delays of the matrices, whose number depended on the properties of the signal to be detected. This could make the use of SOS algorithms problematic in clinical applications since changing the surrounding environment or even examination would mean to continuously update the parameters: Anyway the use of many time delays corresponding to the main characteristics yielded good performances, although not optimal (Section 2.8.3). JADE and SHIBBS could run without any parameters to be set and fICA only had two or three to be chosen (the type of approach, the step size, the possibility to have or not a fine-tune).

The key to assuring that the BSS components cleanly captured the artifact signals and separated them from the components of cardiac activity was to choose a BSS algorithm whose underlying assumptions most closely matched the physical properties of the problem at hand. Such considerations are necessary because BSS solutions could not be validated by directly measuring the cardiac activity.

Among the different methods (TDSEP-EVD, JADE, SHIBBS, fICA, TDSEP-JD), the algorithm to be compared with the standard de-noising algorithm (SVD/PCA) resulted to be TDSEP-JD. The method based on the average of the time-delayed covariance matrices and symmetric EVD (TDSEP-EVD) gave the worse results in terms of noise reduction: Its robustness with respect to the noise was poor, especially when the additive noise was large (case of ICD patients) or it was not possible to estimate precisely the covariance matrix of the noise. Furthermore, the resulting averaged matrix had to be symmetric positive definite, but this property did not always hold after averaging. The alternative approach to EVD was applying the approximate JD procedure on the time delayed matrices. This method gave better results in terms of noise reduction especially for data with low SNR.

Singular Value Decomposition and TDSEP-JD were compared. In RMCG examinations recorded in shielding room, the SNR was sufficiently high: Under this assumption there was a clear distinction between large and small eigenvalues. Since the small eigenvalues in SVD were defined to be related to the noise, the associated eigenvectors could be zeroed. As in TDSEP-JD there was no order in the unmixed data, it was impossible to *a priori* eliminate the last components as in SVD.

To resolve this problem and to further improve the SNR in SVD, methods for automatically detecting the heart signal were developed: kurtosis, beat-to-beat correlation and power spectrum of the Fourier transformed signals (Section 3.2.2). The cardiac detection procedure was

composed in several steps:

1. identification of the continuous or almost continuous noise using kurtosis, already successful for eliminating continuous noise in EEG,MEG, and ECG (Cichocki and Vorobyov (2000); Greco et al. (2005));
2. the detection of the heart beats by means of the correlation in the remaining components;
3. frequency based technique for eliminating residual mains interferences, if any.

Using the thresholds $TK_{svd} = 0.33$, $TK_{tdsep} = 0.78$ (for kurtosis) and $CT_{tdsep} = 0.99$, $CT_{svd} = 0.982$ (for the correlation), found in the identification group, good results were achieved in terms of noise reduction and automatic selection of the heart related components: The sensitivity (Table 3.5 and Table 3.6) had 100% rate successfull applying the thresholds defined above when analyzing the components only related to the cardiac activity. In case the unmixed data with mixed signals were examined, the sensitivity decreased: SVD sensitivity lowered till to 84% whereas TDSEP-JD to 96% after the application of kurtosis; if correlation was used TDSEP had a successfull rate of 77% (96% SVD). Briefly, in case the unmixed data were considered SVD had a better successfull rate than TDSEP if kurtosis was applied, but worse if the correlation was used.

Finally, for RMCG acquisitions with high SNR, SVD performed better than TDSEP although the sensitivity and the specificity related to the automatic recognition of noise and heart related components worked slightly better with TDSEP.

When applying SVD and TDSEP to SMCG the results were different in case of PSMCG or ergometer SMCG. In the former case (PSMCG) it was impossible to find a reliable threshold for the automatic identification of heart related components in SVD: This was due to SVD that was not able to completely separate cardiac signals and disturbances at high (muscular activity) and low frequency (breath, for example). For this reason, the cardiac beats (cardiac sources with low SNR) were still mixed with these extra activities, hampering the correct retrieval of the threshold and a cleaned measurement, as well. On the other hand, applying the TDSEP-JD algorithm to the 15 examinations of the identification group in PSMCG gave two different values of CT (for the rest and stress phase) with low variance. The threshold value estimated during the stress phase was higher than the one during rest ($CT_{t-rest} = 0.973$ and $CT_{t-stress} = 0.987$, respectively): The explanation could be that the number of averaged QRS complexes to be averaged in the stress phase was higher since the RR interval decreased.

In the latter case (ergometer SMCG) SVD was not able to separate the cardiac beats and the noise from the ergonomic disturbances: The orthogonality requirement for signal and noise subspaces (as in SVD) was not sufficient. Apparently, the forces applied to operate the ergometer under typical workloads produced movements and vibrations which somehow transferred to the patient bed, reaching perhaps the structure of the magnetically shielded room and the dewar gantry, thus leading to the generation of vibrations. Two dominant disturbances occurred: one at higher frequency (around 8-10 Hz) and one at lower frequency (lower than 1 Hz). In ergometer SMCG, kurtosis was not used since the number of gaussian noise sources was paltry: For this reason after the correlation procedure a further method based on the frequency was needed to eliminate the frequency-dependent disturbances, in case the first method did not succeed.

Four (TDSEP-JD, JADE, fICA, SHIBBS) out of the 5 BSS algorithms had been tested in ergometer SMCG. All methods succeeded in separating the disturbances caused by the ergometer treatment in almost all acquisitions. Among them, TDSEP-JD and SHIBBS outperformed the other methods with regard to separation quality.

The HOS methods lost some components related to T-wave since the T-wave was covered by the noise in the unmixed data and not detected by the automatic routine.

Finally in case of SMCG (PSMCG and ergometer SMCG) and RMCG (the RMCG during the PRMCG could be considered as a normal rest acquisition, that in this case had a low SNR), TDSEP-JD outperformed the other methods in terms of noise reduction and computing time.

The last application of BSS was related to patients with an already implanted ICD. Because of the properties of the ICD disturbances (partial correlation to the heart beat and respiration), the separation methods by means of correlation and kurtosis, could not be applied for completely detecting the cardiac activity in the unmixed data. Therefore, operator dependent inspection of the arithmetically averaged source signals (or unmixed data) was used to discriminate between the cardiac components and the ICD disturbances. The outcomes of the study clearly indicated that not all BSS methods were able to separate cardiac signal and disturbances from all ICD patients. The TDSEP-JD gave the better results in terms of quality of reconstruction and computational time. The success of the TDSEP-JD method compared with other methods could be due to the ICD disturbances. These might not be completely independent from the heart signal, but having a different spectrum when compared with all other sources. The TDSEP algorithm followed by EVD performed very poorly when compared

to TDSEP-JD. The bad TDSEP-EVD performance was given by the high variance of the set of matrices around the averaged time-delayed correlation matrix. The SVD performed the worst; this result had confirmed that SVD succeeded in case the SNR was not very low and the signal and noise subspace were orthogonal. The methods based on higher order statistics performed with similar results. The method validation should be performed with a higher patient population, although consistent results were already proved (Di Pietro Paolo et al. (2008)).

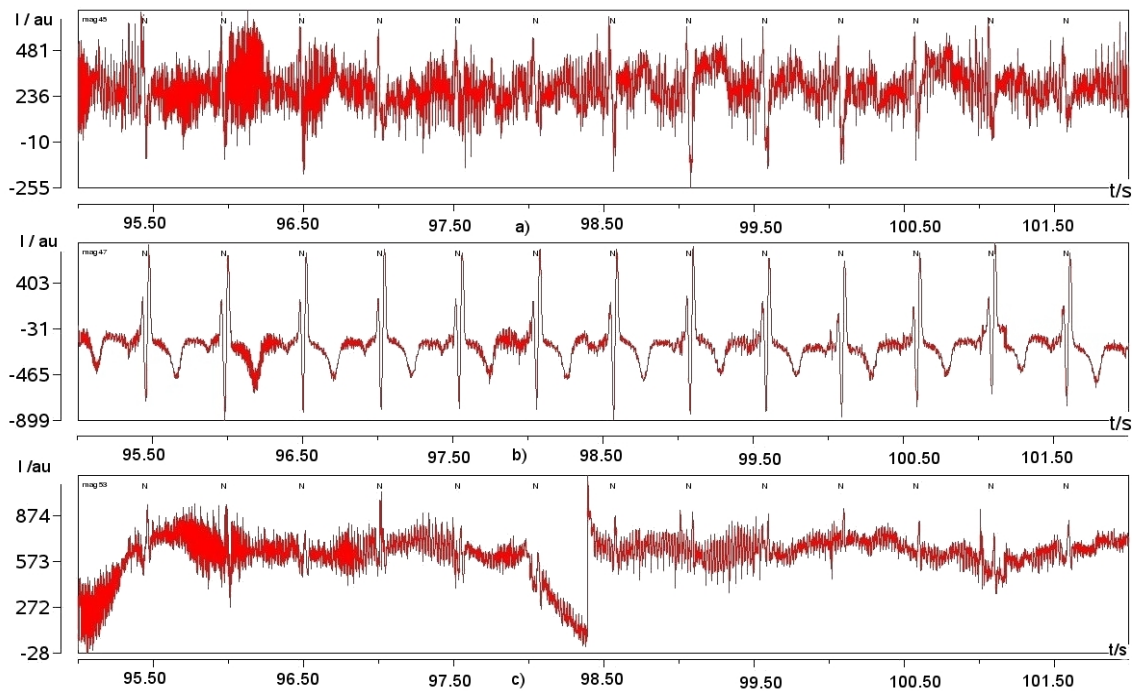


Figure 4.1: Three out of the 55 sources with different SNR. a) and c): Sources with a very low SNR, almost noise overlooked; b) sources with high SNR: in this case the sources is clearly a cardiac sources

This approach however has some limitations. One primary obstacle is that the separation between heart related and noise related data in some unmixed data after applying BSS is not very clear: There were components where it was very difficult to understand whether they were noise dominated, even by the visual inspection of the expert (Figure 4.1).

This question was addressed by the correlation-based method. As a result of applying a low threshold, the identification of these components was more accurate. However, as a side effect the specificity decreased. So the question is: How important are the the components which have been removed with noise or how much noise should be left?

The second limitation to this approach is that the important physiologic information may potentially be lost if an ergometer SMCG examination is analyzed on a patient affected by atrial

flutter or atrial fibrillation. This happens because when using FFT, the important components of the signal around 5 Hz are eliminated by the filter.

Additionally, the references to detect the heart related components, such as the simultaneously recording of ECG data or the MCG data, have to be incorporated to the acquisition in order to get more precise signal interpretation.

Another issue is that the application of SVD and ICA does not imply the existence of neighborhood relationships: Close channels are treated during the analysis as random channels, without considering the distance among them.

Furthermore, the thresholds are estimated according to the SNR of the recorded data: Their value may change if another MCG system with other characteristics is used. In this thesis, a 55 recording channels MCG system has been used: The results obtained were different if another system with other properties was used. In fact if the system does only have 8/9 channels the result would deteriorate since there are too few observations to be evaluated. On the contrary, if a system with a higher number of channels is taken into consideration, the BSS methods will have very similar results or even better to the ones got in this thesis.

Chapter 5

Conclusions

This PhD thesis set out to develop new techniques for improving the SNR in the context of MCG data.

The techniques (based on BSS and averaging procedure) were first discussed and fundamental assumptions, for having a more tractable problem, were made. Two scenarios have been examined:

- MCG data with high SNR where a novel average procedure has been used;
- MCG data with low SNR where BSS methods have been applied.

In the former case, it was for the first time mathematically proved that the SNR in averaged real data does not behave as expected, but reaches a maximum after a *selected* number of beats.

In the latter case, it was proved that among the the different BSS methods, the more suitable for noise reduction in MCG data was TDSEP. This can be explained pointing out that the MCG data have a significant temporal (and spectral) structure: a high autocorrelation among the sources. Furthermore, the use of spatial, time dependency based techniques made for the extraction of information from underlying set of measurements even in ICD patients, who hitherto could not be analyzed due to the strong disturbances.

The problem of TDSEP was that the order of the sources could not determined *a priori*: the noise related components had to be rejected by visual inspection.

In this thesis new algorithms have been developed for the automatic detection of heart related and noise related sources. The algorithms have been thoroughly tested and validated using a data base of more than 100 subjects in different noise environments.

Moreover, it was observed that separating the channels into 2 groups (each of them homogeneously distributed over the sensor area) sufficiently stabilized the estimates. Furthermore, this division of data into 2 subgroups provided as side-effect the huge improvement of the computation speed of the algorithm (last two columns of Table 3.13).

Finally, the use of synergistic methodologies such as the division of the channels into two groups (for reducing the computational time) and the application of new user-independent routines for noise reduction could be very helpful in case MCG would be used in clinical routine. In fact, in clinical environments such methods could enhance the quality of the MCG and simplify the inspection of the MCG recordings for the physicians.

It would be an interesting goal for future research to incorporate prior knowledge into the BSS models. In some preliminary studies (Barros and Cichocki (2001)), it has been observed that, when at the beginning statistically based assumptions are considered, a decomposition of electromagnetic cardiac signals into physiologically meaningful information can be reached. On the other hand, fitting cardiac sources in a classical framework, may be problematic if some temporal overlap is present in their activations. This limitation has to be addressed since patients with cardiac pathologies should be included in the study. In fact, the hypothesis of strict periodicity of the heart signal may influence the performances. Hence, a well balanced use of both, the model and appropriate *a priori* information, will yield a powerful exploratory decomposition technique that is able to extract meaningful information from high-dimensional biomedical data.

List of Figures

1.1	Percentage of death caused by heart disease: Heart disease is the first cause of death in USA according to the National Center for Health Statistic. The trend is the same in almost all industrialized countries (Anderson (2002))	2
1.2	Examples of biomedical applications for Blind Signal Processing (BSP) such as biomedical signals acquired with multi-electrode/channel devices: a) Enhancement of low-level ECG components, noise reduction in EMG signals, separation of residual original heart signal from the transplanted heart signal, separation of heart sounds from gastrointestinal acoustic phenomena, separation of heart sounds from lung sounds, cancellation or reduction of artifacts; b) blind separation of the fetal electrocardiogram (FECG) and maternal electrocardiogram from skin electrode signals recorded from a pregnant woman (Cichocki and Amari (2002))	8
1.3	A schematic representation of the position of the ICD in the patient torso. Overlapped the sensor arrangement of a patient with ICD: Note the different properties of the signal according to the relative position with the ICD	11
2.1	Comparison of selected biomagnetic fields and environmental disturbances: Note the amplitude of the heart MF when compared to the earth magnetic field and urban noise (Vrba (1996))	14
2.2	a) A uniform double-layer model of cardiac activity; b) Another double layer model of the cardiac activity where also the tangential part of the current distribution is shown. These tangential currents produce a MF, but their electrical field is silent (Wikswow et al. (1982))	15

2.3	Electrophysiology of the heart: the relationship between the spread of cardiac electrical activation represented at various time instants by a summing vector and the genesis of the MCG/ECG is shown (Webster (1992))	17
2.4	Schematic illustration of the coupling with a magnetometer, L_i inductance of the antenna and L inductance of the SQUID loop (Andrä and Nowak (2007)) .	18
2.5	Schematic illustration of the coupling with a first order gradiometer, L_i inductance of the antenna and L inductance of the SQUID loop (Andrä and Nowak (2007))	19
2.6	a) Magnetometer (detection of B_z) and different types of gradiometers: b) symmetric gradiometer of the first order (detection of $\delta B_z/\delta z$), c) asymmetric gradiometer of the first order (detection of $\delta B_z/\delta z$), and d) planar gradiometer of the first order (detection of $\delta B_z/\delta x$) (Andrä and Nowak (2007))	19
2.7	Biomagnetic system at the University of Jena: View from the preparation room into the acquisition room with patient support and sensor system	23
2.8	Ergometer used for stress acquisitions at the University of Ulm	24
2.9	Graphical representation of the first steps of the beat detection procedure: In blue the quantity $e(t)$ is drawn, in red a cardiac heart beat $S(t)$ rescaled to $e(t)$. The two vertical lines represent the beginning and the end of the first template $T_0(t)$	31
2.10	Time series of the heart beat signal in 3 out of the 55 channels: The markers in green correspond to the beat suitable for the average, the red ones to the beats that are not used since too noisy, or with a big drift	33
2.11	Schematic illustration of a dendrogram which is the graphical representation of the cluster analysis. Following the arrows at each node, the largest group of beats with the smallest similarity distance is found and thus the starting point for function SNR. The horizontal axis represents the observations (beats), the vertical axis gives the distance (or dissimilarity measure)	34

2.12 Cocktail party example: Two persons are talking simultaneously in a room (like at a cocktail party), a third person is trying to follow one of the discussions. The human brain can handle this sort of auditory source separation problem, but it is a very tricky problem in digital signal processing. In case the number of microphones is equal or larger than the people speaking, ICA is able to extract the source signals from any set of two or more measured signal mixtures (Stone (2004))	37
2.13 The four basic approaches of blind source separation; each approach exploits a particular property of the source: ICA (orange) exploits the independence among sources using the mutual independence; the methods based on the second order use the temporal structure of the data (green); in case the data are not stationary the time-varying variance is used if it does not change fast (blue); the fourth approach exploits the various diversities (yellow). The arrows indicate the possibility of combining or integrating the all above approaches in order to separate or extract sources with various statistical properties and to reduce the influence of noise and undesirable interferences (Cichocki and Amari (2002)) . .	38
2.14 General ICA model: The matrix S represents m independent sources, the constant matrix $A [m \times m]$ the linear mixing of the sources, and $X [m \times n]$, with $m \leq n$ a linear mixture of the sources, i.e., the observations. ICA produces an unmixing matrix W , which unmixes the measurements in order to yield an estimation of the found components $\hat{s}(t)$ (James and Hesse (2005))	42
2.15 Geometrical interpretation of the difference between ICA and SVD: a) Original random sources, b) sources after a linear mixture, c) after the process of uncorrelatness, d) sources after application of ICA	49
2.16 Averaged unmixed data before (in blue) and after the application of the 50 Hz filter (red)	52
2.17 Three unmixed data/sources with different values of frequency: The first picture represents the ergometer noise with a frequency peak of 8.5Hz modulated with a lower frequency signal, the second one corresponding to the QRS complex circa 35 Hz and the last one circa 1Hz. The labels N and N_V correspond to the QRS activity	53

- 3.1 Schematic illustration of the SNR function $R(S/N)$. The values in the ordinate represent the ratio (R) between the signal (S) and the noise (N) according to the number of epochs: (a) the function $R(S/N)$ grows with the square root of the epochs/clusters, reaching its maximum at the extreme case of all clusters used (single-element cluster). This happens in case identical signals and stationary, normally distributed noise are used; (b) For non stationary noise, the function $R(S/N)$ can have its maximum either at the maximum number of epochs (single-element cluster)(a) or at c_{max} : number of epochs/clusters, the maximum SNR is achieved 56
- 3.2 Two representative dendrograms of two patients with different characteristics are shown. The knots indicate where two clusters or group of clusters merge: a) Dendrogram of a measurement where the noise is homogeneous and there is not so much variability among the beats: The dendrogram is in fact almost symmetric; b) Dendrogram coming from a measurement where the beats have a higher level of variability: It is possible to see two main branches, one that contains almost all beats and the other one containing the beats with either more variability or with different shape 59
- 3.3 Two representative overlay plots of 56 averaged signals from the same data set, but with different noise characteristics: a) average calculated over 4 beats shown in the Figure 3.2b, using the left smaller branch b) average calculated over 4 out of the beats shown in the Figure 3.2b using the right bigger branch. The vertical green lines show the markers calculated on the averaged signals: Q-onset, R-peak, Q-end, T-wave, and T-end are visible 60
- 3.4 Raw data of an examination in moderate shielding room: in the first row a channel with low SNR, in the second row a channel with high SNR. The label N stands for Normal beats, the label N_v for normal visual beats 61
- 3.5 Two representative averaged channels with (blue line) and without cluster analysis (red line): a) Channel with low SNR: the signal amplitude after the selection procedure (118 beats out of 273) is greater than in the conventional averaging (all 274 beats); b) Channel with high SNR is shown: using all beats or a subset of them does not make almost any difference 62

- 3.6 Five out 55 sources detected by fICA from a 300s measurement (The label N is in correspondence of the QRS-complexes): There are different kinds of sources related to the cardiac activity: In the first panel the P-wave is clearly visible, in the second and fourth panels the QRS-complex, in the third panel the unmixed data related to T-wave. In the last panel, gaussian noise. The number on the left in each panel corresponds to the channel where the source was found . . . 64
- 3.7 Sources with different values of kurtosis: a) and c) Heart related components; b) and d) non gaussian distribution noise; e) continuous noise 68
- 3.8 Minimum kurtosis value related to cardiac activity in 25 volunteers: The red color is related to the kurtosis values after computing SVD and its error bars, the blue color to the kurtosis values after computing TDSEP and its error bar, the magenta color is TK_{TDSEP} , the green color TK_{SVD} 69
- 3.9 Cardiac sources of the subject 4 in Table 3.3 with different correlations in an examination carried out in noisy environment: a) Correlation value: 1.00 b) Correlation value: 0.981 (this is the minimum correlation value associated with cardiac activity) and c) Correlation value: 0.994 71
- 3.10 Minimum correlation value related to cardiac activity in 25 volunteers: The red curve is related to the correlation value after computing SVD and its error bar, the blue curve to the correlation value after computing TDSEP and its error bar, the magenta curve to the CT_{tdsep} , the green curve to the CT_{svd} 71
- 3.11 Minimum kurtosis value (with error bar) related to the cardiac activity after the application of SVD in 15 patients: The red line is related to the kurtosis value at rest, the blue one to the kurtosis value after stress. The values of SD (error bars) are high, especially when considering the stress case (0.58 vs 0.40) 72
- 3.12 Minimum kurtosis value (with error bar) related to the cardiac activity after the application of TDSEP in 15 patients: The red line is related to the kurtosis value at rest, the blue one to the kurtosis value after stress. The values of SD (error bars) are high, in case of rest MCG even higher than the mean value . . 73
- 3.13 Minimum Correlation value (with error bar) related to the cardiac activity after the application of SVD in 15 volunteers: The red line is related to the correlation value at rest, the blue one to the correlation value during stress. The values of SD (error bars) are high, especially when considering the stress case (0.35) . . . 74

- 3.14 Minimum Correlation value related to cardiac activity in 15 volunteers with error bar after the application of TDSEP: The red curve is related to the correlation value at rest, the blue one to the correlation value during stress. The values of SD are much lower than in SVD (see Figure 3.13): 0.025 and 0.013 at rest and during stress, respectively 74
- 3.15 Time display of the two channels with maximum (upper row) and minimum amplitude (lower row) at R-peak: a) signal with high SNR; b) signal with low SNR; c) Spatio-Temporal representation of the averaged 55 channels in Figure 3.15a: The MF map corresponds to the time instant Q-max (i.e. red line in Figure 3.15a); d) color bar of the MF amplitude related to Figure c); e) MF map corresponding to the time instant Q-max (i.e. red line in Figure 3.15b); f) color bar of the MF amplitude related to Figure e). Note that the MF amplitude in the signal with high SNR is 10 times higher than the MF in the signal with low SNR 76
- 3.16 Three out of the 55 sources using SVD in two examinations a) unmixed data coming from a measurement with low SNR. Upper row: cardiac signal; middle panel: sources with both cardiac and noise signals; lower panel: gaussian noise b) unmixed data coming from a measurement with high SNR. Upper row: gaussian noise; middle panel: cardiac signal; lower panel: cardiac signal 77
- 3.17 Three out of the 55 sources using TDSEP in two examinations a) unmixed data coming from a measurement with low SNR. Upper row: disturbances; middle panel: cardiac signal; lower panel: gaussian noise; b) unmixed data coming from a measurement with high SNR. Upper row: cardiac signal (T-wave); middle panel: cardiac signal (R-peak); lower panel: gaussian noise 78
- 3.18 a) Cleaned signals (SVD) in an examination with low SNR (compare to Figure 3.15b) b) Cleaned signals (SVD) in an examination with high SNR (compare to Figure 3.15a) 79
- 3.19 a) Cleaned signals (TDSEP) in an examinations with low SNR (compare to Figure 3.15b) b) Cleaned signals (TDSEP) in an examination with high SNR (compare to Figure 3.15a) 79

3.20	a) Raw RMCG: in the upper panel a channel with low SNR: Patients artifacts and drifts are displayed; the lower panel displays the channel with maximum amplitude b) Cleaned RMCG signal using TDSEP: the disturbances in 3.20a (upper panel) are vanished, in the channel with maximum amplitude an improvement of the SNR is evident	80
3.21	a) Raw SMCG: in the upper panel a channel with low SNR: Patients artifacts, drifts are displayed; the lower panel displays the channel with maximum amplitude b) Cleaned SMCG signal using TDSEP: the disturbances in 3.21a (upper panel) are vanished, in the channel with maximum amplitude the application of TDSEP caused a drop of the SNR	81
3.22	a) Spectrum of SMCG data before (green) and after (black dots) ICA cleaning in the channel with maximum R-peak amplitude. The arrow indicates the vanishing of the peak between 8 and 9 Hz and below 1 Hz b) Spectrum of rest measurement (rescaled for direct comparison to (a))	82
3.23	Differences in noise reduction in an ergometer SMCG (patient no. 9) using a overlay display: a) Averaged stress measurement with ergometer movement; b) Averaged stress examination after the application of SHIBBS: Note the lower amplitude of T-wave when compared to Figure e); c) Averaged stress examination after the application of SVD: The high frequency disturbances are still present; d) Averaged stress examination after the application of JADE: Note the lower amplitude of T-wave when compared to Figure e); e) Averaged stress examination after the application of TDSEP, f) Averaged stress examination after the application of fICA (using as contrast function the hyperbolic tangent): In this case not only the T-wave has a lower amplitude, but the noise level is higher and power-line noise has been introduced	84
3.24	Differences in noise reduction in an ergometer stress data set in 3 out of the 55 channels. The original averaged raw measurement (green) is compared with the results of the cleaning procedure by applying the BSS and SVD (cyan) methods: a) channel with low SNR); b) channel with maximum positive R-peak; c) channel with maximum negative R-peak	85
3.25	Representative channel showing the interferences caused by the batteries contained in the ICD	86

3.26	Average time signal display of 4 out of the 56 unmixed data components from measurement of patient number six: a) and b) sources representing ICD disturbances, c) the main heart related component d) gaussian noise	86
3.27	Averaged signal before and after the application of TDSEP-Joint: Note the difference in the interval [Q-onset-30, Q-onset] between the two averaged signals: The interval of interest is zoomed	87
3.28	Averaged Signal: sensors arrangement	89
3.29	Averaged Signals: In green are shown the cleaned signals, in red the signals with ICD interferences: the disturbances caused by the ICD disappear	90
3.30	Illustration of QRS fragmentation in two patients: a) QRS fragmentation of a shocked patient, b) QRS fragmentation of a patients that did not shock: Note the difference in the fragmentation level into the two cases	91
4.1	Three out of the 55 sources with different SNR. a) and c): Sources with a very low SNR, almost noise overlooked; b) sources with high SNR: in this case the sources is clearly a cardiac sources	99

List of Tables

1.1	Possible contaminations of a MCG recording and their nature: for each of them the frequency range and time duration are shown	4
2.1	Biomagnetic acquisition systems with name, location and number of channels .	21
2.2	Biomagnetic system acquisitions: Dimensions	22
2.3	Ergometer stress data acquisition: protocol	26
2.4	Protocol of pharmacological stress data acquisition: In bold the acquisition intervals used in the data analysis	27
3.1	<i>Number of components and time necessary to get the unmixed data in 9 patients using five BSS algorithms: G means that the measurement is performed with a gradiometer system, M a magnetometer system is used. One group: All the channels are used simultaneously; two groups: The channels are divided into two groups</i>	65
3.2	Kurtosis in five different sources computed with (second column) and without (first column) histogram	67
3.3	Minimum value of correlation with cardiac activity in the sources: CM1 ($avg = 0.99$ and $\sigma = 0.01$), CM2 ($avg = 0.61$ and $\sigma = 0.14$), CM3 ($avg = 0.51$ and $\sigma = 0.15$). The correlation values with CM1 have lower variability (10 times lower) than the ones obtained by CM2 and CM3. The subject 4 is highlighted since this examination is used for the Figure 3.9	70
3.4	Kurtosis thresholds in PSMCG with SDs	73
3.5	Sensitivity and specificity for Kurtosis: (C) The sensitivity is computed on cardiac related components, (M) the sensitivity is computed on mixed related components	78

3.6	Sensitivity and specificity for correlation: (C) The sensitivity is computed on cardiac related components, (M) the sensitivity is computed on mixed related components	79
3.7	Sensitivity and specificity for Correlation at rest and during stress	80
3.8	Percentage of noise reduction in the 12 subjects: The label "No" for subject 8 means that for that subject data the algorithm did not converge. The highlighted column indicates the noise reduction values for the data drawn in Figure 3.23 .	83
3.9	Percentage of noise reduction in the 6 subjects: The label No indicates those algorithms where the separation was not successful	88
3.10	Computation time of 5 algorithms: SVD and TDSEP have lower CpT compared to HOS methods. FICA show intermediate CpT. SHIBBS and JADE need more than one hour for extracting the sources	91
3.11	Computation time of the 5 algorithms: see table 3.10. In this case a 300s examination is used: The computational time is circa tripled when compared to the results of the 100s measurement	91
3.12	Computation time of the two algorithms, note that a 5 min measurement (300 s) is performed within 2 min	92
3.13	Computation time of the 5 algorithms with different processors. SVD and TDSEP had the better results. HOS methods, specially the ones based on the cumulants have dramatically reduced the computational load when comparing this results with the one in table 3.11	92

Bibliography

- S. Achenbach, W. Moshage, M. Flüg, D. Ropers, V. Schibgilla, and K. Bachmann. Vergleich der Time-Domain-Analyse von Late Potentials im signalgemittelten Elektrokardiogramm und Magnetokardiogramm. *Biomed Tech*, 41:298–299, 1996.
- R. N. Anderson. Deaths: Leading Causes for 2000. *National Vital Statistics Report*, 50(16): 1–86, 2002.
- W. Andrä and H. Nowak. *Magnetism in Medicine: A Handbook*. Wiley-VCH Verlag, 2007.
- A. Azemi, V. R. Sabzevari, M. Khademi, H. Gholizade, A. Kiani, and Z. S. Dastgheib. Intelligent arrhythmia detection and classification using ICA. In *Eng Med Biol Soc, 2006. EMBS '06. 28th Annual International Conference of the IEEE*, volume Suppl., pages 2163–2166. IEEE Service Center, 2007.
- G. H. Bardy, K. L. Lee, D. B. Mark, J. E. Poole, D. L. Packer, R. Boineau, M. Domanski, C. Troutman, J. Anderson, G. Johnson, S. E. McNulty, N. Clapp-Channing, L. D. Davidson-Ray, E. S. Fraulo, D. P. Fishbein, R. M. Luceri, and J. H. Ip. For the sudden cardiac death in heart failure trial investigators: Amiodarone or an implantable cardioverter-defibrillator for congestive heart failure. *N Eng J Med*, 325:225–237, 2005.
- A. C. Barros, A. Mansour, and N. Ohnishi. Removing artifacts from electrocardiographic signals using Independent Component Analysis. *Neural Comput*, 22:173–186, 1998.
- A. K. Barros and A. Cichocki. Extraction of specific signals with temporal structure. *Neural Comput*, 13(9):1995–2003, 2001.
- G. Baule and R. McFee. Detection of the magnetic field of the heart. *Am Heart J*, 66:95–96, 1963.

- A. J. Bell and T. J. Sejnowski. An information maximization approach to blind separation and blind deconvolution. *Neural Comput*, 7:1129–1159, 1995.
- K. Brockmeier, L. Schmitz, J. De Jesus Bobadilla Chavez, M. Burghoff, H. Koch, R. Zimmermann, and L. Trahms. Magnetocardiography and 32-lead potential mapping: repolarization in normal subjects during pharmacologically induced stress. *J Cardiovasc Electr*, 8:615–626, 1997.
- M. Burghoff and P. VanLeeuwen. Separation of fetal and maternal magnetocardiographic signals in twin pregnancy using Independent Component Analysis. *Neurol Clin Neurophysiol*, 39, 2004.
- M. Buxton, N. Caine, D. Chase, D. Connelly, A. Grace, C. Jackson, J. Parkes, and L. Sharples. A review of the evidence on the effects and costs of implantable cardioverter defibrillator therapy in different patient groups, and the modeling of cost-effectiveness an cost-utility for these groups in a UK context. *Health Technol Assess*, 10(27):1–180, 2006.
- M. E. Cain, J. L. Anderson, M. F. Arnsdorf, J. W. Mason, M. M. Scheinman, and L. Waldo. ACC expert document: Signal-averaged electrocardiography. *JACC*, 27(1):238–249, 1996.
- J.-F. Cardoso. High order contrast for Independent Component Analysis. *Neural Comput*, 11: 157–192, 1999.
- J.-F. Cardoso and A. Souloumiac. Jacobi angles for simultaneous diagonalization. *SIAM J Matrix Anal A*, 17(1):161–164, Jan. 1996.
- T. Chow, S. Saghir, C. Bartone, M. Goebel, J. Schneider, T. Booth, and P. S. Chan. Usefulness of microvolt T-wave alternans on predicting outcome in patients with ischemic cardiomyopathy with and without defibrillators. *Am J Cardiol*, 100(4):598–604, 2007.
- A. Cichocki and S. I. Amari. *Adaptive Blind Signal and Image Processing*. John Wiley & Sons, New York Inc, 2002.
- A. Cichocki and S. Vorobyov. Application of ica for automatic noise and interference cancellation in multisensory biomedical signals, 2000.
- D. Cohen, E. A. Edelsack, and J. E. Zimmerman. Magnetocardiograms taken inside a shielded room with a superconducting point-contact magnetometer. *Appl Phys Lett*, 16:178–280, 1970.

- S. Comani, D. Mantini, P. Pennesi, A. Lagatta, and G. Cancellieri. Independent Component Analysis: fetal signal reconstruction from magnetocardiographic recordings. *Comput Meth Prog Bio*, 75(2):163–177, 2004.
- S. Comani, van Leeuwen P, S. Lange, D. Geue, and D. Grnemeyer. Processing the fetal magnetocardiogram: comparison of methods based on independent component analysis (ica) and component subtraction. *Biomed Tech*, 54:29–37, 2009.
- P. Comon. Independent Component Analysis- a new concept? *Signal Process*, 36:287–314, 1994.
- W. Craelius, M. Restivo, M. A. Assadi, and N. El-Sherif. Criteria for optimal averaging of cardiac signals. *IEEE T Biomed Eng*, 33:957–966, 1986.
- T. W. Dawson, M. A. Stuchly, K. Caputa, A. Sastre, R. B. Shepard, and R. Kavet. Pacemaker interference and low-frequency electric induction in humans by external fields and electrodes. *IEEE T Biomed Eng*, 47:1211–1218, 2000.
- L. de Lathauwer, D. Callaerts, B. de Moor, and J. Vandewalle. Fetal electrocardiogram extraction by source subspace separation. In *In Proc. IEEE Workshop on HOS*, pages 134 – 138, June 1995.
- L. de Lathauwer, B. de Moor, and J. Vandewalle. Fetal electrocardiogram extraction by blind source subspace separation. *IEEE T Biomed Eng*, 47(5):567–572, 2000.
- L. De Lathauwer, B. de Moor, J. Vandewalle, and J.-F. Cardoso. Independent Component Analysis of largely underdetermined mixtures. In *Proc. 4th Int. Symp. on Independent Component Analysis and Blind Signal Separation (ICA 2003)*, pages 29–34, Nara, Japan, April 2003.
- A. Delorme, S. Makeig, and T. Sejnowski. Automatic artifact rejection for eeg data using high-order statistics and independent component analysis. In *International workshop on ICA (San Diego, CA)*, 2001.
- A. Delorme, T. Sejnowski, and S. Makeig. Enhanced detection of artifacts in eeg data using higher-order statistics and independent component analysis. *NeuroImage*, 34:1443–1449, 2007.

- F. Deprettere. *SVD and Signal Processing: Algorithms, Analysis and Applications*. Elsevier Science Publishers, Amsterdam, 1988.
- D. Di Pietro Paolo, H.-P. Müller, and S. N. Erne. A novel approach for the averaging of magnetocardiographically recorded heart beats. *Phys Med Biol*, 50(10):2415–2426, 2005.
- D. Di Pietro Paolo, H.-P. Müller, G. Nolte, and S. N. Erne. Noise reduction in magnetocardiography by Singular Value Decomposition and Independent Component Analysis. *Med Biol Eng Comput*, 44(6):489–499, 2006a.
- D. Di Pietro Paolo, H.-P. Müller, W. Tedeschi, M. DeMelis, and S. N. Erne. Comparison of BSS algorithms in SMCG data. In *International Congress Series 1300 (Biomag2006)*, pages 213–216, August 2006b.
- D. Di Pietro Paolo, H.-P. Müller, W. Tedeschi, J. W. Park, F. Jung, and S. N. Erne. Noise reduction in CHD patients by means of BSS. In *International Congress Series 1300 (Biomag2006)*, pages 217–20, August 2006c.
- D. Di Pietro Paolo, M. Schlosser, M. Goernig, and S. N. Erne. Biomagnetic risk stratification by QRS-fragmentation in patients with implanted cardioverter defibrillators. In *Proc. of the International Conference on Electrocardiology*, page in press, Saint Petersburg, Russia, 2008.
- D. Di Pietro Paolo, H.-P. Müller, M. Görnig, J. Haueisen, and S. N. Erne. Cardiac signal extraction in patients with implantable cardioverter defibrillators. *Med Eng Phys*, in press: –, 2009.
- S. Dutz, M. E. Bellemann, U. Leder, and J. Haueisen. Passive vortex currents in magneto- and electrocardiography: comparison of magnetic and electric signal strengths. *Phys Med Biol*, 51(1):145–151, 2006.
- P. Endt, H.-D. Hahlbohm, D. Kreiseler, M. Oeff, U. Steinhoff, and L. Trahms. Fragmentation of bandpass-filtered QRS-complex of patients prone to malignant arrhythmia. *Med Biol Eng Comp*, 36:723–728, 1998.
- S. N. Erne. High resolution magnetocardiography: modeling and sources localization. *Med Biol Eng Comput*, 23:1447–1450, 1985.

- S. N. Erne, R. Fenici, H.-D. Hahlbohm, W. Jaszczyk, H.-P. Lehmann, and M. Masselli. High-resolution magnetocardiographic recordings of the ST segment in patients with electrical late potentials. *Il Nuovo Cimento D*, 2(2):340–345, 1983.
- S. N. Erne, L. Trahms, and Z. Trontelj. Clustering - a novel approach for selected averaging of biomagnetic signals. In K. Atsumi, M. Kotani, S. Ueno, T. Katila, and S. J. Williamson, editors, *Biomagnetism*, pages 298–301. Tokyo Denki University Press, 1987.
- S. N. Erne, A. Pasquarelli, H. Kammrath, S. Della Penna, K. Torquati, V. Pizzella, R. Rossi, C. Granata, and M. Russo. Argos55 - the new MCG system in Ulm. In *Proceeding of the 12th International Conference on Biomagnetism*, pages 27–30, Sendai, Japan, 1998.
- R. Fenici, G. L. Romani, and S. N. Erne. High-resolution magnetic measurements of human cardiac electro-physiological events. *Il Nuovo Cimento D*, 2(2):231–247, 1983.
- R. Fenici, G. Melillo, A. Capelli, C. DeLuca, and M. Masselli. Magnetic localisation of a pacing catheter. In S. J. Williamson, M. Hoke, G. Stroink, and M. Kotani, editors, *Advances in Biomagnetism*, pages 361–364. New York, Plenum Press, 1989.
- M. Ferdjallah and R. E. Barr. Frequency-domain digital filtering technique for the removal of power-line noise applications to electrocardiogram. *Comput Biomed Res*, 23:473–489, 1990.
- J. R. Glover. Comments on *Digital filters for real-time ECG signal processing using microprocessors*. *IEEE T Biomed Eng*, 34:962, 1987.
- G. Gomez-Herrero and E. Huupponen. Blind Source Separation techniques for processing electroencephalographic recordings. Technical report, Department of Signal Processing, Tampere university of Technology, September 2004.
- A. Greco, N. Mammone, f C Morabito, and M. Versaci. Kurtosis, renyis entropy and independent component scalp maps for the utomatic artifact rejection from eeg data. *IJBS ISSN 1306-1216*, 1:12–16, 2005.
- T. He, G. Clifford, and L. Tarassenko. Application of Independent Component Analysis in removing artefacts from the electrocardiogram. *Neural Comput Appl*, 15(2):105–116, Apr. 2006.

- K. E. Hild, G. Alleva, S. Nagarajan, and S. Comani. Performance comparison of six Independent Component Analysis algorithms for fetal signal extraction from real fMCG data. *Phys Med Biol*, 52(2):449–462, 2007.
- S. H. Hohnloser, T. Klingenhöfen, Y. G. Li, M. Zabel, J. Peetermans, and R. J. Cohen. T-wave alternans as a predictor of recurrent ventricular tachyarrhythmias in ICD recipients: Prospective comparison with conventional risk markers. *J Cardiovasc Electr*, 9:1258–1268, 1998.
- M. Hoke, B. Ross, R. Wickesberg, and B. Lutkenhoner. Weighted averaging—theory and application to electric response audiometry. *Electroen Clin Neuro*, 57(5):484–489, 1984.
- D. Hoyer, E. Heinicke, S. Jaekel, F. Tetschke, D. Di Pietro Paolo, J. Haueisen, E. Schleuner, and U. Schneider. Indices of fetal development derived from heart rate patterns. *Early Hum Dev*, 85(6):379–86, 2009.
- R. Hren, U. Steinhoff, C. Gessner, P. Endt, P. Goeddle, R. Agrawal, M. Oeff, R. L. Lux, and L. Trahms. Value of magnetocardiographic QRST integral maps in the identification of patients at risk of ventricular arrhythmias. *Pace*, 22:1292–1304, 1999.
- J. C. Huhta and G. Webster. 60hz interference in electrocardiography. *IEEE T Biomed Eng*, 20(2):91–101, 1973.
- A. Hyvärinen. Independent Component Analysis: Algorithms and applications. *Neural Networks*, 13(4-5):411–430, 2000.
- A. Hyvärinen. Survey on Independent Component Analysis. *Neural Computing Surveys*, 2: 94–128, 1999.
- A. Hyvärinen, J. Sürelä, and R. Vigario. Spikes and bumps: Artefacts generated by Independent Component Analysis with insufficient sample size. In *Proc. Int. Workshop on Independent Component Analysis and Blind Signal Separation (ICA '99)*, pages 425–429, 1999.
- A. Hyvärinen, J. Karhunen, and E. Oja. *Independent Component Analysis*. John Wiley & Sons, New York Inc, 2001.
- C. J. James and C. W. Hesse. Independent Component Analysis for biomedical signals. *Physiol Meas*, 26:15–39, 2005.

- R. Jane, H. Rix, P. Caminal, and P. Laguna. Alignment methods for averaging of high-resolution cardiac signals: a comparative study of performance. *IEEE T Biomed Eng*, 38: 571–579, 1991.
- I. T. Joliffe. *Principal Component Analysis*. Springer, New York, 1986.
- T.-P. Jung, C. Humphries, T.-W. Lee, M. J. McKeown, V. Iragui, S. Makeig, and T. J. Sejnowski. Removing electroencephalographic artefacts by Blind Source Separation. *Psychophysiology*, 37:163–178, 2000a.
- T.-P. Jung, S. Makeig, T.-W. Lee, M. J. McKeown, G. Brown, A. J. Bell, and T. J. Sejnowski. Independent Component Analysis of biomedical signals. In *Proceeding of the 2nd International Workshop on Independent Component Analysis and Signal Separation*, Helsinki, Finland, 2000b.
- A. Kandori, H. Kanzaki, K. Miyatake, S. Hashimoto, S. Itoh, N. Tanaka, T. Miyashita, and K. Tsuda. A method for detecting myocardial abnormality by using a total current-vector calculated from ST-segment deviation of a magnetocardiogram signal. *Med Biol Eng Comput*, 39:21–28, 2001.
- K. Kobayashi, Y. Uchikawa, T. Simizu, K. Nakai, and M. Yoshizawa. The rejection of magnetic noise from the wire using Independent Component Analysis for magnetocardiogram. *IEEE T Magn*, 41(10):4152–4154, 2005.
- H. Koch. SQUID magnetocardiography: Status and perspectives. *IEEE T Appl Supercon*, 2(1):49–59, 2001.
- P. Korhonen, T. Husa, I. Tierala, H. Väänänen, M. Mäkijärvi, T. Katila, and L. Toivonen. Increased intra-QRS fragmentation in magnetocardiography as a predictor of arrhythmic events and mortality in patients with cardiac dysfunction after myocardial infarction. *J Cardiovasc Electr*, 17(4):396–401, 2006.
- O. Kosch, P. Meindl, U. Steinhoff, and L. Trahms. Physical aspects of cardiac magnetic fields and electric potentials. In *Proc. of the 12th int. conf. on Biomagnetism*, pages 553–556, August 2000.
- P. Lander, E. J. Berbari, and R. Lazzara. Optimal filtering and quality control of signal-averaged ECG. *Circulation*, 91(5):1495–1505, 1995.

- U. Leder., L. Frankenstein, J. Haas, V. Baier, J. Haueisen, H. Nowak, and H. R. Figulla. Temporal properties of high frequency intra-QRS signals in myocardial infarction and healthy hearts. *Biomed Tech*, 45:243–247, 2000.
- H. N. Lee, T. S. Park, S. Y. Lee, and Y. Huh. Spatial filters based on independent component analysis for magnetic noise reduction in the magnetocardiogram. *Med. Biol. Eng. Comput.*, 42:532–534, 2004.
- M. Liehr, J. Haueisen, M. Görnig, P. Seidel, J. Nenonen, and T. Katila. Vortex shaped current sources in a physical torso phantom. *Ann Biomed Eng*, 33(2):240–247, 2005.
- A. Link, L. Trahms, R. Zimmermann, and M. Oeff. Complex binomial bandpass filters for analysis phase and envelope of high frequency components in cardiac signals. *Computer in Cardiology*, pages 617–629, 1994.
- B. Lutkenhoner, M. Hoke, and C. Pantev. Possibilities and limitations of weighted averaging. *Biol Cybern*, 52:409–416, 1985.
- M. Mäkijärvi, J. Montonen, L. Toivonen, P. Siltanen, M. Nieminen, M. Leiniö, and T. Katila. Identification of patients with ventricular tachycardia after myocardial infarction by high-resolution magnetocardiography and electrocardiography. *J. Electrocardiol*, 26:117–124, 1993.
- K. Matsuoka, M. Kawamoto, and M. Kawamoto. A neural net for blind separation of nonstationary signals. *Neural Networks*, 3(8):411–419, 1995.
- C. D. McManus, K. D. Neubert, and E. Cramer. Characterization and elimination of AC noise in electrocardiograms: a comparison of digital filtering methods. *Comput Biomed Res*, 26(1):48–67, 1993.
- L. Molgedey and H. G. Schuler. Separation of mixture of independent signals using time delayed correlations. *Phys Rev Lett*, 23(72):3634–3637, 1994.
- J. Montonen. Magnetocardiography in identification of patients prone to malignant arrhythmias. In C. Baumgartner, L. Deecke, G. Stroink, and S. J. Williamson, editors, *Biomagnetism: Fundamental research and clinical applications*, pages 606–610. IOS Press, 1995.

- J. Montonen, M. Mäkijärvi, M. Paavola, M. Leiniö, P. Siltanen, and T. Katila. Comparison of time domain and spectrotemporal domain analysis of high resolution magneto- and electrocardiographic recordings of myocardial infarction patients with and without ventricular tachycardia. In C. Baumgartner, L. Deecke, G. Stroink, and S. J. Williamson, editors, *Biomagnetism: Fundamental research and clinical applications*, pages 624–627. IOS Press, 1995.
- D. W. Mortara. Digital filters for signals ECG. *IEEE Comp. in Cardiology*, pages 511–514, 1977.
- W. Moshage, K. Göhl, S. Achenbach, B. Seese, S. Schneider, and K. Bachmann. Ablation of idiopathic ventricular tachycardias and accessory conduction pathways guided by multi-channel MCG. In C. Baumgartner, L. Deecke, G. Stroink, and S. J. Williamson, editors, *Biomagnetism: Fundamental research and clinical applications*, pages 599–601. IOS Press, 1995.
- A. J. Moss, H. Greenberg, R. B. Case, W. Zareba, W. J. Hall, M. Brown, J. P. Daubert, S. McNitt, M. L. Andrews, and A. D. Elkin. For the multicenter automatic defibrillator implantation trial-ii research group: Long-term clinical course of patients after termination of ventricular tachyarrhythmia by an implanted defibrillator. *Circulation*, 110:3760–3765, 2004.
- R. Mühler and H. von Specht. Reduction of background noise in human auditory brainstem response by means of classified averaging. In J. Syka, editor, *Acoustical Signal Processing in the Central Auditory System*, pages 599–604. New York, Plenum Press, 1996.
- R. Mühler and H. von Specht. Sorted averaging-principle and application to auditory brainstem responses. *Scand Audiol*, 28(3):145–149, 1999.
- H.-P. Müller, P. Gödde, K. Czerski, M. Oeff, R. Agrawal, P. Endt, W. Kruse, U. Steinhoff, and L. Trahms. Magnetocardiographic analysis of the two-dimensional distribution of intra-QRS fractionated activation. *Phys Med Biol*, 44:105–120, 1999.
- H.-P. Müller, G. Nolte, D. Di Pietro Paolo, and S. N. Erne. Using Independent Component Analysis for noise reduction of magnetocardiographic data in case of exercise with an ergometer. *J Med Eng Technol*, 30(3):158–65, may-jun 2006.

- Y. Nakaya and H. Mori. Magnetocardiography. *Clin Phys Physiol M*, 13(3):191–229, 1992.
- S. Noel, S. B. Yim, and H. Szu. Detecting electrocardiogram abnormalities with Independent Component Analysis. In *Proceeding of the 15th Annual International Symposium on Aerospace/Defense Sensing, Simulation, and Controls*, Orlando, Florida, 2001.
- G. Nolte and G. Curio. The effect of artifact rejection by signal-space projection on source localization accuracy in MEG measurement. *IEEE T Biomed Eng*, 46:400–408, 1999.
- M. Oeff, M. Burghoff, L. Hennig, M. Dulce, H. Hahlbohm, K. J. Wolf, and R. Schröder. Magnetocardiographic guiding for catheter ablation of accessory pathways. In L. Deecke, C. Baumgartner, G. Stroink, and S. J. Williamson, editors, *Recent Advances in Biomagnetism: 9th International Conference on Biomagnetism*, page 318. Tohoku University Press, 1993.
- M. Oeff, U. Leder, P. Endt, K. Brockmayer, L. Hennig, and L. Trahms. Abnormal intraventricular activation in patients with malignant tachyarrhythmias detected by magnetocardiography. *Pace*, 18:925, 1995.
- M. I. Owis, A. B. M. Youssef, and Y. M. Kadah. Characterisation of electrocardiogram signals based on Blind Source Separation. *Med Biol Eng Comput*, 40(5):557–564, 2002.
- A. Pasquarelli and S. Di Luzio. Instrumentation and methods for biomagnetic measurement. *Phys Med*, 9:249–266, 1993.
- A. Pasquarelli, B. G. Schless, H.-P. Müller, V. Hombach, and S. N. Erne. A non-magnetic ergometer for MCG stress testing. In *Proceeding of the 13th International Conference on Biomagnetism*, pages 949–951, Jena-Germany, 2002.
- J. L. Patrick, D. W. Hess, J. H. Tripp, and D. E. Farrell. The magnetic field produced by the conduction system of the human heart. *Il Nuovo Cimento D*, 2(2):255–265, 1983.
- R. Phlypo, Y. D. Asseler, I. Lemahieu, and V. Zarsoso. Extraction of the atrial activity from the ECG based on Independent Component Analysis with prior knowledge of the source kurtosis signs. In *Conf Proc IEEE Eng Med Biol Soc*, pages 6500–6503. IEEE Service Center, 2007.
- H. Riedel, M. Granzow, and B. Kollmeier. Single- sweep- based methods to improve the quality of auditory brain stem response. part ii: Averaging methods. *Z Audiol*, 40(2):94–128, 1999.

- J. J. Rieta, V. Zarzoso, J. Millet-Roig, R. Garcia-Civera, and R. Ruiz-Granell. Atrial activity extraction based on Blind Source Separation as alternative to QRS cancellation for atrial fibrillation analysis. *Computers in Cardiology*, 27:69–72, 2000.
- J. J. Rieta, J. Millet-Roig, V. Zarzoso, F. Castells, R. Sanchez Garcia-Civera, and S. Morell. Atrial flutter and normal sinus rhythm discrimination by means of Blind Source Separation and Spectral Parameters Extraction. *Computers in Cardiology*, 29:25–28, 2002.
- J. J. Rieta, F. Castells, C. Sanchez, V. Zarzoso, and J. Millet. Atrial activity extraction for atrial fibrillation using Blind Source Separation. *IEEE T Biomed Eng*, 51(7):1176–1186, 2004.
- G. L. Romani, S. J. Williamson, and L. Kaufman. Tonotopic organization of the human auditory cortex. *Science*, 216:1339–1340, 1982a.
- G. L. Romani, S. J. Williamson, L. Kaufman, and D. Brenner. Characterization of the human auditory cortex by the neuromagnetic method. *Exp Brain Res*, 47:381–393, 1982b.
- O. Rompelman and H. Ros. Coherent averaging technique: a tutorial review. part 1: Noise reduction and the equivalent filter. *J. Biomed. Eng.*, 8:24–29, 1986a.
- O. Rompelman and H. Ros. Coherent averaging technique: a tutorial review. part 2: Trigger jitter, overlapping responses and non-periodic stimulation. *J Biomed Eng*, 8:30–35, 1986b.
- C. Rosendorff. *Essentials in Cardiology - Principle and Practice 2nd editions*. Humana Press, New Yersey, 2005.
- P. Siltanen. Magnetocardiography. In P. W. Macfarlane and T. D. V. Lawrie, editors, *Comprehensive Electrocardiology. Theory and Practice*, volume 2, pages 1405–1438. Pergamon Press, New York, 1989.
- U. Steinhoff. Signal identification and noise suppression in multi-channel ECG and MCG by Independent Component Analysis (ICA). *Biocybernetics and Biomedical Engineering*, 25(4): 59–68, 2005.
- J. V. Stone. *Independent Component Analysis: A Tutorial Introduction*. The MIT Press, 2004.

- G. Stroink, D. Vardy, R. Lamothe, and M. Gardner. Magnetocardiographic and electrocardiographic recordings of patients with ventricular tachycardia. In W. S. J., H. M., S. G., and K. M., editors, *Advances in Biomagnetism*, pages 305–322. New York, Plenum Press, 1989.
- G. Stroink, W. Moshage, and S. Achenbach. Cardiomagnetism. In W. Andrä and H. Nowak, editors, *Magnetism in Medicine- A Handbook*, pages 136–189. Berlin: Wiley VCH, 1998.
- I. Tavarozzi, S. Comani, C. Del Gratta, S. Di Luzio, G. L. Romani, S. Gallina, M. Zimarino, D. Brisinda, R. Fenici, and R. De Caterina. Magnetocardiography: current status and perspectives. part I: Physical principles and instrumentation. *Ital Heart J*, 3:75–85, 2002a.
- I. Tavarozzi, S. Comani, C. Del Gratta, G. L. Romani, S. Di Luzio, D. Brisinda, S. Gallina, M. Zimarino, R. Fenici, and R. De Caterina. Magnetocardiography: current status and perspectives. part II: Clinical applications. *Ital Heart J*, 3:151–165, 2002b.
- N. V. Thakor and V. S. Zhu. Application of adaptive filtering to ECG analysis: Noise cancellation and arrhythmia detection. *IEEE T Biomed Eng*, 38:785–793, 1991.
- Y. Uchikawa and S. N. Erne. Modeling the Wolff Parkinson White syndrome for magnetocardiography. In *Proc. of the 6th int. conf. on Biomagnetism*, pages 322–25, August-Tokyo 1987.
- M. Unser and A. Aldroubi. A review of wavelets in biomedical applications. In *Proceeding of the IEEE*, volume 84, April 1996.
- S. Vorobyov and A. Cichocki. Blind noise reduction for multisensory signals using ICA and subspace filtering, with application to EEG analysis. *Biol Cybern*, 86:293–303, 2002.
- J. Vrba. SQUID gradiometers in real environments. In H. Weinstock, editor, *SQUID Sensors: Fundamentals, Fabrication and Application*, pages 117–178. Kluwer Academic Publishers, 1996.
- J. G. Webster. *Medical instrumentation : application and design*, 2nd ed. Houghton Mifflin, Boston NA, 1992.
- P. Weissmüller, K. Abraham-Fuchs, S. Schneider, P. Richter, W. Härer, M. Kochs, J. Edrich, and V. Hombach. Magnetocardiographic localization of single ventricular premature beats with a multichannel system in patients with ventricular tachycardia. In M. Hoke, S. N.

- Erne, Y. Okada, and G. L. Romani, editors, *Biomagnetism: Clinical Aspects*, pages 459–464. Amsterdam, Elsevier Science Publications, 1992a.
- P. Weissmüller, K. Abraham-fuchs, S. Schneider, P. Richter, M. Kochs, and V. Hombach. Magnetocardiographic non-invasive localization of accessory pathways in the Wolff-Parkinson-White syndrome by a multichannel system. *Eur Heart J*, 13:616–622, 1992b.
- B. Widrow and E. Walach. *Adaptive inverse control*. Prentice Hall, Upper Sadde River, New York, 1996.
- J. P. Wikswo. Theoretical aspects of the ECG-MCG relationship. In S. J. Williamson, G. L. Romani, L. Kaufman, and I. Modena, editors, *Biomagnetism: An interdisciplinary approach*, chapter 9, pages 311–326. Plenum Press in collaboration with NATO Scientific Affairs Division, 1983.
- J. P. Wikswo, J. R. Barach, and J. P. Barach. Possible sources of new information in the magnetocardiogram. *J Theor Biol*, 95:721–729, 1982.
- J. R. Willemsen, A. C. Linnenbank, M. Potse, and C. A. Grimbergen. Signal averaging of non-stationary noise. In *Proceeding of the 21st annual international conference of the IEEE EMBS*, 1999.
- V. Zarzoso, A. K. Nandi, and E. Bacharakis. Maternal and foetal ECG separation using Blind Source Separation methods. *IMA J Math Appl Med*, 14:207–225, 1997.
- A. Ziehe, K. R. Müller, G. Nolte, B. M. Mackert, and G. Curio. Artifact reduction in biomagnetic recordings based on time-delayed second order correlations. *IEEE T Biomed Eng*, 47: 75–87, 2000.
- D. P. Zipes, A. J. Camm, and M. Borggrefe. ACC/AHA/ESC 2006 guidelines for management of patients with ventricular arrhythmias and the prevention of sudden cardiac death: a report of the american college of cardiology/american heart association task force and the european society of cardiology committee for practice guidelines. *Circulation*, 114(10):385–348, 2006.

Acknowledgments

Here I am, at the last page of the thesis, ready to thank who gave me support and helped me in these *German* years. In fact, this thesis would not have been possible without the support and understanding of many people. Therefore, I would like to thank all of them, including those I may not have chance to mention here.

I start expressing my deep and sincere gratitude to Dr. rer. nat. Sergio Nicola Erne. His wide knowledge, his logical way of thinking and detailed instructions have been of great basis for me to finish the thesis work and gave me the possibility to reach one of the greatest and valuable goals in my live. With his important support throughout this work and guidance during my first steps into the signal processing, Magnetocardiography and C++ programming, he provided me a fine environment to finish this thesis.

I wish to thank my supervisor Prof. Dr.-Ing. habil. Jens Haueisen for his support for my work, giving me important comments on this manuscript and for the possibility he gave to me to defend my PhD thesis. The work presented here would certainly not have been accomplished without his influence and support. From my supervisor, I have learned a great deal about problem solving and presentation of the results of my research work.

I thank Torsten Krummel, the chief of the company I am working with, that gave me the opportunity to combine research and every day work.

I would like to give my special thanks to all my colleagues and to all those gave me the possibility to complete this thesis: Dr. rer. nat. Hans Peter Mueller for his detailed and constructive comments and kind help throughout this work and for his tireless help at the time it was needed most: In the thesis revising, he gave me great support and suggestions.

A special thank goes to Annett Veit, my roommate at work in the last years, for her nice collaboration on software development and for her patience and availability.

I would like to thank all the Mittelstr. community: Vito, Andrea, Felix, Terry, Tati and the others for their support and dinners... As Italian leaving abroad I do not know whether I could

have written my dissertation without the food provided by them: the nice dinners including the kicker games (as gymnastic for the body: mens sana in corpore sano) at Felix and Andrea's place were a wonderful break during the writing.

Furthermore I wish to thank Maria and Michela for their advices (my mental status is not too easy to rule); with them I spent long evenings in the fitness center talking about food and new recipes to taste....

My sincere thanks go to my friends Paola Oriana and Sabrina, my parents and my sister who gave me support in all their lives.

I dedicate this thesis to Tony: Thanks for the nice evenings spent together in Ancona.

Curriculum Vitae

Dania Di Pietro Paolo

Karl-Liebknechtstr. 3

07749 Jena

Date of Birth: August 21, 1978

Citizenship: Italian

Phone: 0049- 01787743731

Fax: 0049- 03641-9325789

Email: ddpp@bmddsys.de

Education

Ph.D. , University of Ilmenau, *since* 2006

PhD Thesis title: Numerical methods for improved signal to noise ratios in spatio-temporal biomedical data

Graduate electrical engineer (Dipl. Ing.) , Università Politecnica delle Marche, 2003

Thesis title: Automatic Recognition of Sharp Transients during Human Locomotion

High school graduation, Liceo Scientifico A. Orsini, 1997

Junior high school, S. Egidio alla Vibrata (Italy), 1992

Primary school, Ripe di Civitella del Tronto (Italy) 1989

Work Experience

Guest Scientist, University of Jena, since January 2006

BMDDSys Production GmbH, Magdeburg, Germany, since September 2009

BMDDSys GmbH, Jena, Germany, November 2005 - August 2009

Guest Scientist, University of Ulm, June 2003-September 2005

AtB s.r.l., Pescara, Italy, June 2003-October 2005

Awards

August 2008: Poster Award for the work *Magnetic cardiac signal extraction from measurements of patients with Implantable Cardioverter Defibrillators (ICD)* conferred at the 16th International Conference on Biomagnetism, Biomag2008, 25-29 August, Sapporo, Japan.

Publications

Peer Reviewed original papers

D. Di Pietro Paolo, H.-P. Müller and S. Erne. A novel approach for the averaging of magnetocardiographically recorded heart beats. *Phys Med Biol*, 50(10):2415-426, 2005.

D. Di Pietro Paolo, H.-P. Müller, G. Nolte and S. Erne. Noise reduction in magnetocardiography by singular value decomposition and independent component analysis. *Med Biol Eng Comput*, 44(6):489-99, 2006.

H.-P. Müller, G. Nolte, **D. Di Pietro Paolo** and S. Erne. Using independent component analysis for noise reduction of magnetocardiographic data in case of exercise with an ergometer. *J Med Eng Technol*, 30(3):158-65, may-jun 2006.

M. Görnig, M. De Melis, **D. Di Pietro Paolo**, W. Tedeschi, M. Liehr, H.R. Figulla and S. Erne. Stress testing in coronary artery disease by Magnetic Field Imaging: a 3D current distribution model. *Anadolu Kardiyol Derg*, 7(1):191-92, 2007.

D. Hoyer, E. Heinicke, S. Jaekel, F. Tetschke, **D. Di Pietro Paolo**, J. Haueisen, E. Schleuner and U. Schneider. Indices of fetal development derived from heart rate patterns. *Early Hum Dev*, 85(6):375-86, 2009.

D. Di Pietro Paolo, H.-P. Müller, M. Görnig, J. Haueisen and S. Erne. Cardiac signal extraction in patients with implantable cardioverter defibrillators. *Med Eng Phys*, in press, 2009.

Conference Proceedings

D. Di Pietro Paolo, F. Verdini, M. Marcucci and T. Leo. Automatic Recognition of sharp transients during human locomotion. *Gait & Posture - Book of abstracts*, 18(2):80-

123, 2004.

B.G. Schless, **D. Di Pietro Paolo**, H.-P. Müller, A. Pasquarelli, M. DeMelis, V. Hombach and S.N. Erne. ST-Variability Detection by Multichannel Magnetocardiography and Principal Component Analysis. *Biomed Tech*, 48(2):153-55, 2004.

B.G. Schless, **D. Di Pietro Paolo**, H.-P. Müller, A. Pasquarelli, M. DeMelis and S.N. Erne. QRS-Fragmentation Detected by Filtering with Binomial Non-Recursive Filters. In *Proc. of the 14th int. conf. on Biomagnetism*, pages 177-78, August 2004.

B.G. Schless, R. Zhu, M. DeMelis, H.-P. Müller, A. Pasquarelli, **D. Di Pietro Paolo** and S.N. Erne. Magnetocardiographic study of heart repolarization disturbances. In *Proc. of the 14th int. conf. on Biomagnetism*, pages 179-80, August 2004.

M. DeMelis, I. De Cesaris, **D. Di Pietro Paolo**, H.-P. Müller, G. Nolte and S.N. Erne. Noise reduction in MEG Data recorded by a new 500-Channel MEG vectorgradiometer system. In *Proc. of the 14th int. conf. on Biomagnetism*, pages 153-54, August 2004.

D. Di Pietro Paolo, H.-P. Müller, I. De Cesaris, G. Nolte and S.N. Erne. Noise reduction in MCG Data by Singular Value Decomposition and Independent Component Analysis. In *Proc. of the 14th int. conf. on Biomagnetism*, pages 155-56, August 2004.

D. Di Pietro Paolo, H.-P. Müller, I. De Cesaris, G. Nolte and S.N. Erne. Noise reduction in MCG Data by Singular Value Decomposition and Independent Component Analysis. In *Biomed Tech*, 49(2):728-29, 2004.

D. Di Pietro Paolo, H.-P. Müller, W. Tedeschi, J.W. Park, F. Jung and S.N. Erne. Noise Reduction in CHD patients by means of BSS. In *International Congress Series 1300 (Biomag2006)*, pages 217-20, August 2006.

D. Di Pietro Paolo, H.-P. Müller, W. Tedeschi, M. DeMelis and S.N. Erne. Comparison of BSS algorithms in SMCG data. In *International Congress Series 1300 (Biomag2006)*, pages 213-16, August 2006.

M. DeMelis, **D. Di Pietro Paolo**, W. Tedeschi, M. Görnig and S.N. Erne. RT-Matcher of data with different heart beats rate. In *International Congress Series 1300 (Biomag2006)*, pages 221-24, August 2006.

M. DeMelis, H.-P. Müller, **D. Di Pietro Paolo**, W. Tedeschi, M. Görnig and S.N. Erne. Epicardial Current Source Distribution with an Ellipsoidal Model. In *International Congress Series 1300 (Biomag2006)*, pages 129-32, August 2006.

D. Di Pietro Paolo, M. Schlosser, M. Goernig and S.N. Erne. Biomagnetic risk stratification by QRS-fragmentation in patients with implanted cardioverter defibrillators. *Proc. of the International Conference on Electrocardiology*, August 2008.

M. Görnig, **D. Di Pietro Paolo**, J. Haueisen and S.N. Erne. Biomagnetic risk stratification by QRS fragmentation in patients with Implanted Cardioverter Defibrillators. In *Proc. of the 4th European Congress for Medical and Biomedical Engineering*, November 2008.

Oral presentations at scientific conferences

B.G. Schless, **D. Di Pietro Paolo**, H.-P. Müller, A. Pasquarelli, M. DeMelis, V. Hombach and S.N. Erne. "ST-Variability Detection by Multichannel Magnetocardiography and Principal Component Analysis" in *4th International Conference on noninvasive functional source imaging*, Chieti 2003.

D. Di Pietro Paolo, H.-P. Müller, I. De Cesaris, G. Nolte and S.N. Erne "Noise reduction in MCG Data by Singular Value Decomposition and Independent Component Analysis" in *BMT*, Ilmenau 2004.

D. Di Pietro Paolo "Using ICA for pre-processing Dania Di Pietro Paolo magnetic cardiac data" in *1st International Summer school in Biomedical Engineering*, Erfurt 2006.

D. Di Pietro Paolo, M. Schlosser, M. Goernig and S.N. Erne "Biomagnetic risk stratification by QRS-fragmentation in patients with implanted cardioverter defibrillators" in *XXXV International Congress on Electrocardiology*, St. Petersburg 2008.

Erklärungen

Ich versichere, dass ich die vorliegende Arbeit ohne unzulässige Hilfe Dritter und ohne Benutzung anderer als der angegebenen Hilfsmittel angefertigt habe. Die aus anderen Quellen direkt oder indirekt übernommenen Daten und Konzepte sind unter Angabe der Quelle gekennzeichnet.

An der inhaltlich-materiellen Erstellung der vorliegenden Arbeit waren keine weiteren Personen beteiligt. Insbesondere habe ich hierfür nicht die entgeltliche Hilfe von Vermittlungs- bzw. Beratungsdiensten (Promotionsberater oder anderer Personen) in Anspruch genommen. Niemand hat von mir unmittelbar oder mittelbar geldwerte Leistungen für Arbeiten erhalten, die im Zusammenhang mit dem Inhalt der vorgelegten Dissertation stehen.

Die Arbeit wurde bisher weder im In- noch im Ausland in gleicher oder ähnlicher Form einer Prüfungsbehörde vorgelegt.

Ich bin darauf hingewiesen worden, dass die Unrichtigkeit der vorstehenden Erklärung als Täuschungsversuch angesehen wird und den erfolglosen Abbruch des Promotionsverfahrens zu Folge hat.

(Ort, Datum)

(Unterschrift)

Thesen zur Dissertation

Magnetocardiography (MCG) is a technique to detect the magnetic fields related to the electrical activity of the heart using extremely sensitive devices such as the Superconducting Quantum Interference Device (SQUIDs). The heart magnetic field is very small compared to the earth magnetic field; therefore, the interpretation of the signal is jeopardized by different kinds of disturbances and noise, causing difficulties during its analysis.

The goal of the thesis is to present a general strategy, how to cope with the different noise sources in MCG signals in order to make MCG applicable in clinical use. Two different noise reduction procedures are applied according to the SNR of the signal:

1. an optimized averaging approach
2. a method based on the blind source separation (BSS) techniques

In the optimized average approach, the main assumption is that the cardiac signal and the noise are uncorrelated and that the noise is piecewise stationary. The Signal to Noise ratio (SNR) can be optimized to a maximum value by using a selected number of beats. Herefore, a mathematical prove is given.

Five BSS methods are applied to different types of MCG examinations in order to find the most suitable method for each typology of measurement. Hereby, Temporal decorrelation source separation (TDSEP) is found to be the most effective in terms of separation and time performances.

The problem of the BSS methods is that the order of the components cannot be determined a priori. Routines for the automatic detection of cardiac and noise related components are developed. The validity of the algorithms is proved separating the patients enrolled into two groups: one identification group where the thresholds are calculated and a validation group where these thresholds are tested. In order to have a quantitative result the sensitivity and specificity of the methods are calculated.

BSS methods are applied to patients with an implanted ICD, as well. TDSEP is the most effective method, but no automatic extraction of the heart related components is possible.

Moreover, good performances are achieved in terms of computation load. It can be observed that separating the channels into 2 groups (each of them homogeneously distributed over the sensor area) provides a huge improvement of the computation speed of the algorithm.

The use and the development of the spatial, time dependency based techniques (kurtosis, correlation and frequency) make for a more flexible set of tools available to extract information from underlying set of measurements.

In clinical environments such methods could enhance the quality of the MCG and simplify the inspection of the MCG recordings for the physicians.